Evaluation of drug therapies targeting calcium homeostasis in a mouse model of hypertrophic cardiomyopathy

Dissertation

In the fulfillment of the requirements for the degree
Doctor of Natural Sciences

Submitted to the Department of Biology, Faculty of Mathematics,
Informatics and Natural Sciences

by
Frederik Flenner
from Münster

Hamburg 2015

Genehmigt vom Fachbereich Biologie
der Fakultät für Mathematik, Informatik und Naturwissenschaften
an der Universität Hamburg
auf Antrag von Frau Professor Dr. L. CARRIER
Weiterer Gutachter der Dissertation:
Priv.-Doz. Dr. H. LÜTHEN
Tag der Disputation: 16. Januar 2015

Professor Dr. C. Lohr
Vorsitzender des
Fach-Promotionsausschusses Biologie

Universitätsklinikum Hamburg-Eppendorf

Zentrum für Molekulare Neurobiologie

Research Group: Neuronal Translational Control

Falkenried 94
20251 Hamburg

Dr. Kent Duncan
Telefon: +49(40) 7410-56274
Telefax: +49(40) 7410-53436

kent.duncan@zmnh.uni-hamburg.de
www.zmnh.uni-hamburg.de

Universitätsklinikum Hamburg-Eppendorf   Martinistraße 52   20246 Hamburg
Zentrum für Molekulare Neurobiologie - Forschergruppen

English language Thesis Certification: Frederik Flenner

To whom it may concern:

Frederik Flenner, who was born on 02.07.1981 in Münster, is submitting his doctoral dissertation in English. The title of his thesis is: '**Evaluation of drug therapies targeting calcium homeostasis in a mouse model of hypertrophic cardiomyopathy**'.

I hereby certify as a native speaker and molecular biologist that the English language used in this thesis is sufficiently correct for submission.

Dr. Kent Duncan, Ph.D.

Universität Hamburg
Universitätsklinikum Hamburg-Eppendorf
Zentrum für Molekulare Neurobiologie
AG Duncan
Falkenried 94 · D-20251 Hamburg

October 24, 2014

Table of contents

1. Introduction

1.1. Heart function

The heart is a central organ of many classes of animals, as it supplies all organs of the body with blood and therefore with all nutrients and oxygen needed to function. In mammals, low-oxygen blood arrives through the venae cavae at the right atrium and is passed on through the tricuspidal valve into the right ventricle (RV). The RV pumps the blood to the lung where it gets re-oxygenized and is redirected through the pulmonary vein to the left atrium. From there it reaches the left ventricle (LV) through the mitral valve, and the contraction of the LV sends the blood to the rest of the body through the aorta. The contraction of the heart is highly coordinated and originates in just a small number of cells of the right atrium, the sinoatrial node. These cells generate an electrical signal which initiates contraction. It spreads over the atria and is then passed onto the ventricles through the atrioventricular node and the ventricular parts of the cardiac conduction system, consisting of the left and right bundle branches and their slender branch-offs, the purkinje fibers. After contraction, the heart muscle relaxes and hereby allows the re-filling of the chambers before the next beat is initiated. In human adults, this cycle is repeated 70 times a minute and can be accelerated to beating rates of close to 200 bpm in stress or exercise situations. Flawless activity of the heart is essential for a healthy organism, and impairment of heart function will inevitably lead to problems in many parts of the body.

1.2. Hypertrophic cardiomyopathy: A cardiac genetic disease

Cardiovascular diseases are one of the major causes of death worldwide. This is especially true for western industrial nations in which people have the longest expectancy of life (WHO 2012). Many of those deaths are due to acquired heart diseases which can be caused by multiple factors like dietary habits, lifestyle or environmental influences. Besides this, genetic defects can cause or trigger cardiac dysfunctions. The most common form of Mendelian-inherited heart disease is hypertrophic cardiomyopathy (HCM), affecting 0.2% of people worldwide (Maron et

al. 1995, Ashrafian et al. 2007). Patients which are clinically diagnosed with HCM have an increase of left-ventricular wall thickness of ≥15 mm in one or more segments of the LV which cannot be explained by changed cardiac loading conditions (Klues et al. 1995, Maron et al. 2003, Maron et al. 2009, ACCF/AHA guidelines 2011, ESC guidelines 2014). This hypertrophy is most of the time asymmetrical and can be associated with mild right-ventricular hypertrophy. About 70% of hospitalized HCM patients suffer from LV outflow obstruction (HOCM) due to pronounced hypertrophy (Maron et al. 2006). HCM-associated cardiac hypertrophy is usually accompanied by myocardial fibrosis and cardiomyocyte disarray (McLeod et al. 2009). The clinical phenotype, however, varies widely. Most carriers of disease-associated mutations do not suffer from any symptoms and therefore remain undiagnosed their whole life (Watkins et al. 1995). Symptomatic HCM patients show exertional dyspnea as a result of diastolic dysfunction as an early sign (Maron et al. 2006), which typically occurs in early adulthood, but disease onset can also happen in early childhood or later phases of life (Maron et al. 2003, Decker et al. 2009, Maron et al. 2012). Disease progression is also highly variable and HCM is not a relentlessly progressive disease (Maron et al. 2012), but a subset of patients develops severe heart failure which sometimes even requires heart transplantation (Spirito et al. 1997, Maron 2002, Maron et al. 2003, ACCF/AHA guidelines 2011). More than three quarters of HCM-diagnosed patients have ECG abnormalities (Niimura et al. 1998, McLeod et al. 2009) and in 20% of patients, episodes of atrial fibrillations are reported (Olivotto et al. 2001). Furthermore, HCM is considered to be the most common cause of sudden cardiac death (SCD) in young people <35 years of age, particularly in athletes (Maron et al. 1996, Elliott et al. 2000, Maron et al. 2009, Maron 2010), which sadly often occurs in patients which had been asymptomatic before.

The incomplete penetrance of HCM is most impressive in affected families, where disease phenotypes also vary from asymptomatic to severe disease forms between family members carrying the same mutation. This indicates a possible role for modifier genes, environmental factors and the patients' lifestyle. Also, the time of disease onset varies widely, with presentation of the disease at any age from infancy to old age (Maron 2002, Maron et al. 2003), resulting in an increased penetrance with patient cohorts' age. Individuals who carry a disease-associated mutation at the homozygous state usually have a poor prognosis (Ho et al. 2000, Nanni et al. 2003,

Wessels et al. 2014), and also double or triple mutations are associated with a severe course of the disease (Ingles et al. 2005, Girolami et al. 2010, Maron et al. 2012). In addition, identification of the pathogenic mutation is lacking in 30-40% of patients (Bos et al. 2009, Force et al. 2010, Landstrom et al. 2010, Maron et al. 2012). The vast majority of identified mutations occurs in genes encoding proteins of the sarcomere, the contractile units of muscles, and often lead to alterations in their function (Marian et al. 2001, Arad et al. 2002, Richard et al. 2003, Bos et al. 2009, Friedrich et al. 2012). Remarkably, although hundreds of different mutations in over 20 genes have been identified, about 70% percent of patients who have been genotyped successfully have mutations in only two different genes, namely β-myosin heavy chain (*MYH7*) and cardiac myosin-binding protein C (*MYBPC3*; fig. 1.1).
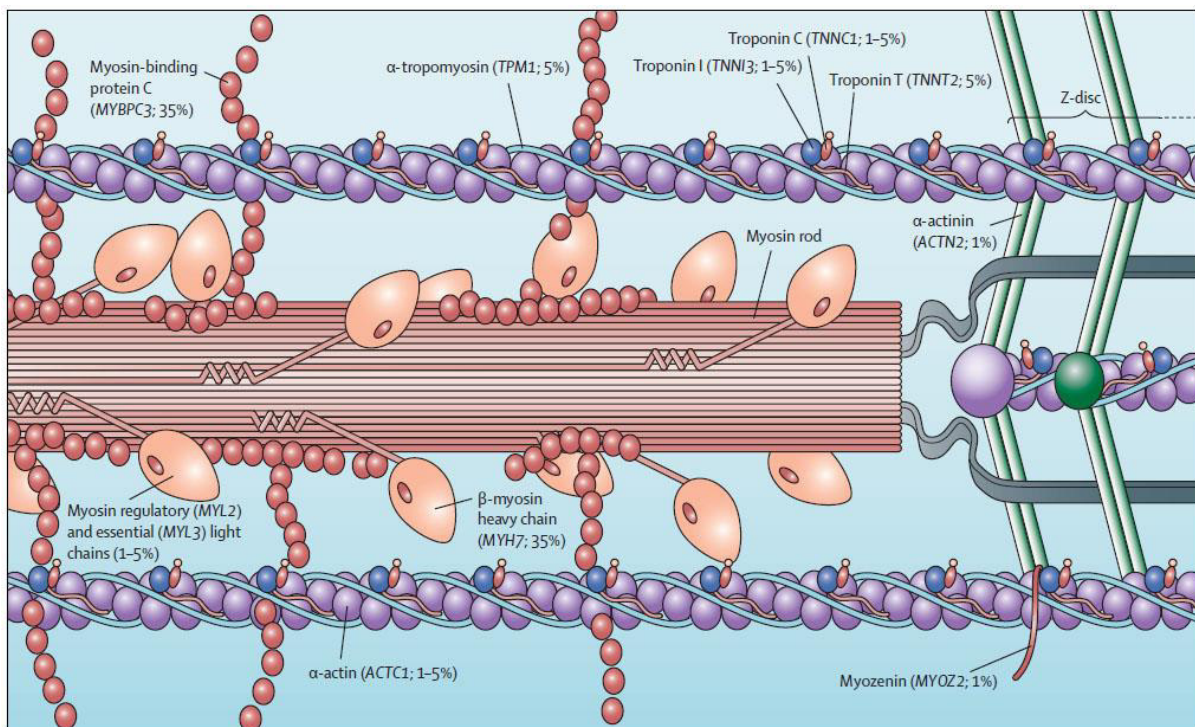
Fig. 1.1: Locations of HCM-causing genes within the sarcomere (Maron et al. 2013): Prevalence of every gene is shown in parenthesis (data from HCM patients with positive genotyping).

The pathogenic pathways leading from mutations to the HCM phenotype are largely unclear and are topic of often controversial debate. Several mechanisms have been proposed, such as altered calcium cycling and sensitivity, disturbed stress sensing, deficits in energy homeostasis or microvascular dysfunction (for review, see Frey et al. 2012). These theories are not mutually exclusive and there might not be a unifying molecular mechanism underlying every developed HCM. However, perturbed

function of the sarcomere is certainly one of the key aspects of the disease. In order to understand which consequences an altered sarcomere function can have, the basic principles of cardiac contraction are explained in the next paragraphs.

1.3. Cardiac contraction and relaxation

Cardiac contraction is regulated by a process called excitation-contraction coupling (for review, see Bers 2002, Bers 2008, Eschenhagen 2010). Central for this process is the regulation of intracellular Ca^{2+} levels, which increase and decrease during each action potential and cardiac beat. When the cellular membrane potential is depolarized in the early phase of the cardiac action potential, which is mediated by the opening of voltage-sensitive Na^+ currents in ventricular cells, L-type Ca^{2+} channels (LTCC) get activated, leading to Ca^{2+} influx into the cell. These channels are located primarily in cellular junctions, where the sarcolemma and the sarcoplasmic reticulum (SR), a cellular compartment enriched with Ca^{2+} (up to 1 mM inside the SR (Shannon et al. 2000), are in close vicinity to each other (fig. 1.2). In these areas, the LTCCs are one major component of local Ca^{2+} signaling complexes, so-called couplons. The other main actors in this complex are ryanodine receptors (RyR), which are Ca^{2+} release channels located in the SR membrane. They get activated by the Ca^{2+} ions entering the cell through LTCCs, and this elevates the cytoplasmic Ca^{2+} concentration locally to 200-400 µM (Bers 2008), a process called Ca^{2+}-induced Ca^{2+} release (CICR). This concentration rapidly declines with distance from the release site, but global depolarization of a myocyte leads to activation of ~20,000 couplons, which increases cytosolic Ca^{2+} to a level sufficient to initiate cardiac contraction at the sarcomere.
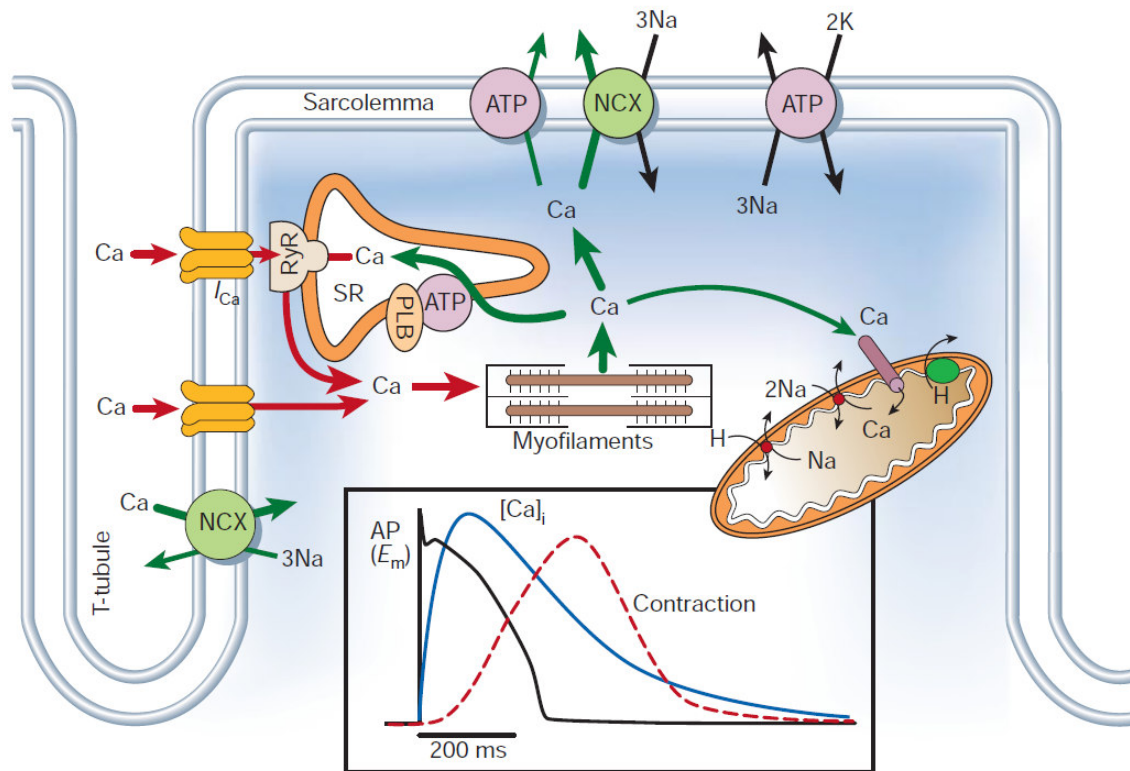
Fig. 1.2: Ca^{2+} transport in ventricular myocytes (Bers 2002): Red arrows depict fluxes which increase cytoplasmic Ca^{2+} concentration and initiate contraction, green arrows depict those which decrease cytoplasmic Ca^{2+} and are involved in relaxation. SR: Sarcoplasmic reticulum; RyR: Ryanodine receptor; PLB: Phospholamban; ATP: ATPase; NCX: Sodium-calcium exchanger Inset shows the time courses of a typical action potential, calcium transient and contraction process in a rabbit ventricular cardiomyocyte. E_m: Membrane potential of the sarcolemma.

The sarcomere is the functional unit of myofibrils, which are the main components of cardiac myocytes, which for their part make up most of heart mass. Sarcomeres consist of proteins which form two main contractile compartments, the so-called thick and thin filaments. The thick filament mainly comprises the multimeric protein myosin and cardiac myosin binding protein C (cMyBP-C). Titin, a giant protein which is often considered to be the "third filament", anchors the thick filament at the sarcomere's border, named Z-disc (fig. 1.3). The thin filament is composed of actin, α-tropomyosin (α-TM) and the cardiac troponin (cTn) complex, which includes three troponin types: cTnT, cTnI and cTnC.
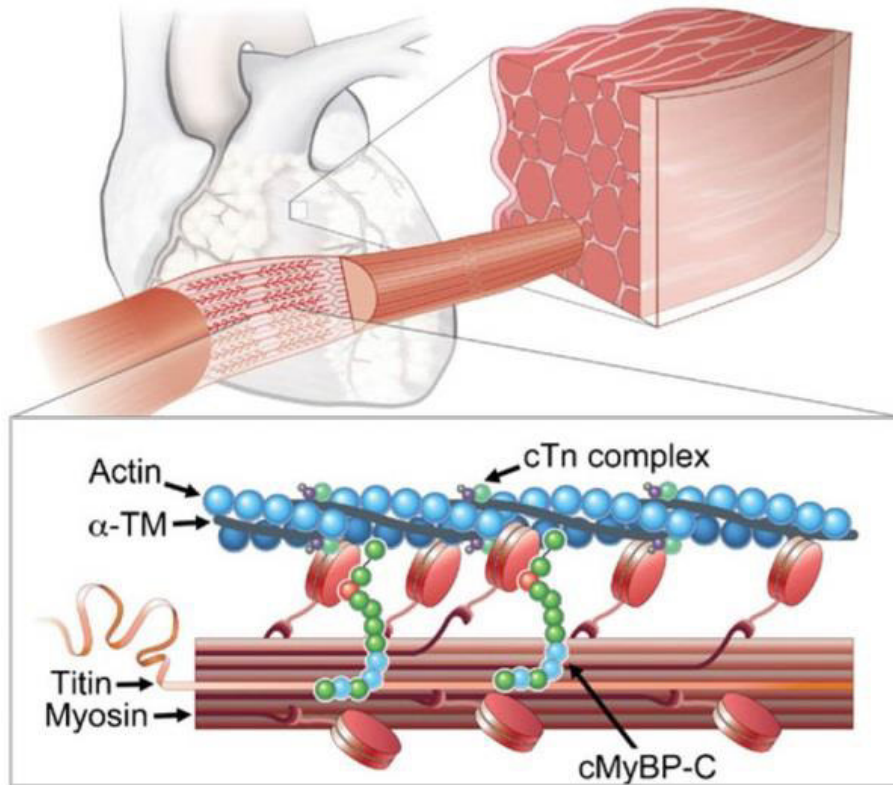
Fig. 1.3: Main components of the sarcomere and its localization in the heart (Sadayappan et al. 2014).

Sarcomeric contraction is initiated when Ca^{2+} binds to cTnC. This in turn binds cTnI more strongly and hereby withdraws it from its actin-binding site. This causes movement of troponin and tropomyosin, which are connected via cTnT, deeper into the cleft of actin. After this, myosin heads, comprised of the molecules' S1 domain which is sticking out of the multimeric protein, are able to form crossbridges with actin (Bers 2008). In the beginning of this phase, ATP is bound to the S1 domain of myosin (fig. 1.4); before binding to actin, ATP gets hydrolyzed to ADP + P_i by the enzymatic part of the molecule, which induces myosin-actin interaction. Subsequently, a conformational change of myosin heads is induced, which pulls the thin filament to the middle of the sarcomere and is accompanied by release of ADP + P_i from its myosin-binding site. After binding of a new ATP molecule, myosin detaches from actin and the contractile cycle can start again.
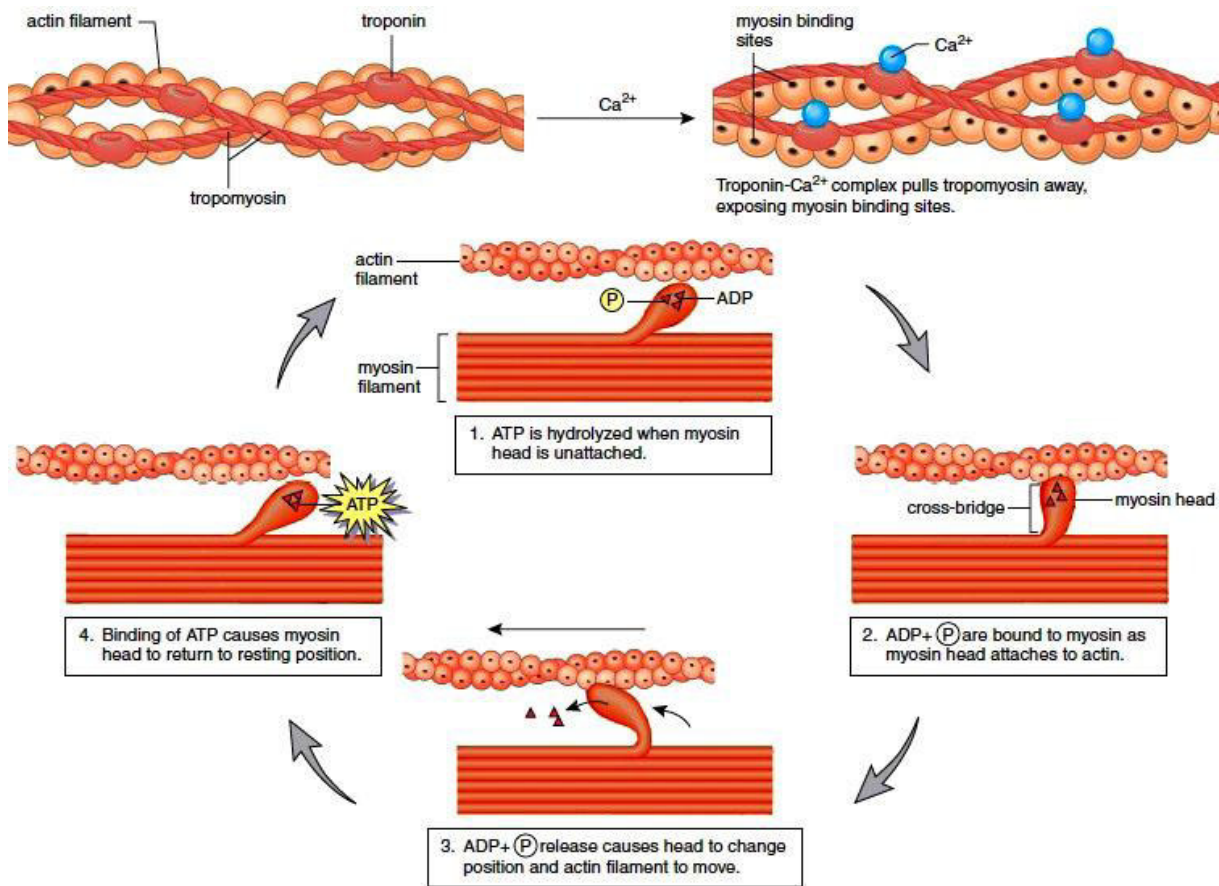
Fig. 1.4: Crossbridge cycle of muscle contraction at the myofilament (from encyclopedia.lubopitko-bg.com): Steps of contraction and relaxation are described in the figure.

This repeated crossbridge-cycling at countless myosin-actin interaction sites of numerous sarcomeres and myofilaments generates muscle contraction. The contractile process ends when the intracellular Ca^{2+} concentration ($[Ca^{2+}]_i$) decreases again and the troponin/tropomyosin complex moves back to its initial position, hindering interaction of myosin and actin. The decrease of the Ca^{2+} transient is mediated on the one hand side by inactivation of LTCCs and RyRs via Ca^{2+}- and membrane potential-mediated effects, and, on the other hand, of the transport of Ca^{2+} out of the cytosol. This task is mainly fulfilled by two molecules and pathways: The energy-demanding SR Ca^{2+} ATPase (SERCA) pumps Ca^{2+} into the SR, and the sodium-potassium exchanger (NCX) transports Ca^{2+} to the extracellular side in an electrogenic exchange for Na^+ ions.

1.4. Modulation of excitation-contraction coupling

The heart is able to adapt its output to the requirements of different situations in life, which happens on the subcellular level by the regulation of excitation-contraction coupling. The major pathway of this regulation is sympathetic stimulation of the heart through β-adrenergic receptors. Activation of these G-protein coupled receptors increases the activity of protein kinase A (PKA) via the enhancement of production of cyclic AMP. PKA in turn phosphorylates multiple components involved in excitation-contraction coupling, thereby altering their functionality (fig. 1.5). Phosphorylation of LTCCs increases their open probability, which allows more Ca^{2+} influx per excitation cycle. At the same time, SERCA activity is upregulated by phosphorylation of the SERCA-inhibiting molecule phospholamban; as a result, diastolic SR Ca^{2+} load increases, and upon RyR stimulation, more Ca^{2+} is released, which in turn increases sarcomeric contraction (= positive inotropy). This might additionally be supplemented by increased RyR open probability after phosphorylation. The enhanced SERCA activity also leads to a faster decrease in the cytosolic Ca^{2+} transient and therefore enables the sarcomere to relax faster (= positive lusitropy). In addition, cTnI phosphorylation by PKA speeds up Ca^{2+} dissociation from the myofilament by sustaining the inhibitory effect of cTnI on myosin-actin crossbridges. While this effect is too weak to significantly counteract the positive inotropic effect of β-adrenergic stimulation, it contributes to positive lusitropy.
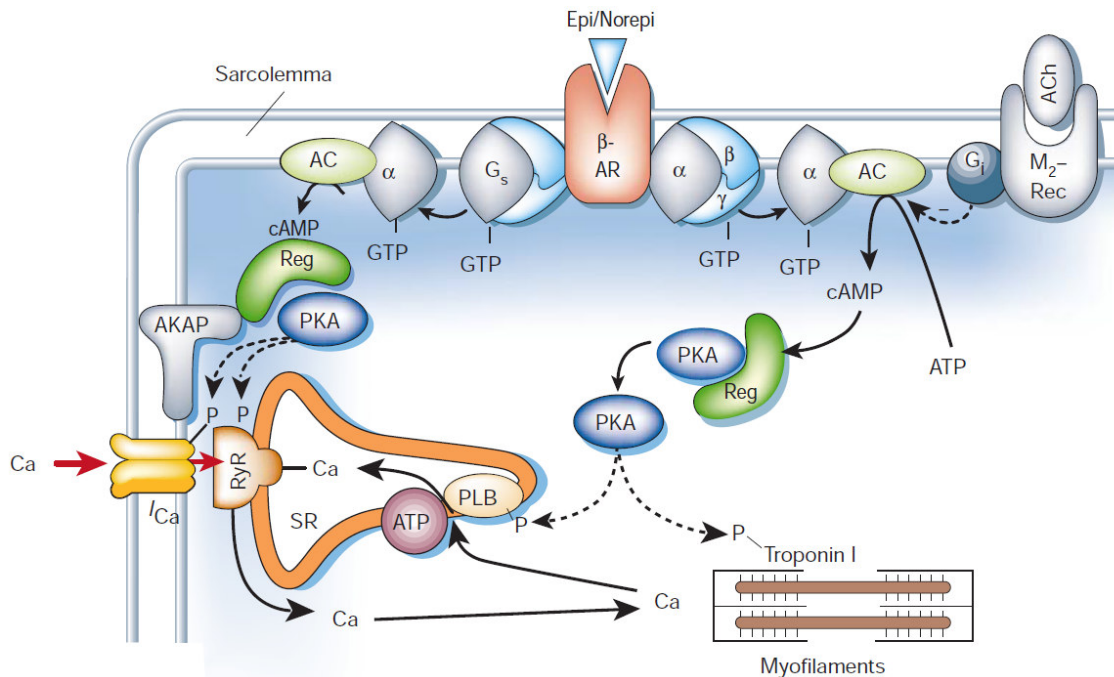
Fig. 1.5: Sympathetic regulation of excitation-contraction coupling (Bers 2002): The major components of β-adrenergic receptor (β-AR) signaling and the main phosphorylation targets of protein kinase A (PKA) are schematically illustrated. G_s, G_i, α/β/γ = receptor-coupled G-proteins and subunits; AC = adenylate cyclase; ACh = acetylcholine; AKAP = A kinase anchoring protein; M_2-Rec = M_2 muscarinic receptor; PLB = phospholamban; Reg = PKA regulatory subunit.

The elevation of the cytosolic Ca^{2+} transient additionally leads to an increase in the activation of Ca^{2+}/calmodulin-dependent protein kinase II (CaMKII). This kinase also phosphorylates LTCC, SERCA and RyR and therefore synergistically contributes to β-adrenergic signaling, whereby its efficacy is generally more moderate than that of PKA.

Ca^{2+}-handling proteins are not the only components which are important for regulation of cardiac excitation-contraction coupling. The myofilament-associated protein cMyBP-C is not only another target of post-translational modification, but seems to be a regulator of excitation-contraction coupling itself; mice lacking cMyBP-C are viable, but show severe perturbations of sarcomere, cell and heart morphology and their heart function is impaired (Harris et al. 2002, Carrier et al. 2004, Pohlmann et al. 2007). The next paragraph describes how the modulatory function of cMyBP-C is potentially carried out as it describes its structure, interactions with neighboring molecules and its regulation through phosphorylation.

1.5. Cardiac myosin-binding protein C and the sarcomere

Cardiac myosin-binding protein C is a large protein (~140-150 kDa) which is built up by immunoglobulin (Ig) and fibronectin domains, together providing 11 modules of the molecule (fig. 1.6). These domains are in general connected with 4 nm long repeats; between domains C1 and C2, there is a MyBP-C specific motif, the so-called M-domain. The cardiac isoform differs from its skeletal protein family members in three major aspects: An additional Ig-domain at the N-terminus called C0, a 30 residue stretch in the C5 domain and four phosphorylation sites in the M-domain (Gautel et al. 1995, Mohamed et al. 1998, Flashman et al. 2004, Barefield et al. 2010). Interestingly, the proline- and alanine-rich area, which connects the cardio-specific C0 domain with the C1 domain, is differently organized in species with different heart rates, suggesting this area helps to adapt cardiac contraction to the respective beating frequency (Shaffer et al. 2009).
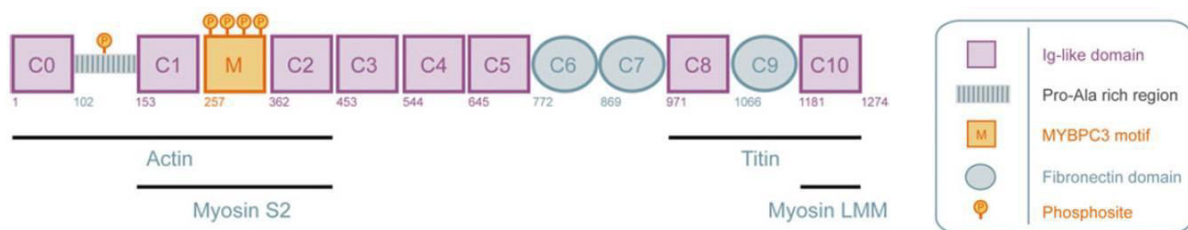
Fig. 1.6: Modular organization of cMyBP-C (adapted from Sequeira et al. 2014): Lines below the scheme indicate areas of putative interactions with other proteins.

Inside the sarcomere, cMyBP-C is located on both sides of the M-line in the C-zones of the A-band (fig. 1.7), a region where myosin-actin crossbridges are formed (Luther et al. 2008). On each side of the M-line, 9 cMyBP-C molecules form transversal stripes at every third level of myosin heads, which leads to a distance of 43 nm between these stripes.
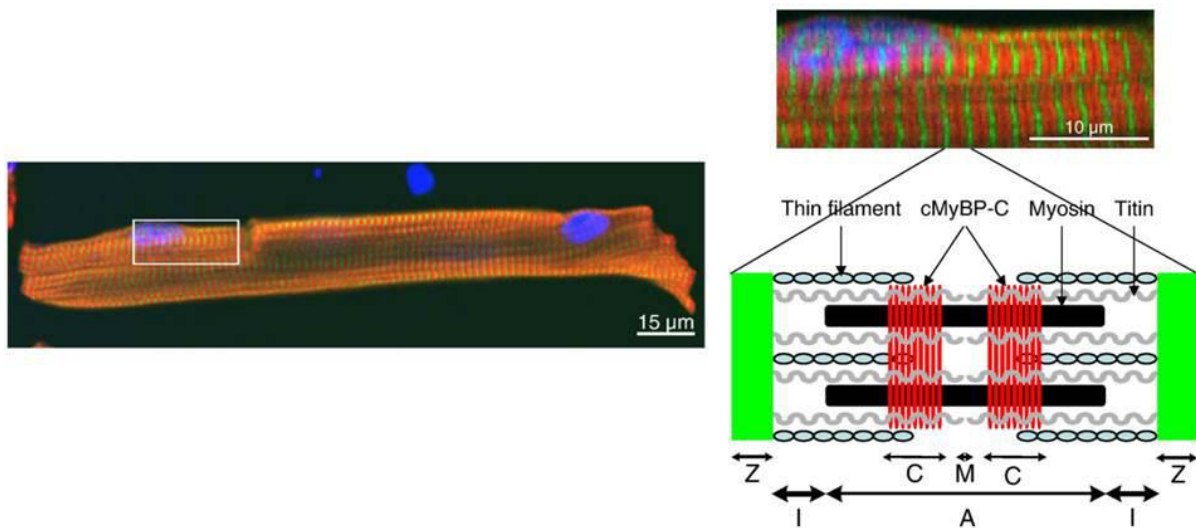
Fig. 1.7: Sarcomeric localization of cMyBP-C (adapted from Schlossarek et al. 2011): Left: Adult mouse ventricular myocyte stained for the Z-line component α-actinin (green), cMyBP-C (red) and nuclei (blue). Right: Higher magnification of the boxed area of the left picture and schematic diagram of a sarcomere between two Z-lines.

Many studies have tried to unravel how cMyBP-C is interacting with other proteins, and the main interaction areas are depicted in fig. 1.8. The C-terminal region anchors the protein to the thick filament of the sarcomere, with the C10 domain binding to light meromyosin subunits of myosin and areas of domains C8 – C10 binding to titin (Gilbert et al. 1999, Flashman et al. 2004). These interactions might lead to cMyBP-C forming a trimeric collar around the thick filament (Winegrad 1999, Moolman-Smook et al. 2002), but different organization patterns have also been proposed (Squire et al. 2003). The N-terminal region seems to bind to both actin (Kulikovskaya et al. 2003, Shaffer et al. 2009, Howarth et al. 2012) and the S2 fragment of myosin (Gruen et al. 1999), tethering the myosin heads to the tail of the molecule. Although the exact mechanism is not entirely understood, this simultaneous interaction with myosin and actin regulates their interaction, and modification of cMyBP-C also modifies myosin-actin binding. Basically, cMyBP-C reduces the probability of myosin-actin binding by physically restraining myosin head motility (Pohlmann et al. 2007). Additionally, it also can activate actin-myosin binding and influence their movement velocity differentially (Kunst et al. 2000, Herron et al. 2006, Razumova et al. 2006). Its activity is highly regulated, mainly by post-translational modification in the form of phosphorylation, and until now, 17 putative phosphorylation sites have been identified (Kooij et al. 2013). The four main phosphorylation sites are in the M-domain

(see fig. 1.5) and are targets of multiple kinases like PKA, protein kinase C (PKC), protein kinase D (PKD) and CaMKII (for review, see Barefield et al. 2010, Bardswell et al. 2012, Kuster et al. 2012). Their phosphorylation reduces the binding of cMyBP-C to both actin (Shaffer et al. 2009) and myosin S2 (Colson et al. 2008, Tong et al. 2008) and therefore enables establishment of strong crossbridges (fig. 1.8). In tissue samples of heart failure and HCM models and patients, phosphorylation status of these sites is lower than in healthy cardiac tissue (Sadayappan et al. 2005, El-Armouche et al. 2007, Jacques et al. 2008).
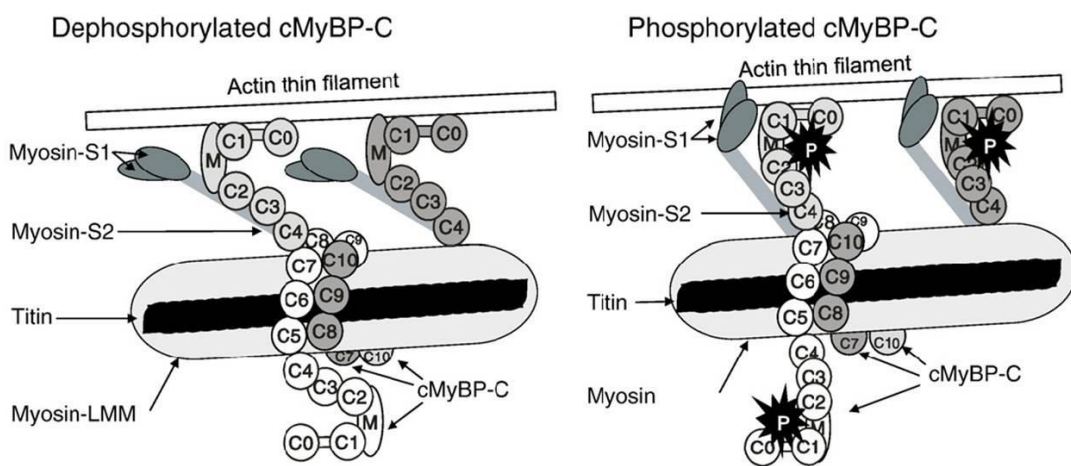
Fig. 1.8: Scheme of interaction of cMyBP-C with sarcomere components ("collar"-model) and conformational changes upon phosphorylation (Schlossarek et al. 2011).

1.6. Cardiac myosin-binding protein C in hypertrophic cardiomyopathy

More than 350 HCM-associated mutations in *MYBPC3*, the gene encoding for cMyBP-C, have been found until now (Behrens-Gawlik et al. 2014). The majority of these (~64%) are nonsense- and frameshift-mutations which produce mRNAs encoding for C-terminally truncated protein versions (for reviews, see Richard et al. 2006, Alcalai et al. 2008, Carrier et al. 2010). Interestingly, truncated versions of cMyBP-C were not detectable by Western Blot in myocardial samples from HCM patients (Marston et al. 2009, van Dijk et al. 2009), and even when transiently overexpressed in cell systems, these *MYBPC3* variants produced only relatively low amounts of proteins (Flavigny et al. 1999, Sarikas et al. 2005). Accordingly, studies

show that *MYBPC3* nonsense- and frameshift-mutations produce unstable mRNAs and/or proteins, which are degraded by cellular quality control systems (for review, see Schlossarek et al. 2011). In the vast majority of cases, patients carry the HCM-associated mutations at the heterozygous state, but the wild-type (WT) allele can only partially compensate the lack of protein caused by the mutation, so HCM is caused by cMyBP-C haploinsufficiency (Marston et al. 2009, van Dijk et al. 2009). This haploinsufficiency is also repeatedly seen in murine and also feline models carrying *MYBPC3* mutations (Meurs et al. 2005, Vignier et al. 2009), which leads to the conclusion that this is a unifying mechanism underlying HCM. Accordingly, phenotypes of *MYBPC3* knock-out and mutation-carrying knock-in models are similar in many aspects (Harris et al. 2002, Carrier et al. 2004, Vignier et al. 2009). Besides cardiac hypertrophy, impaired cardiac function, fibrosis and myofilament disarray, one phenotypic aspect which many models share is higher Ca^{2+} sensitivity of the myofilament (Cazorla et al. 2006, Fraysse et al. 2012). This is also repeatedly found in HCM models with mutations in other genes than *MYBPC3* and also in patient samples (for review, see Marston et al. 2012). Although there have also been contradictory findings of HCM-mutations leading to unchanged or even decreased myofilament Ca^{2+} sensitivity (Watkins et al. 1996, Miller et al. 2001, Soergel et al. 2004, Neulen et al. 2009), the paradigm has been formulated that increased Ca^{2+} sensitivity leads to HCM, while decreased Ca^{2+} sensitivity causes dilated cardiomyopathy (DCM).

In case of cMyBP-C haploinsufficiency, the elevated Ca^{2+} sensitivity is likely caused by the partial lack of the myosin-actin interaction block, which is underlined by the finding that isolated atria of a KO mouse model were able to beat even in the nominal absence of external Ca^{2+} (Pohlmann et al. 2007). Isolated cardiac myocytes of this mouse model also show decreased diastolic sarcomere lengths at physiological external Ca^{2+} concentrations, which is in line with reports about compromised diastolic relaxation in HCM, probably caused by residual actin-myosin interaction at low Ca^{2+} concentrations (Iorga et al. 2008, van Dijk et al. 2009, Huke et al. 2010). Furthermore, Ca^{2+}-sensitized myofilaments might buffer Ca^{2+} and thereby cause diastolic dysfunction and arrhythmia development (Pohlmann et al. 2007, Baudenbacher et al. 2008, Vignier et al. 2009, Huke et al. 2010).

Despite the remaining uncertainties about the exact mechanisms and consequences of increased myofilament Ca^{2+} sensitivity, the fact that numerous different mutations in many different genes cause similar phenotypes indicates that altered myofilament Ca^{2+} sensitivity and cellular Ca^{2+} homeostasis are promising therapeutic targets. Pharmacological regulation of these could help to improve the situation of many HCM patients.

1.7. Therapy of hypertrophic cardiomyopathy

Therapeutical concepts for treatment of HCM are largely empirical and mainly aim to ameliorate HCM-related symptoms based on the individual patient's situation. Severe disease states, such as the occurrence of HOCM, can require invasive strategies. In these cases, surgical septal myectomy or, in a subset of patients, septal alcohol ablation, are the treatment options (Sigwart 1995, Ommen et al. 2005, ESC guidelines 2014), which are most effective concerning long-term survival and reduction of risk of SCD (Wigle et al. 1995, Ball et al. 2011). The second group of patients in which invasive therapy is indicated is the one at high risk for SCD. Implantation of a cardioverter-defibrillator has shown to raise their life expectancy substantially (Sanders et al. 2005).

The majority of patients receive pharmacological treatment. First line agents recommended by guidelines (Maron et al. 2003, ACCF/AHA guidelines 2011, ESC guidelines 2014) are β-adrenoceptor antagonists (β-blockers). They are especially effective in patients displaying outflow obstruction in exercise situations and can relieve them from angina and dyspnea by lowering cardiac workload and increasing time for diastolic filling (Spirito et al. 1997, Marian 2009).

The second standard treatment drug is verapamil, a Ca^{2+} channel blocker which is primarily applied in patients with non-obstructive HCM. This treatment has been shown to improve LV function in early diastole and prolong LV filling time (Hanrath et al. 1980, Choudhury et al. 1999). Both classes of agents however are unable to stop disease progression or even reverse hypertrophy (for review, see Frey et al. 2012, Hamada et al. 2014).

Diltiazem, a non-dihydropyridine Ca^{2+} channel blocker which is recommended as an alternative for patients who are intolerant to verapamil (ESC guidelines 2014), has been shown to prevent cardiac dysfunction and development of fibrosis in HCM mouse models (Semsarian et al. 2002, Westermann et al. 2006) and is currently tested regarding its potential to prevent HCM development in genotype-positive individuals (NCT00319982). It is highly interesting to see if progression of the disease can be decelerated or even stopped in already established HCM.

Other drug classes have been tested, e.g. anti-arrhythmic agents and drugs influencing the renin-angiotensin-aldosterone system (for review, see Spoladore et al. 2012), but while some positive effects could be reported, agents were either not feasible for long-term treatment or did not have enduring efficacies. A therapy which tried to improve cardiac energy utilization with perhexiline has shown some promising effects concerning symptoms, exercise capability and diastolic dysfunction (Abozguia et al. 2010), and the approach to improve cardiac energy metabolism is pursued in a clinical trial with trimetazidine (NCT01696370). However, long-term effects of this approach are unclear.

Besides pharmacological therapy, animal studies have provided promising results in gene therapy approaches aiming at correction of mutations or introduction of the correct gene (for review, see Behrens-Gawlik et al. 2014), and these concepts certainly have the potential to change HCM outcome or even prevent disease development (Mearini et al. 2014). Nevertheless, as this way of treatment is far from clinical stages, the application of already approved pharmacological agents in HCM is an important option which should be considered.

Another promising agent for HCM therapy is the late sodium current inhibitor ranolazine. The late I_{Na} has been reported to be higher in myocytes isolated from myectomies of HOCM patients (Coppini et al. 2013), which caused, in synergy with higher Ca^{2+} and lower K^+ currents, problems in repolarization of the analyzed cells leading to high incidence of arrhythmias. Ranolazine was able to improve the myectomy-derived cell phenotype in this study and also improved diastolic dysfunction in spontaneously hypertensive rats (Williams et al. 2014). In addition, another study, which investigated diastolic dysfunction in a hypertensive mouse model, reported improvement of cardiac function by ranolazine through myofilament

Ca^{2+} desensitization (Lovelock et al. 2012). Ranolazine is standardly used as an anti-anginal drug (Banon et al. 2014) and has shown protective potential for atrial and ventricular fibrillation (Verrier et al. 2013), all of which are appearing symptoms in HCM. Therefore, ranolazine might have multiple beneficial effects in treatment and is currently tested in HCM patients suffering from chest pain (NCT01721967).

1.8. Objective

The main goal of this thesis was to test pharmacological therapy approaches in a mouse model of hypertrophic cardiomyopathy. Assuming that the repeatedly reported increased myofilament Ca^{2+} sensitivity is one of the central problems of the disease, I tried to prove the following hypotheses:

1) Higher myofilament Ca^{2+} sensitivity is a central disease mechanism of HCM. Thus, a Ca^{2+} sensitizer should induce a HCM-like phenotype in WT cardiac myocytes, while a Ca^{2+} desensitizer should improve HCM-associated phenotypic aspects in *Mybpc3*-KI cardiac myocytes.

2) Pharmacological agents which decrease intracellular Ca^{2+} load or desensitize the myofilament towards Ca^{2+} improve HCM cardiomyocyte and heart function (fig. 1.9).

To define the functional phenotype of KI cardiac myocytes, I used the IonOptix system, which monitors movement of sarcomeres during contraction and can evaluate intracellular Ca^{2+} levels with the help of fluorescent dyes. The same system was used to test the effects of the Ca^{2+} sensitizer EMD 57033, the Ca^{2+} desensitizing myosin ATPase inhibitor Blebbistatin as well as the efficacies of the Ca^{2+} channel blocker diltiazem and the late Na$^+$ current inhibitor ranolazine on single cardiac myocytes. The acute effects of EMD 57033 were additionally evaluated *in vivo* by echocardiography.

I further evaluated the therapeutical potential of diltiazem and ranolazine in *Mybpc3*-KI mice and compared the effects to a classical therapy approach with the β-receptor-antagonist metoprolol in a 6-month treatment study. Echocardiographic

recordings of mitral blood flow and movement of the left ventricle were used to determine cardiac function and its changes upon pharmacological treatment. In a subset of mice, cardiac function was further evaluated by intraventricular hemodynamic measurements at the end of the study. Additionally, body parameters were monitored throughout the whole study.
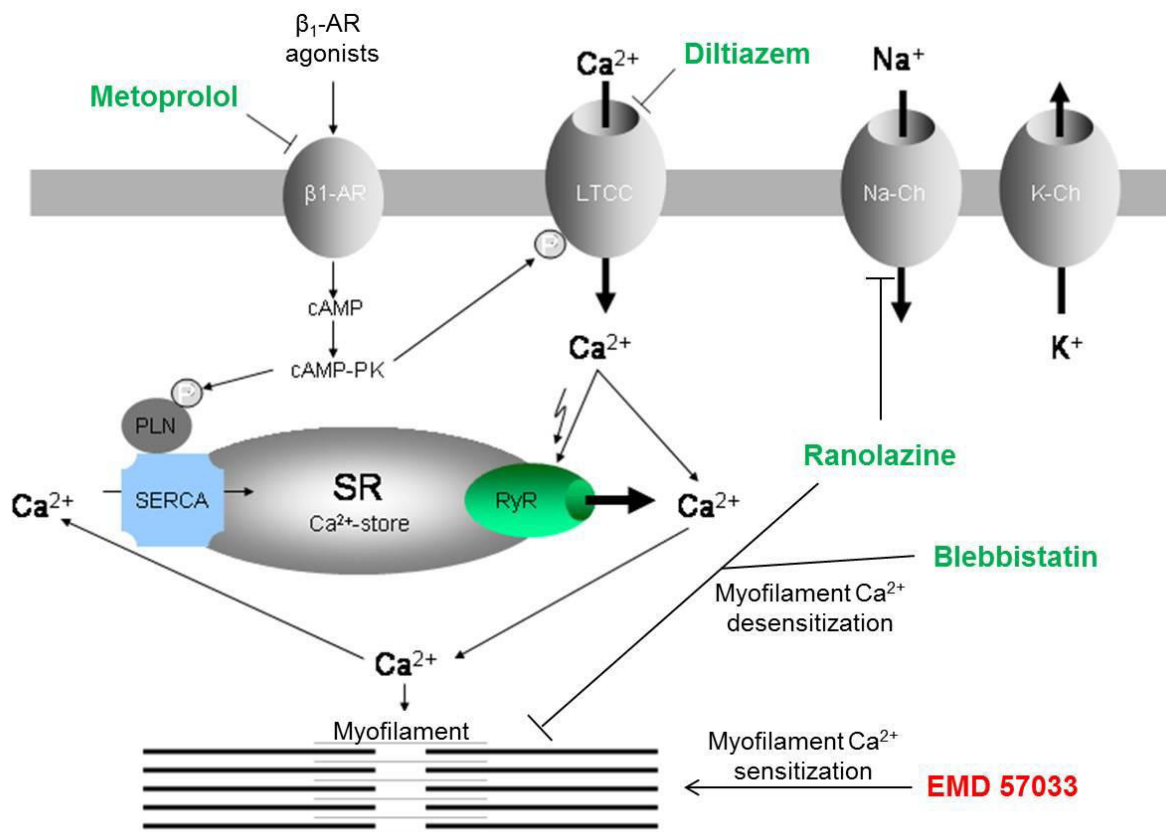
Fig. 1.9: Main components of cardiac excitation-contraction coupling and targets of drugs used in this study (adapted from calcium.ion.ucl.ac.uk): Substances with a supposed beneficial effect are displayed in green, those with a supposed detrimental effect are displayed in red.

2. Methods

2.1. *Mybpc3*-targeted knock-in mouse model

The *Mybpc3* knock-in (KI) mouse model used in this study had been generated previously (Vignier et al., 2009). Specifically, a G>A transition frequently found in HCM patients was introduced in the last nucleotide of exon 6 of the *Mypbc3* gene by gene targeting. This G>A transition is located in a consensus sequence for donor splice sites. This mutation leads to different *Mybpc3* mRNA splice variants, encoding either for missense (E264K), truncated (premature stop codon in exon 9) or slightly shortened (deletion/insertion or in-frame deletion) versions of cMyBP-C. However, truncated protein versions could neither be detected in mouse nor in patient samples until now. Accordingly, the presence of the mutated allele leads to drastically lower amounts of cMyBP-C, resulting in 21% and 90% lower protein quantity in heterozygous and homozygous KI mice, respectively. Phenotypically, homozygous KI mice develop left ventricular and myocyte hypertrophy with diastolic and systolic dysfunction. Taken together, these mice show key features of HCM.

2.2. Isolation of adult ventricular cardiomyocytes

Intact ventricular cardiomyocytes were isolated from adult mouse hearts by retrograde perfusion of the myocardium with recombinant collagenases as described by O'Connell et al. 2007 and Pohlmann et al. 2007. Fifteen minutes (min) prior to the preparation, mice were injected intraperitoneally with heparin (200 units) to avoid blood clotting in the vessels during preparation. Mice were anesthetized with CO_2 and then killed by cervical dislocation. The thorax was opened and the heart was quickly excised while cutting the aorta ~2-5 mm above its entry into the heart. The aorta was slid onto a buffer-filled cannula with fine forceps and fixed with a surgical thread. The cannulated heart was then mounted on a temperature-controlled perfusion system and perfused at a rate of 3 ml/min with the buffer heated to 37 °C.
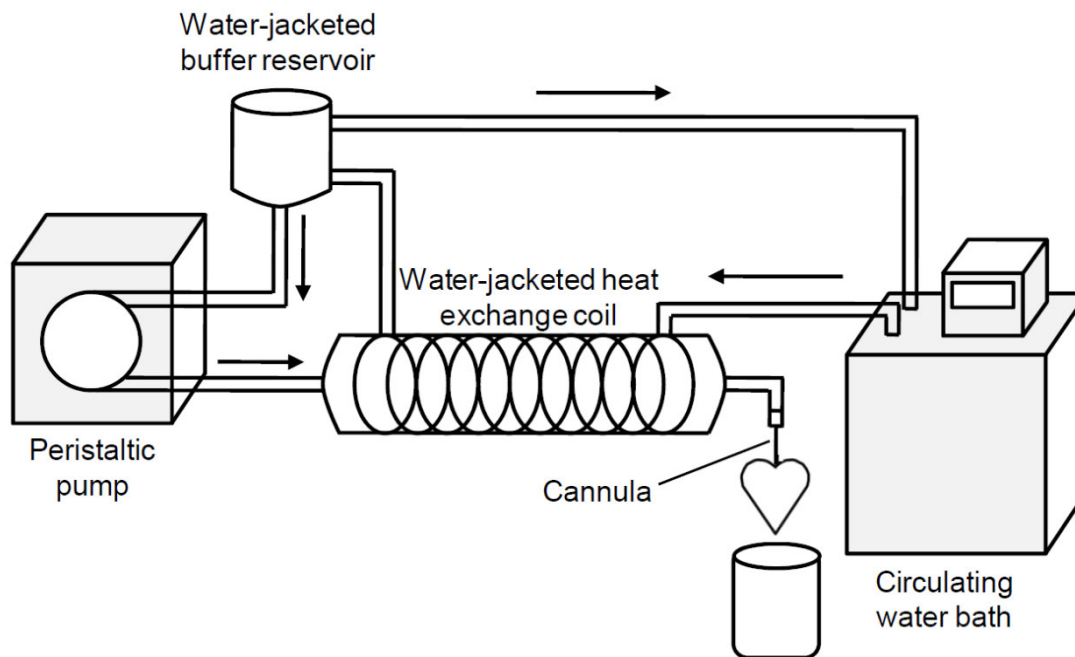
Fig. 2.1: Schematic drawing of a heart perfusion system according to Langendorff: With the help of a circulating water bath and a peristaltic pump, an extracted heart is perfused with a mix of recombinant collagenases via the aorta. This results in digestion of fibroblasts and connective tissue, and single ventricular myocytes can be isolated.

After a washing period of 6 min 30 sec, in which the heart was perfused with Ca^{2+}-free buffer containing the myosin inhibitor 2,3-butanedione monoxime (BDM) (113 mM NaCl, 4.7 mM KCl, 0.6 mM KH_2PO_4, 0.6 mM Na_2HPO_4, 1.2 mM $MgSO_4$, 12 mM $NaHCO_3$, 10 mM $KHCO_3$, 10 mM HEPES pH 7.46, 30 mM taurine, 5.55 mM glucose, 10 mM BDM, 5 mM penicillin/streptomycin), perfusion was switched to digestion buffer (perfusion buffer containing 12.5 µM $CaCl_2$ and 0.075 mg/ml Liberase TM, a mix of recombinant collagenases and proteases designed by Roche). After additional 7 to 8 min of perfusion, ventricles were separated from the rest of the heart and placed into a dish containing digestion buffer. The degree of digestion was tested by applying sheer stress to the tissue with forceps. If the tissue was digested sufficiently, enzyme activity was inhibited by addition of 5% fetal bovine serum. Tissue was then gently dissected using scissors and forceps. Single cardiomyocytes were isolated from homogenized tissue by repeated pipetting through a 10-ml wide-mouth pipette. Debris was separated from cardiomyocytes by one minute sedimentation, and the supernatant was transferred to a new tube. Cardiomyocytes were allowed to sediment for 10 min and then resuspended in fresh buffer. Ca^{2+} was slowly and gradually raised to a final concentration of 1 mM over 20 min. Cardiomyocyte number

was calculated using a Fuchs-Rosenthal chamber. For further experiments, cardiomyocytes were transferred to IonOptix buffer (135 mM NaCl, 4.7 mM KCl, 0.6 mM KH_2PO_4, 0.6 mM Na_2HPO_4, 1.2 mM $MgSO_4$, 10 mM HEPES pH 7.46, 20 mM glucose, 1.5 mM $CaCl_2$).

2.3. IonOptix measurements and analysis

The contractile properties of isolated adult ventricular cardiomyocytes as well as their intracellular Ca^{2+} transient shapes were analyzed with the IonOptix system (IonOptix Corporation, Milton, MA, USA). This system combines video-optical recordings of sarcomere movements with fluorescent dye-based monitoring of the intracellular Ca^{2+} transient in electrically stimulated cardiomyocytes. Thereby, it enables the user to analyze these two parameters of cardiomyocyte contractility in parallel.

The intracellular sarcomeric organization of heart muscle cells with their thick and thin myofilament elements is visible in light microscopy as a regular alternating pattern of dark and light areas. The IonOptix MyoCamS^{Tm} records the optical density of a series of these visible sarcomeres and the acquisition software (IonWizard) analyzes the resulting sinusoidal curve of this pattern, in which the wavelength of the sine represents sarcomere length.
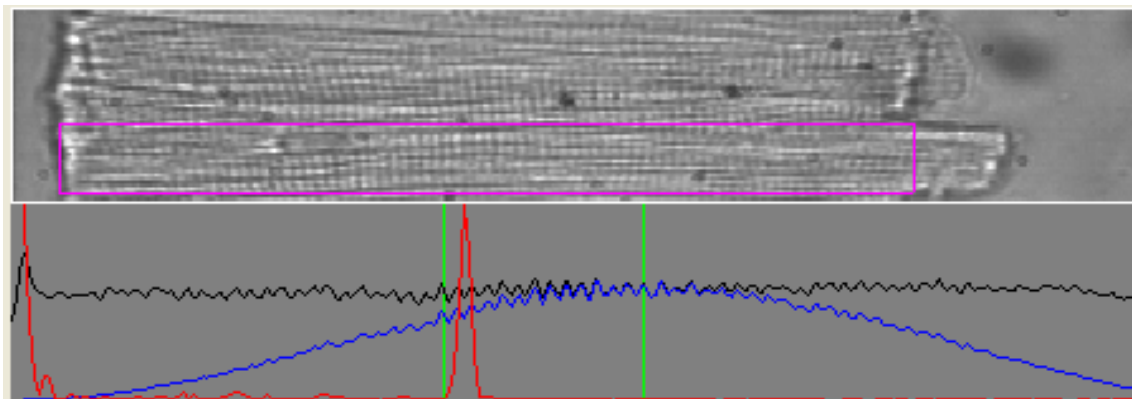
Fig. 2.2: Averaged sarcomere length measurement of a single murine cardiomyocyte (IonWizard screenshot): The acquisition software transforms the optical density pattern of all sarcomeres detected in the pink box (represented by the black trace in the lower picture) of the upper picture into an average sarcomere length (red peak in the lower picture).

With the help of a Fast Fourier Transform of this wavelength, sarcomere length can be calculated once the system is calibrated with a defined scale pattern stage micrometer. Changes in sarcomere length upon electrical stimulation of the recorded cell can be traced by the MyoCamS^{Tm}, which has an image sampling frequency of up to 500 Hz. Parallel recording of the electrical pacing signal, which is integrated by the Fluorescence System Interface, enables the IonWizard software to calculate not only contraction amplitude of the cell, but also contraction kinetics with time and velocity parameters.
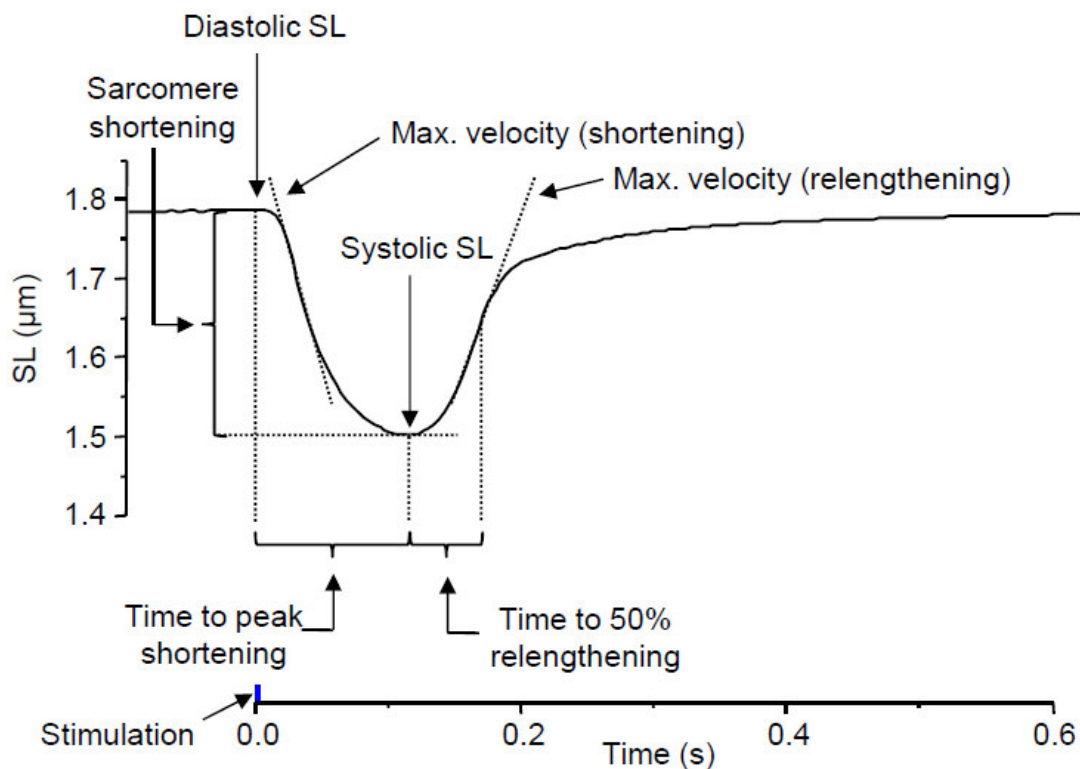
Fig. 2.3: Averaged contraction and analysis parameters (image from IonOptix manual): Video-optical recordings follow the change of sarcomere length of a cardiomyocyte during contraction and the analysis software can measure and calculate contractile parameters depicted in the figure.

For the analysis of this study, about 20-30 contractions of one recording condition were averaged for the analysis of contractile properties.

The fluorescent Ca^{2+} chelator Fura-2 was used to record intracellular Ca^{2+} concentration changes upon electrical stimulation of ventricular cardiomyocytes. The maximum in the excitation spectrum of this fluorescent dye changes upon binding to

Ca^{2+}. In the non-Ca^{2+} bound state, the maximum is at 380 nm, and the binding of Ca^{2+} shifts it to 340 nm.
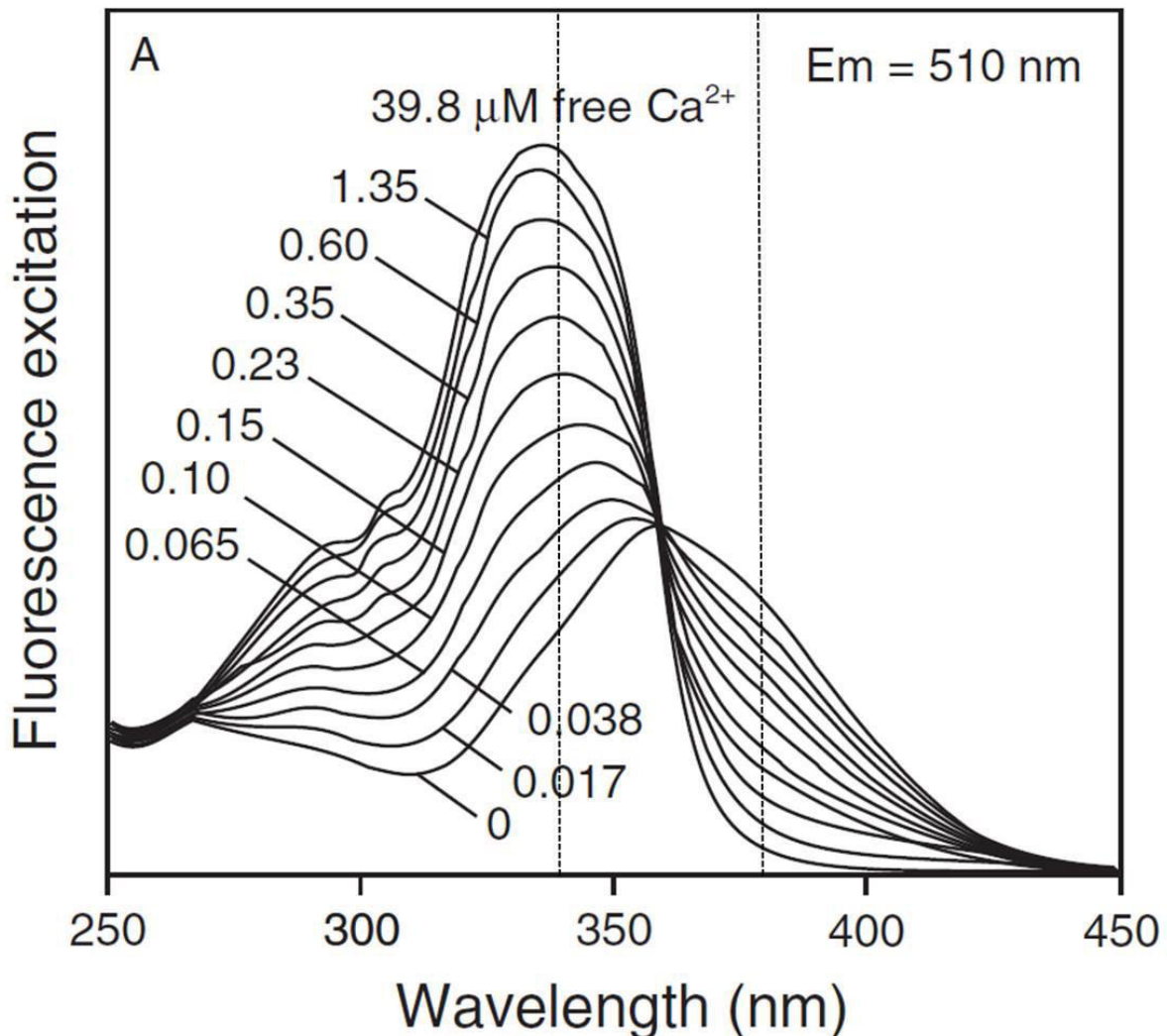
Fig. 2.4 Absorption spectra of Fura-2 in solutions of different Ca^{2+} concentrations (image taken from the Invitrogen manual): The curves describe the relative absorption spectra of Fura-2 between 250 and 450 nm in response to different concentrations of free Ca^{2+}. Dotted lines indicate excitation wavelengths (340 and 380 nm) for ratiometric measurements.

As Fura-2 in its active fluorescent form is not cell permeable and the recorded cardiomyocytes needed to stay intact, the acetoxymethyl (AM) form of the chelator was used in the experiments of this study. In this form of the molecule, carboxylic acids have been modified with AM ester groups, resulting in an unpolar, membrane-permeable molecule. Nonspecific esterases inside the cell cleave these lipophilic blocking groups, creating a charged form of the molecule which leaks out of cells at very low rates.

In both states, Ca^{2+}-bound and -unbound, Fura-2 emits light with a maximum at 510 nm. The two different excitation maxima make it a ratiometric fluorescent dye, meaning that the ratio of light emitted upon stimulation at 340 nm divided by the light emitted upon stimulation at 380 nm directly reflects the available free Ca^{2+} concentration inside the cell. The IonOptix HyperSwitch Dual Excitation Light Source emits the 340 nm / 380 nm wavelength pair 250 times per second, which provides a time resolution sufficient to record real-time Ca^{2+} transients of Fura-2-loaded cells. This high time resolution is reached by a high-speed galvanometer-driven mirror, which reflects the light of a 75-W Xenon arc lamp to two different light paths in an alternating pattern. On the first path, light enters a dichroic cube through an emission filter first, then passes a dichroic mirror and is at the end of the cube focused onto a liquid light guide which leads to the microscope. On the second path, light is steered into the cube at a 90° angle and passes a different emission filter, before it is reflected by the dichroic mirror and focused onto the light guide.
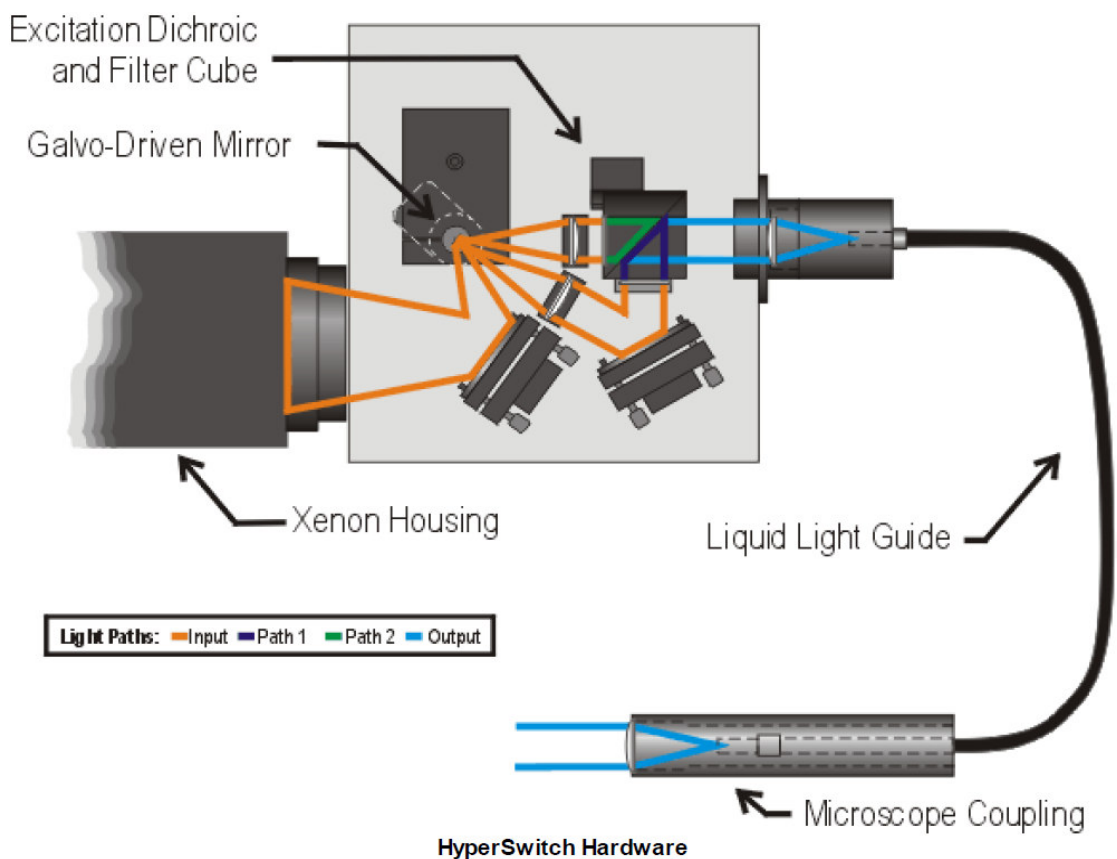
Fig. 2.5: Schematic drawing of the IonOptix HyperSwitch dual excitation light source (image taken from the IonOptix manual): Light is guided from the light source through the filters for the excitation wavelengths of Fura-2 (340 and 380 nm) by mirrors and passed on to the microscope over a liquid light guide.

At the microscope, the light coming from the HyperSwitch Light Source is directed to the microscope table holding the glass-bottomed chamber with the cardiomyocytes. The returning light emitted by the cells is, together with the light of the microscope light source, then directed towards another cube containing the cell framing adapter, which reduces the recorded signal to the measured cell, and again, a dichroic mirror. Light with wavelengths >510 nm passes the mirror and builds up the signal for the MyoCamS^{Tm}. Wavelengths of 510 nm and below are reflected onto a photo multiplier tube (PMT) which generates current for every sensed photon. Its signal is also integrated into the recording via the Fluorescence System Interface.
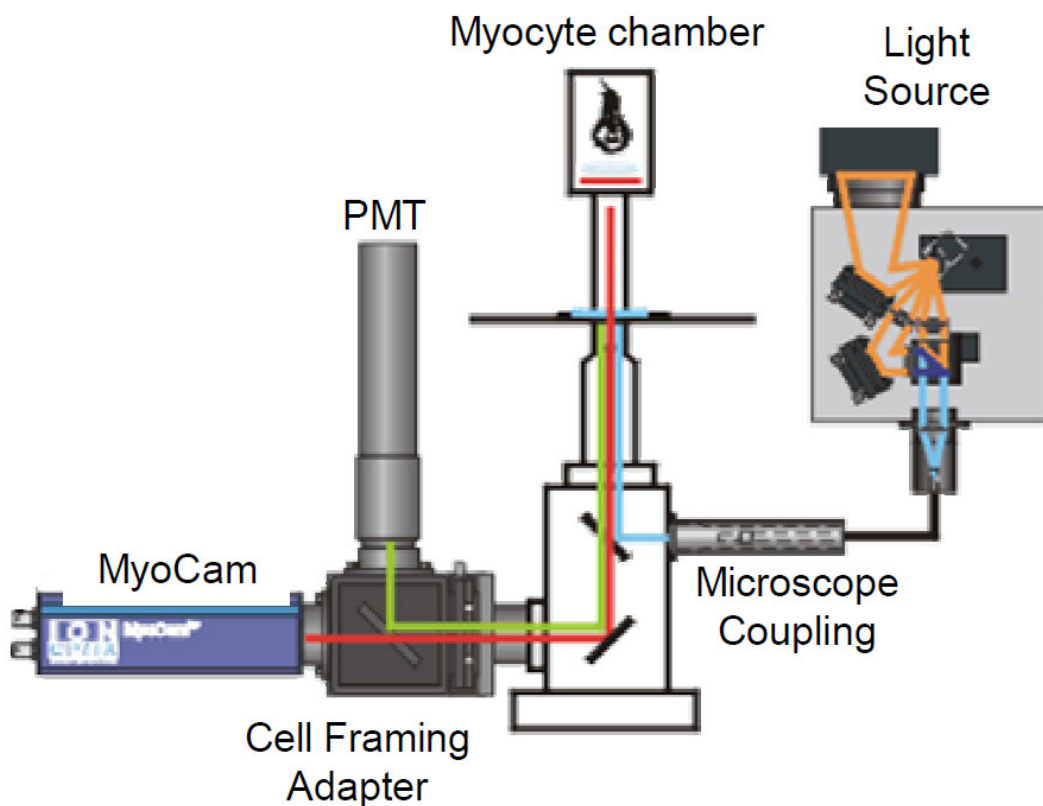
Fig. 2.6: Schematic drawing of IonOptix components involved in signal generation and detection (image adapted from IonOptix manual): Excitation light is transferred from the light source to the cell sample on the microscope table. Emitted light from Fura-2-loaded cells and light from the microscope lamp are then passed on to the MyoCamS for detection of contractions and to the photomultiplier tube (PMT) for registration of the fluorescence signal.

As for the contraction analysis, 20-30 Ca^{2+} transients were averaged and amplitude and kinetic parameters were calculated.
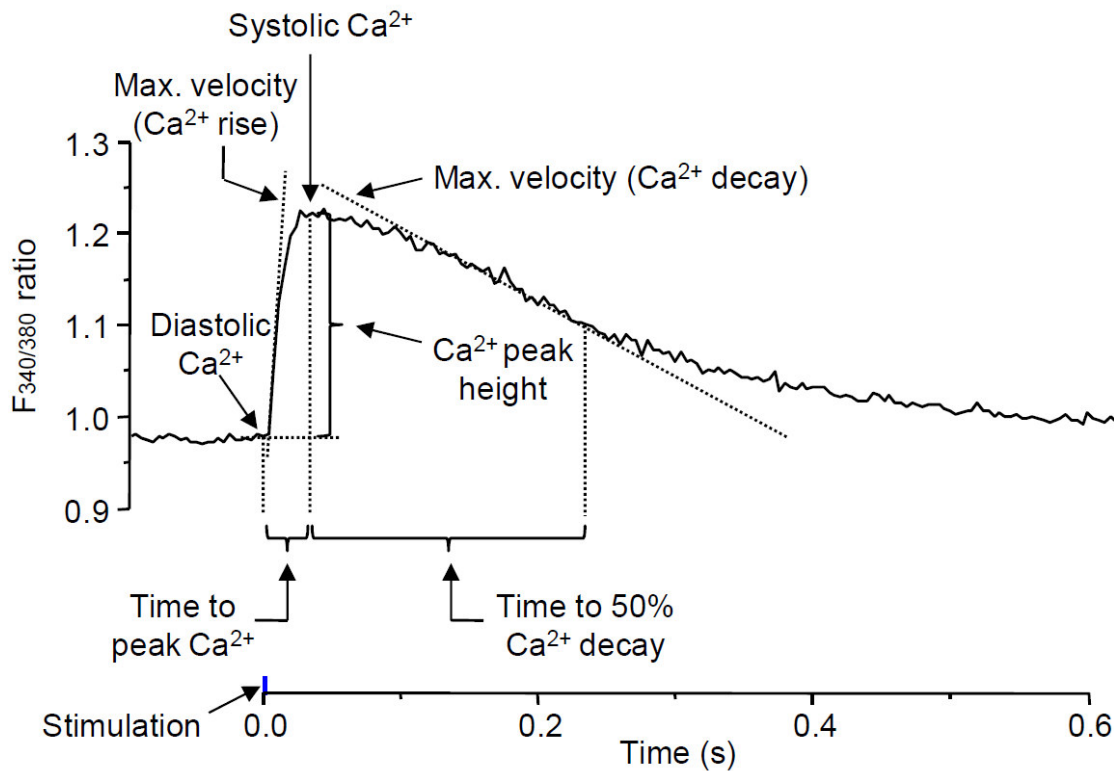
Fig. 2.7: Averaged Ca^{2+} transient and analysis parameters: The PMT detects changes in Fura-2 fluorescence upon cell stimulation, and the IonWizard software allows the calculation of the parameters depicted in the scheme. Here, an example for an excitation-elicited Ca^{2+} transient, measured by change in Fura-2 340/380 ratio over time is shown. The descriptions in the graph show the most important kinetic parameters.

Fura-2 acts as a Ca^{2+} buffer, as Ca^{2+} bound by Fura-2 is not available in the cell to activate myofilament contraction. This leads to non-negligible alterations of contraction kinetics. Therefore, recordings of contraction and Ca^{2+} transients were done in parallel in this study, but detailed analysis of contractile parameters were done in cells which were not loaded with Fura-2.

Isolated cardiomyocytes were diluted to a concentration of 10,000 to 20,000 cells per ml buffer for measurements. For measurements of Ca^{2+} transients, cells were loaded with 0.6 µM Fura-2 AM for 15 min in a lightproof tube. Then, cells were washed in fresh IonOptix buffer for 15 min to end loading and enable intracellular de-esterification of Fura-2. Before measurements, cells were taken up in fresh buffer.

For measurements, 400 µl of cell suspension was pipetted into a cell perfusion chamber (Cell MicroControls, Norfolk, VA, USA), which was then inserted into a cutout in the table of an inverted microscope. The chamber was perfused with pre-

warmed IonOptix buffer, creating a controlled temperature of ~37 °C in the chamber. Flow (1 ml/min) and temperature were controlled by cFlow 8 channel flow controller (Cell MicroControls, Norfolk, VA, USA), a TC2BIP2 2/3 channel bipolar heat controller and a MPRE8 8 channel pre-heater. This 8-channel pipette allowed rapid switching between solutions containing the substances which were tested. Excessive solution was removed from the chamber by a peristaltic pump (Gilson Inc., Middleton, WI, USA). To elicit Ca^{2+} transients and myocyte contraction, cells were electrically field-stimulated with two platinum iridium electrodes connected to a MyoPacer, which allows stimulation of cells at different frequencies.

Cells measured had to fulfill the following criteria: a) rod-shaped size without damaged membrane parts or blebs, b) clear and regular striated sarcomere pattern, c) no spontaneous activity without stimulation and d) stable contraction amplitude without extrasystoles or missing beats.

Concentration-response experiments to determine EC_{50} values of used substances were recorded at 1 Hz pacing frequency. An increased workload protocol (fig. 2.8) was designed the following way: Cells were paced at 1 Hz and recorded for minimum 30 sec before 30 nM isoprenaline (ISO) was infused into the chamber. When ISO stimulation was in full effect, pacing was switched to 5 Hz for 1 min and subsequently put back to 1 Hz. Recording was ended 30 sec later. The effect of 3 µM EMD 57033, 300 nM blebbistatin, 1 µM diltiazem or 10 µM ranolazine was tested in this protocol. As control experiments, ISO stimulation at 1 Hz for 5 min or switch to 5 Hz pacing without ISO stimulation were performed in the presence or absence of the pharmacological agents.
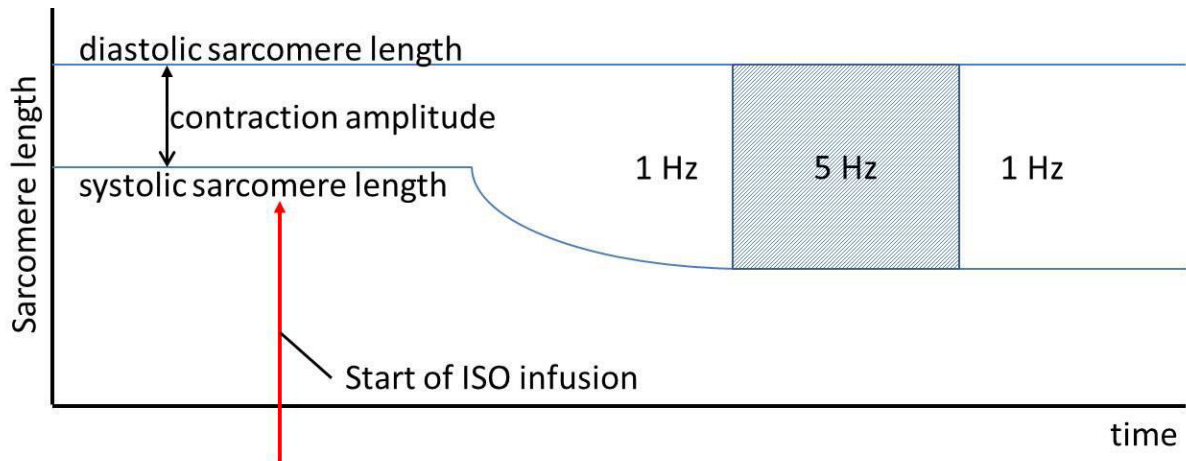
Fig. 2.8: Design of the increased workload protocol: Sarcomere length of an isolated cardiomyocyte is measured monitored under different stimulation conditions which are depicted in the figure.

2.4. Isometric force measurements

To test the sensitivity of cardiac tissue to β-adrenergic stimulation and the effect of ranolazine, isometric force measurements on left ventricular muscle strips were performed. To prepare these muscle strips, WT and KI mice were sacrificed by cervical dislocation and hearts were quickly excised. Atria were removed, ventricles were opened from base to apex and longitudinally divided into strips. Muscle strips were mounted in an organ bath between a fixed clamp and a force transducer.
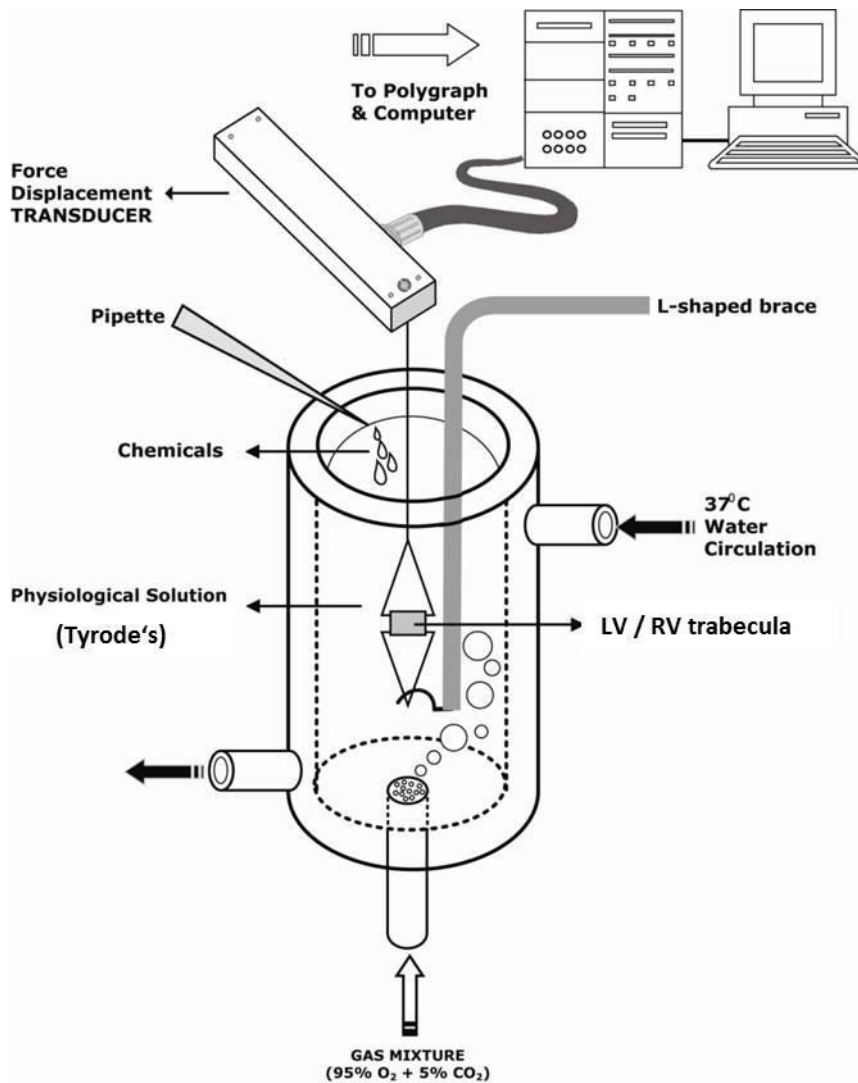
Fig. 2.9: Schematic drawing of a ventricular muscle piece mounted for isometric force measurements (image adapted from intechopen.com): A ventricular muscle strip or trabecula is mounted between a steady post and a hook, which is connected to a force transducer. It is immersed in a 37 °C physiological solution and stimulated to twitch by electrical field stimulation. Pharmacological agents can be added to the solution and their impact on twitch force and kinetics can be evaluated.

In this configuration, muscles were electrically stimulated and the force of the elicited twitches was measured. To keep the muscles working for several hours, they were bathed with carbogen-saturated Tyrode's solution (NaCl 126.9 mM, KCl 5.4 mM, $CaCl_2$ 1.8 mM, $MgCl_2$ 1.05 mM, $NaHCO_3$ 22 mM, NaH_2PO_4 0.45 mM, EDTA 0.04 mM, ascorbic acid 0.2 mM, pyruvate 5 mM, glucose 5 mM, pH 7.4). Solution and organ baths were heated to maintain an environment of 37 °C. ISO-induced (0.1 nM

– 30 µM) changes in contraction force were obtained in the presence or absence of different concentrations of ranolazine (1 µM – 100 µM) at 2-Hz pacing frequency.

2.5. Long term and acute drug treatment, echocardiography and haemodynamic measurements

To test the effects of long-term drug treatment on the HCM phenotype in mice, groups of 10 WT and KI mice were supplied with chow or water containing either ranolazine, metoprolol or diltiazem; control groups were also included in the study. Treatment started at 6-8 weeks of age and was maintained for 6 months. In the ranolazine-treatment approach, mice received chow containing either 0.5% ranolazine and 0.03% ketoconazole (treatment group) or 0.03% ketoconazole only (control group). Ketoconazole was added as a cytochrome P450 (CYP3A4) inhibitor to slow down first-pass-effect metabolism for better ranolazine bioavailability. Based on food consumption, mice were dosed with 800 mg/kg/day of ranolazine (recommended by Gilead Sciences). Metoprolol (1 g/l) and diltiazem (250 mg/l) were dissolved in drinking water, while control groups received normal water. Based on their water consumption, mice were dosed with 100 mg/kg/day metoprolol (recommended by M. Jelinek and PD Dr. A. Schwörer, Department of Physiology of the UKE) and 25 mg/kg/day diltiazem (as used by Westermann et al. 2006), respectively.

For acute dose-response measurements, EMD 57033 was injected intraperitoneally (IP) in a cumulative manner (from 0.4 to 6.4 mg/kg body weight (BW)). Echocardiographic measurements were performed before the first injection and then 5 min after each new injection.

To assess cardiac function, transthoracic echocardiography was performed using the Vevo 2100 system (VisualSonics, Toronto, Canada) with a MS400 transducer. Measurements were performed directly before the start of treatment and subsequently every 8 weeks until the end of the study (fig. 2.10).
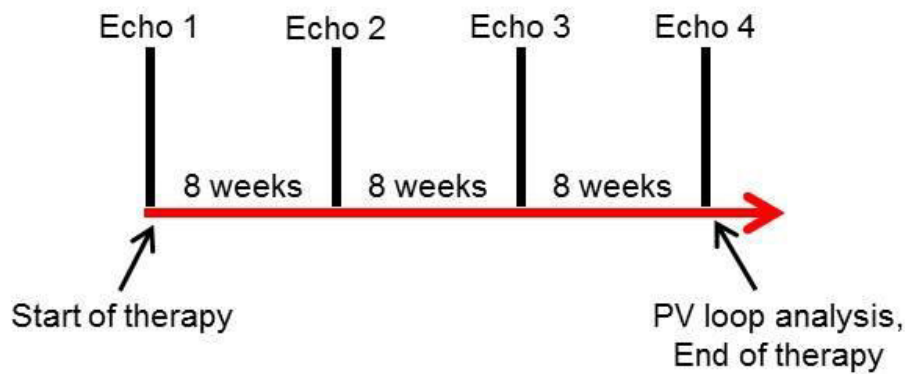
Fig. 2.10: Course of events in the long term therapy.

Six to eight week old mice received pharmacological treatment while their cardiac function was monitored by echocardiography regularly as indicated. After 6 months, hemodynamic measurements of left ventricular function were performed in some mice. All mice were sacrificed and hearts were collected for optional histologic and molecular analysis.

Mice were anaesthetized with isoflurane (1-2 %), placed on a warming platform in a supine position and chest hair was removed with depilatory cream. B-mode images were obtained in a parasternal long and short axis view at mid-papillary muscle level to obtain left ventricular dimensions (fig. 2.11).
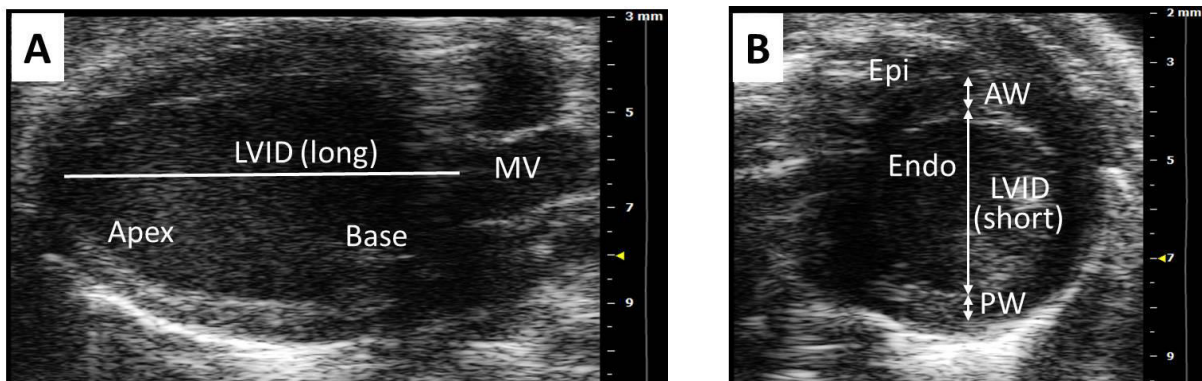
Fig. 2.11: B-mode images of the left ventricle in long (A) and short (B) axis view (Vevo2100 screenshots): A) Long axis view of the left ventricle. B) Short axis view of the left ventricle. AW = Anterior wall of the LV; Endo = Endocardial side; Epi = Epicardial side; LVID = Left ventricular inner diameter of (long) and (short) axis view; MV = Mitral valve; PM = Papillary muscles; PW = Posterior wall of the LV.

On the basis of measurements depicted in fig. 2.11, the left ventricular mass (LVM) was calculated with the values obtained in diastole (d):

LVM = 1.053 * ((LVID;d + LVPW;d + LVAW;d)^3 − LVID;d^3).

In addition to these measurements, the endo- and epicardial borders of the LV were marked in systole (s) and diastole in the short axis view and the Vevo2100® software calculated the LV wall area. Based on the area values, fractional area shortening (FAS) was calculated:

FAS = 100 * ((Area;d – Area;s) / Area;d).

Pulsed-wave Doppler echocardiography was used to measure blood flow velocities though the mitral valve (fig. 2.12).
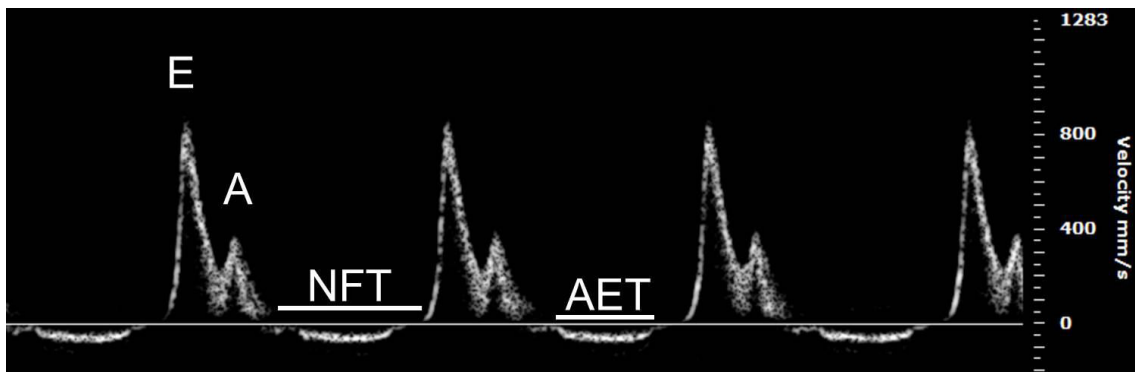
Fig. 2.12: Blood flow velocity measurement at the mitral walve with pulsed-wave tissue Doppler (Vevo2100 screenshot): E = Peak velocity of early diastolic filling; A = Peak velocity of late diastolic filling; NFT = non-filling time; AET = aortic ejection time.

Based on the measurements depicted in fig. 2.12, the myocardial performance index (MPI) was calculated:

MPI = (NFT - AET) / AET.

Hemodynamic measurements were performed in an open-chest approach. Mice were analyzed at the age of 34 weeks after being treated with drugs for 6 months. Mice were anesthetized with isoflurane (3.5% for induction, 2% during the recording) and buprenorphine (0.5 mg/kg BW) was administered for analgesia. Animals were assured to a warming platform in a supine position and the abdomen and the anterior neck were shaved. Tracheotomy was performed and mice were artificially ventilated with a rodent ventilator (MiniVent Type 845, Hugo Sachs). The abdomen was opened subxiphoidally. The diaphragm was incised via a transversal subcostal approach and the pericardium was opened. The left ventricle was entered via an apical stab with a 25 gauge needle, followed by a 1.2F Transonic© catheter.
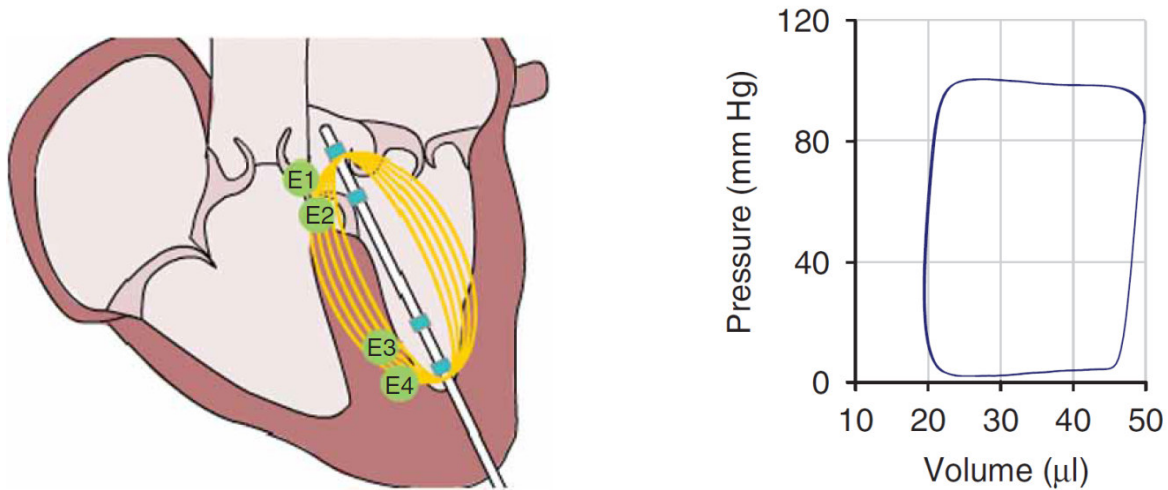
Fig. 2.13: Haemodynamic measurement of LV pressure-volume loops (adapted from Pacher et al. 2008).
Left: Placement and working principle of the Transonic© catheter: LV volume change is measured by the change of electrical resistance of the blood pool in the LV with the help of four ring electrodes (E1-E4), and the catheter itself senses changes in pressure. Right: Schematic example of a pressure-volume loop representing one cycle of systole and diastole.

After a stabilization period of 5 min, heart rate, left ventricular enddiastolic and endsystolic pressure and systolic (dP/dt_{max}) and diastolic function (dP/dt_{min}) were recorded with the Scisense ADVANTAGE System.

2.6. Protein analysis

Fractions of 20,000 to 50,000 adult ventricular cardiomyocytes were then incubated for 30 min at room temperature in IonOptix buffer alone or buffer containing 30 nM ISO ± 10 µM ranolazine. Next, cells were centrifuged for 4 min at 1000x g. The supernatant was removed, cell pellets were dissolved in 100 to 150 µl lysis buffer (30 mM Tris, pH 8.8, 5 mM EDTA, 30 mM NaF, 3% sodium dodecyl sulfate (SDS), 10% glycerol) and then stored at -20 °C until they were used for Western blot analysis.

Protein concentration was determined using the Bradford protein assay (Bradford, 1976). This colorimetric assay uses the dye Coomassie Brilliant Blue G-250, whose absorbance at 595 nm shifts upon the binding to arginine or hydrophobic amino acid residues of proteins. Bovine serum albumin was used to create a standard absorption

curve with defined amounts of protein. Cardiomyocyte protein extracts were diluted 1:5, and 5 µl of the diluted sample was intermingled with 795 µl 0.1 M NaOH and 200 µl Bradford reagent. Samples were measured in duplicates and results were corrected for blank values.

For Western blot analysis, samples containing 20 µg protein per lane were separated by SDS-polyacrylamide-gel electrophoresis (SDS-PAGE). Samples were mixed with Laemmli buffer (10 mM Tris base, pH 6.8, 2% SDS, 10% glycerol, 100 mM DTT, 0.01% bromphenol blue) and boiled for 5 min at 95 °C to denature proteins. Next, proteins were loaded onto a polyacrylamide gel consisting of a stacking gel (125 mM Tris pH 6.8, 5% acrylamide/bis acrylamide solution (29:1), 0.1% SDS, 0.1% ammonium persulfate (APS), 0.01% tetramethyethylenediamine (TEMED)) and a running gel (125 mM Tris, pH 8.8, 12% acrylamide/bis acrylamide solution (29:1), 0.1% SDS, 0.1% APS, 0.004% TEMED), which was placed into a electrophoresis chamber filled with electrophoresis buffer (25 mM Tris base, 192 mM glycine, 0.1% SDS). The Precision Plus Protein[Tm] Standard (Bio-Rad) was used as a standard molecular weight marker. Separation of proteins by gel electrophoresis was conducted at 120 V for 90 to 120 min.

Proteins were then transferred to a polyvinyledene fluoride (PVDF) membrane (GE healthcare) using a mini trans-blot chamber system filled with transfer buffer (25 mM Tris base, 190 mM glycine, 20% methanol). Transfer was conducted at 300 mA for 90 min. Subsequently, PVDF membranes were washed with 0.1% TBS-Tween (TBS-T) buffer and then incubated for one hour at room temperature in TBS-T containing 5% milk powder to block unspecific antibody binding sites. After this, membranes were incubated with primary antibodies diluted in TBS-T overnight at 4 °C. After a washing step (TBS-T, 3x 5 min), membranes were incubated with peroxidase-conjugated antibodies diluted in TBS-T containing 5% milk powder. PVDF membranes were again washed three times for 5 min and then incubated with detection reagents (Amersham[Tm] ECL[Tm] Prime, GE Healthcare or SuperSignal[®] West Dura, Thermo Scientific). These reagents contain peroxidase substrates whose products produce a chemiluminiscent signal. This signal was detected with the Chemie Genius[2] Bio Imaging System and quantified with Gene Tool Software (Syngene, Cambridge).

Used antibodies and dilutions were: Rabbit anti-calsequestrin (Dianova ABR-01164) 1:2500; rabbit anti-cTnI (Cell signaling #4002) 1:1000; rabbit anti-phospho-cTnI serine 23/24 (Cell signaling #4004) 1:1000; mouse anti-phospholamban (Badrilla A10-14) 1:2000; rabbit anti-phospho-phospholamban serine 16 (Badrilla A10-12) 1:5000; anti-rabbit IgG horseradish peroxidase-conjugated (Sigma-Aldrich A0545) 1:5000; anti-rabbit IgG horseradish peroxidase-conjugated (Dianova 111-035-045); anti-mouse IgG horseradish peroxidase-conjugated (Dianova 515-035-003) 1:5000.

2.7. Statistics

Data are displayed as mean±SEM. Data transformation, normalization, curve fittings and calculation of p-values were performed with GraphPad Prism 5 software. Comparisons were performed with two-tailed paired t-test, extra sum-of-squares F-test, or with one-way or two-way ANOVA followed by Dunnett's or Bonferroni's post-tests. A value of $P<0.05$ was considered statistically significant and is depicted with one, a value of $P<0.01$ with two and a value of $P<0.001$ with three asterisks/hash keys.

3. Results

3.1. Contractile deficits in isolated knock-in cardiomyocytes under elevated workload

To test the functional consequences of the reported higher Ca^{2+} sensitivity of the myofilaments in KI cardiac trabeculae (Fraysse et al. 2012), cardiomyocytes were isolated from hearts and tested regarding their contractile and Ca^{2+} transient properties. Isolation of single adult ventricular cardiomyocytes was established before in the institute, but had to be refined for the KI mouse model in the black swiss background. For WT black swiss mice at the age of 12 to 30 weeks, 7-min perfusion of the cannulated heart with buffer containing 0.075 mg/ml Liberase TM led to the best isolation yields, resulting in ≥400,000 living cardiomyocytes per heart. KI mice of the same age already displayed pronounced cardiac hypertrophy and fibrosis, which demanded longer digestion times and led to lower cell yield. After digestion times from 7:30 to 8 min, ≥150,000 living cardiomyocytes could generally be obtained.

As already reported for this model (Fraysse et al. 2012) and also for the *Mybpc3*-KO mouse (Pohlmann et al. 2007), cardiomyocytes isolated from KI mouse hearts showed lower diastolic sarcomere lengths than WT cardiomyocytes (fig. 3.3A). In baseline conditions (external Ca^{2+} concentration 1.5 mM, 1-Hz pacing frequency), their contractile properties did not significantly differ from WT cells. To test their behavior under conditions of increased intracellular Ca^{2+} load, cardiomyocytes were stimulated with 30 nM ISO. Additionally, pacing frequency was increased to 5 Hz once the ISO had set in and led to a new steady state of contraction and Ca^{2+} transient amplitude. Isolated cardiomyocytes are not able to work at physiological beating frequencies (450 – 750 bpm; Detweiler et al. 2004). Three hundred beats per minute is close to the performance limit of murine cardiomyocytes *ex vivo* and was therefore considered as a simulation of physiologic stress.

In WT cardiomyocytes, stimulation with 30 nM ISO normally led to a 2-fold increase of the contraction amplitude at 1-Hz pacing frequency (fig. 3.1 and 3.4A). An additional increase in pacing frequency to 5 Hz for 1 min only had minor effects and did not significantly increase contractility further. Throughout the whole recording time

(up to 5 min), cells were able to follow the pacing signal and contract in a regular manner.
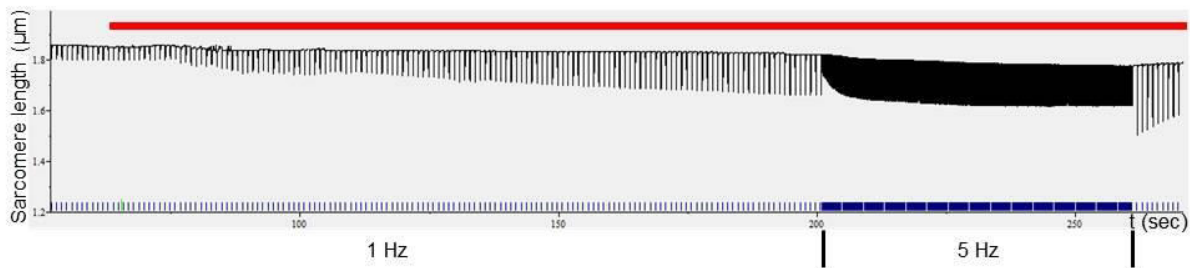
Fig. 3.1: Contraction trace of a WT cardiomyocyte paced at 1 and 5 Hz and stimulated with 30 nM ISO: Representative sarcomere length measurement of a WT cardiomyocyte. The change of sarcomere length upon electrical field stimulation (blue marks) is recorded over time. The red line indicates the period of ISO stimulation.

KI cardiomyocytes showed a 3-fold increase of their contraction amplitude when stimulated with 30 nM ISO (fig. 3.2 and 3.4A). Additionally, some cells developed arrhythmias or had problems to maintain stable contraction amplitudes. Upon simulation at 5 Hz, rhythm problems increased and diastolic sarcomere lengths dropped markedly in the majority of measured cells. In extreme cases, this relaxation deficit was so pronounced that cells shrunk up to half of their size and did barely contract anymore. These cells were taken out of the analysis. Regardless of the degree of shortening of diastolic sarcomere length, cells were generally unable to recover fully after pacing frequency was set back to 1 Hz. Neither ISO (30 nM) stimulation nor 5-Hz pacing alone induced this detrimental effect in KI cardiomyocytes (data not shown).
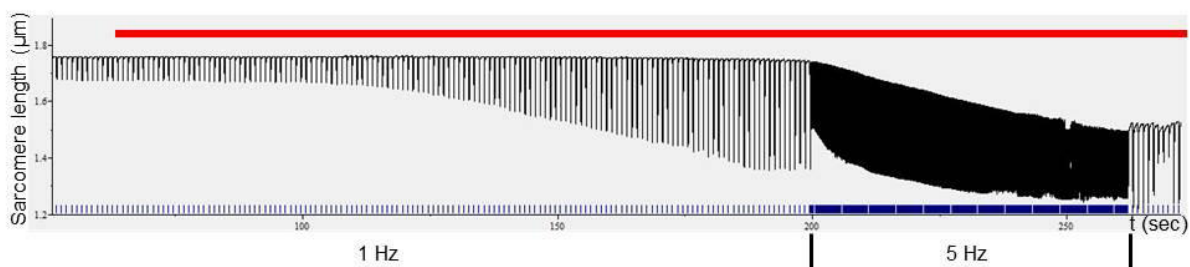
Fig. 3.2: Contraction trace of a KI cardiomyocyte paced at 1 and 5 Hz and stimulated with 30 nM ISO: Representative sarcomere length measurement of a KI cardiomyocyte. The change of sarcomere length upon electrical field stimulation (blue marks) is recorded over time. The red line indicates the period of ISO stimulation.

Fig. 3.3A represents the changes in diastolic sarcomere length of a set of cells undergoing the same recording protocol as shown in the representative traces in fig. 3.1 and 3.2. In fig. 3.3B, the diastolic Ca^{2+} load of cells undergoing the same recording protocol is represented. Contractile parameters of Fura-2-loaded cells were also measured and evaluated, but not represented here, as Fura-2 buffers Ca^{2+} in significant matter and therefore interferes with contractile processes. KI cardiomyocytes tended to have a higher intracellular Ca^{2+} concentration than WT cells, but at fully increased workload (ISO stimulation and 5-Hz pacing), diastolic Ca^{2+} load was not significantly higher than in the WT group. Therefore, the significant drop in diastolic sarcomere length seen in KI cardiomyocytes is most likely not caused by intracellular Ca^{2+} overload.
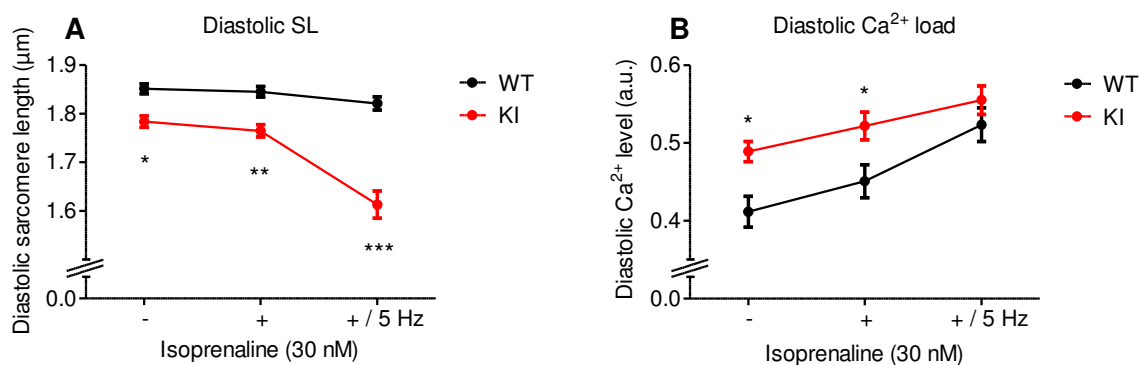
Fig. 3.3: Effect of ISO and pacing on diastolic sarcomere length and diastolic Ca^{2+} load of cardiomyocytes: A) Diastolic sarcomere length (SL) of WT (black) and KI (red) cardiomyocytes at 1-Hz pacing (-), 1-Hz pacing and 30 nM ISO (+), 5-Hz pacing and 30 nM ISO (+ / 5 Hz); n=24-26. B) Diastolic intracellular Ca^{2+} concentration measured by Fura-2 340/380 nm ratio under the same recording conditions as in A); n=19. Two-way ANOVA with Bonferroni's post-test; *P<0.05, **P<0.01, ***P<0.001 vs. WT value in the same condition.

As already seen in the representative traces, ISO induced a significant increase in contraction amplitude in WT and KI cells, but ISO response of KI cardiomyocytes concerning intensity of sarcomere shortening was much stronger than in WT cells. Ca^{2+} transient amplitudes on the contrary significantly increased in the same rate in cells of both genotypes with ISO. An additional increase in pacing frequency did not change contraction or transient amplitudes in both groups (fig. 3.4).
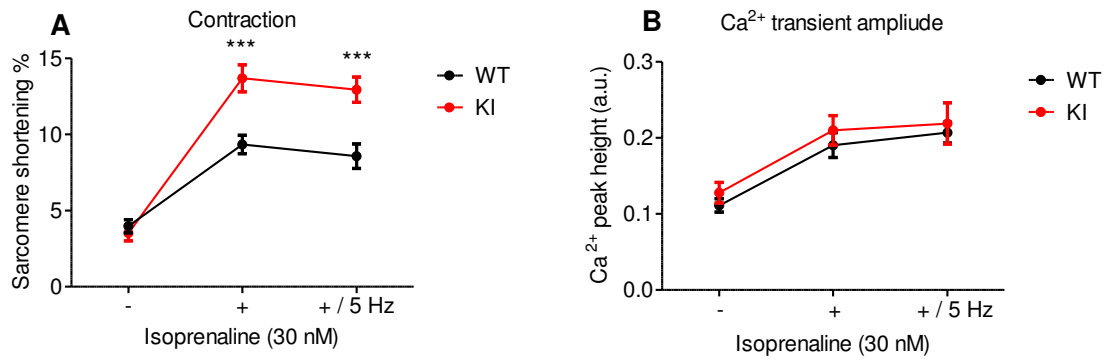
Fig. 3.4: Effect of ISO and pacing on contraction and Ca^{2+} transient amplitude of cardiomyocytes: A) Contraction amplitude of WT (black) and KI (red) cardiomyocytes at 1-Hz pacing (-), 1-Hz pacing and 30 nM ISO (+), 5-Hz pacing and 30 nM ISO (+ / 5 Hz); n=24-26. B) Ca^{2+} transient amplitude changes relative to baseline (1 Hz) measured by Fura-2 340/380 nm ratio under the same recording conditions as in A); n=19. Two-way ANOVA with Bonferroni's post-test; ***P<0.001 vs. WT value in the same condition.

Time to peak shortening (TTP), as a parameter of the cells' velocity of contraction, did not differ between WT and KI cells at baseline pacing of 1 Hz. After stimulation with ISO, TTP was significantly longer in KI cardiomyocytes. Upstroke kinetics of the Ca^{2+} transient did not differ between genotypes in any recorded condition (fig. 3.5A).
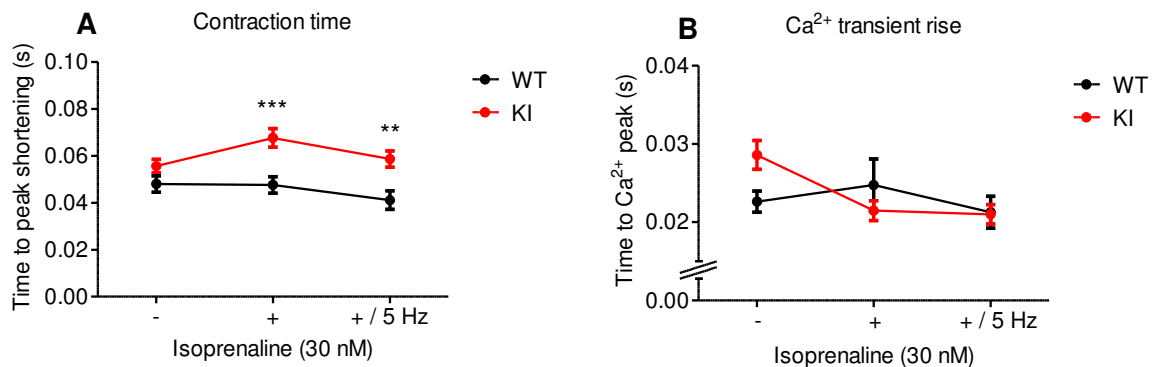
Fig. 3.5: Effect of ISO and pacing on contraction and Ca^{2+} transient rise kinetics of cardiomyocytes: A) Time from pacing signal to peak shortening of WT (black) and KI (red) cardiomyocytes at 1-Hz pacing (-), 1-Hz pacing and 30 nM ISO (+), 5-Hz pacing and 30 nM ISO (+ / 5 Hz); n=24-26. B) Time from pacing signal to maximal Fura-2 340/380 nm ratio under the same recording conditions as in A); n=19. Two-way ANOVA with Bonferroni's post-test; **P<0.01 and ***P<0.001 vs. WT value in the same condition.

KI cardiomyocytes showed slightly, but not significantly longer relaxation times at 1-Hz pacing than WT counterparts. The differences between KI and WT cells were more pronounced under ISO stimulation at 1 and 5 Hz. Nevertheless, ISO exerted its typical lusitropic effect independent of cell genotype. Again, no significant differences in Ca^{2+} transient parameters occurred between KI and WT cells when the time of decay was measured (fig. 3.6).
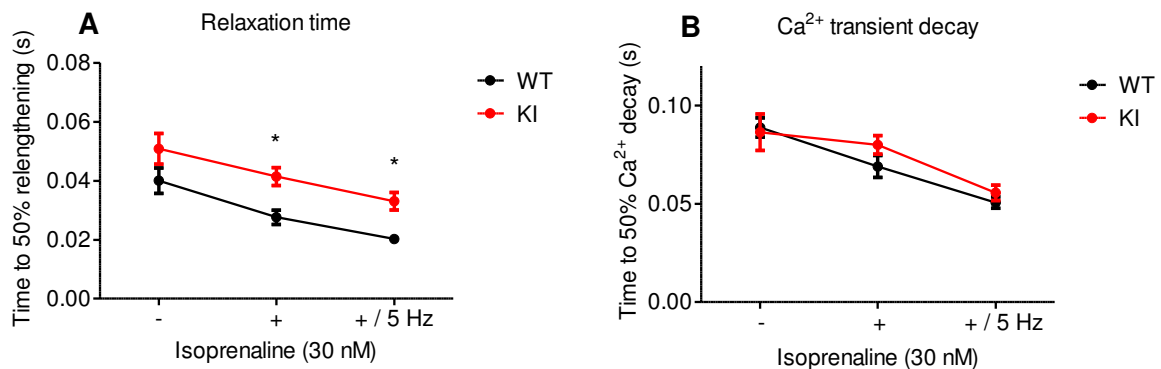
Fig. 3.6: Effect of ISO and pacing on relaxation and Ca^{2+} transient decay kinetics of cardiomyocytes: A) Time from peak of contraction to 50% of sarcomere relengthening of WT (black) and KI (red) cardiomyocytes at 1-Hz pacing (-), 1-Hz pacing and 30 nM ISO (+), 5-Hz pacing and 30 nM ISO (+ / 5 Hz); n=24-26. B) Time from peak of Fura-2 340/380 nm ratio to 50% decay of the signal under the same recording conditions as in A); n=19. Two-way ANOVA with Bonferroni's post-test; *P<0.05 vs. WT value in the same condition.

Taken together, cardiomyocytes isolated from hypertrophic KI hearts were more sensitive to β-adrenergic stimulation with 30 nM ISO and had difficulties to withstand an increased workload protocol of ISO stimulation plus 5-Hz pacing frequency. This protocol induced deficits in contraction as well as relaxation processes in KI cells. Despite the finding that intracellular Ca^{2+} concentration tended to be higher in diastole in unstimulated KI cardiomyocytes, no differences occurred in Ca^{2+} load, transient changes and kinetics during the increased workload protocol. Therefore, pathologically elevated intracellular Ca^{2+} levels are not the problem underlying the bad performance of the KI cells in the increased workload protocol.

3.2. Increased myofilament Ca^{2+} sensitivity as the underlying pathomechanism: Proof of principle with EMD 57033 and Blebbistatin

Changes in myofilament Ca^{2+} sensitivity are not exclusively caused by mutations in genes encoding for proteins of the myofilament or post-translational modifications like protein phosphorylation, but can also be induced pharmacologically by drugs that influence these proteins and their modifications. Unlike many other comparable substances, the inotropic agent EMD 57033 sensitizes the myofilament to Ca^{2+} with only minor inhibiting impact on phosphodiesterases (Endoh 2008) and rather seems to act on troponin C (Kawai et al. 2000), a component of the contractile apparatus of the cell. Therefore, I used EMD 57033 to mimic the KI phenotype in WT cardiomyocytes.

For the opposing experiment, the attempt to improve the KI phenotype with a Ca^{2+} desensitizer, the selection of the right agent was even more difficult. Drugs that directly act on the myofilament are rare and, like e.g. epigallocatechin-3-gallate (EGCg), known for their versatile off-target effects in the therapeutic concentration range (Feng et al. 2012). Here, I used the myosin ATPase inhibitor blebbistatin to improve the performance of KI cardiomyocytes under increased workload.

3.2.1. EMD 57033 elicits a knock-in-like phenotype in wild-type cardiomyocytes

To assess the right concentration of EMD 57033 to mimic the phenotype of KI myocytes in WT cells, concentration-response curves from 100 nM to 30 µM on isolated cells paced at 1 Hz were performed. Because of the resulting long measurement times and the toxic effect of EMD 57033, cumulative concentration experiments were not reliable as cells started to get arrhythmic early during the course of experiments. Therefore, only one EMD 57033 concentration per cell was applied. At concentrations ≥ 3 µM, the EMD 57033 effect occurred instantaneously. In order to reach the full effect also at lower concentrations, cells were allowed to develop a new contractile steady state for at least 3 min before the analysis.

Results

EMD 57033 showed a very narrow range of safely active concentrations. A positive inotropic effect was seen in concentrations ≥ 3 µM, but already at concentrations > 30 µM, cells lost their ability to relax completely, leading to cell death. Fig. 3.7B illustrates this partially: At 10-30 µM, diastolic sarcomere (dSL) length decreased ~0.2 µm, at the next tested concentration (100 µM), dSL could not be measured anymore as all cells had shrunken to about 1/3 of their original size. Therefore, EC_{50} values were not determined for EMD 57033 effect on dSL.
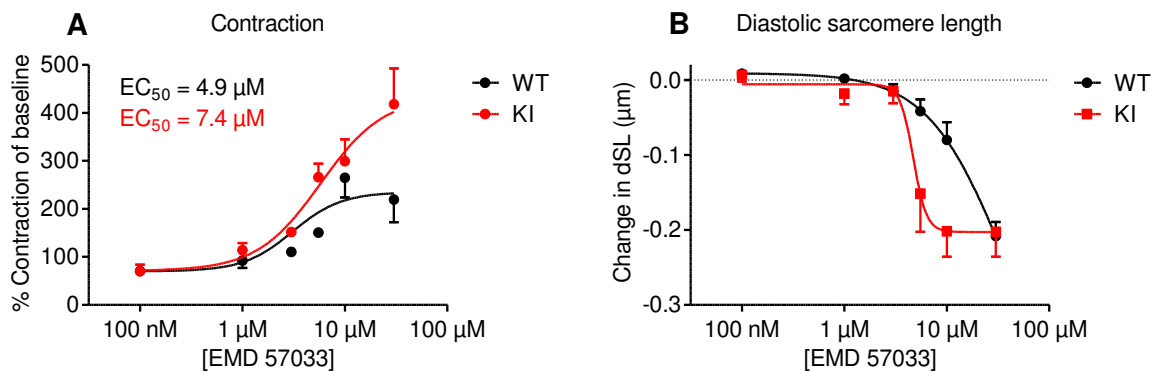
Fig. 3.7: EMD 57033 concentration-response curves on contractile parameters of wild-type and knock-in cardiomyocytes: A) Increase of WT (black) and KI (red) cardiomyocyte sarcomere shortening upon stimulation with different concentrations of EMD 57033. B) Corresponding changes of diastolic sarcomere length of the same cells measured in A); n=6.

For proof-of-principle experiments, WT cardiomyocytes were incubated with 3 µM EMD 57033, a concentration with moderate effects on inotropy and lusitropy, for 5 min before the cells were subjected to the increased workload protocol. Control cells were kept in buffer containing 0.03% dimethyl sulfoxide (DMSO), as this was used as a solvent for the drug. The EMD 57033 treated cells behaved remarkably similar to KI cardiomyocytes (fig. 3.8A). Their dSL was significantly shorter compared to DMSO controls already at baseline and decreased further upon stimulation of the cells with 30 nM ISO and 5-Hz pacing, while this did not affect cells incubated with DMSO only. Accordingly, the EMD 57033 cell group showed an inotropic response to ISO which was again twice as strong as the effect in the control group (3-fold increase in sarcomere shortening, fig. 3.8B).
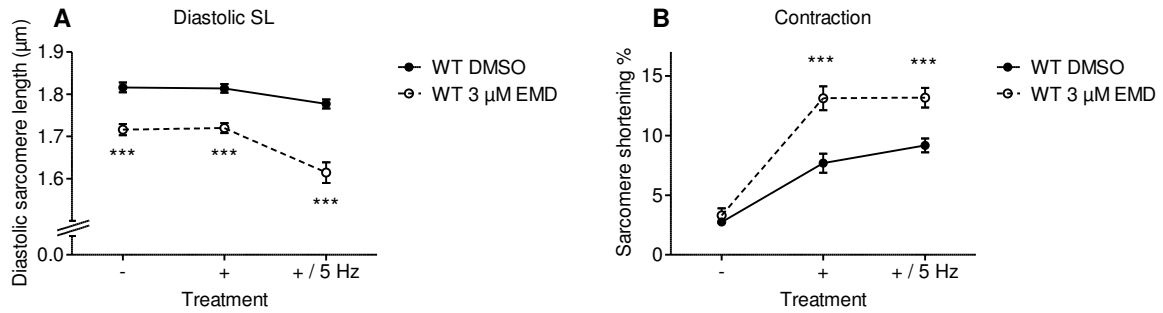
Fig. 3.8: Effect of ISO and pacing on diastolic sarcomere length and contraction amplitude of cells treated with EMD 57033: A) Diastolic sarcomere length (SL) of WT DMSO control cells (black, filled circles, straight lines) and WT cells treated with 3 µM EMD 57033 (black, hollow circles, dotted lines) at 1-Hz pacing (-), 1-Hz pacing and 30 nM ISO (+), 5-Hz pacing and 30 nM ISO (+ / 5 Hz). B) Contraction amplitudes of the same cells; n=10-13. Two-way ANOVA with Bonferroni's post-test; ***$P<0.001$ vs. WT DMSO value.

Contraction and relaxation kinetics were also different in WT cells treated with EMD 57033 or with 0.03% DMSO only (fig. 3.9). As seen before in KI cardiomyocytes, time to peak and time to 50% relaxation tended to be longer in EMD 57033 treated cells. This could again be witnessed in contraction after the ISO effect had set in, but in relaxation this was more pronounced at baseline (1 Hz, no ISO) and the difference faded upon β-AR stimulation.
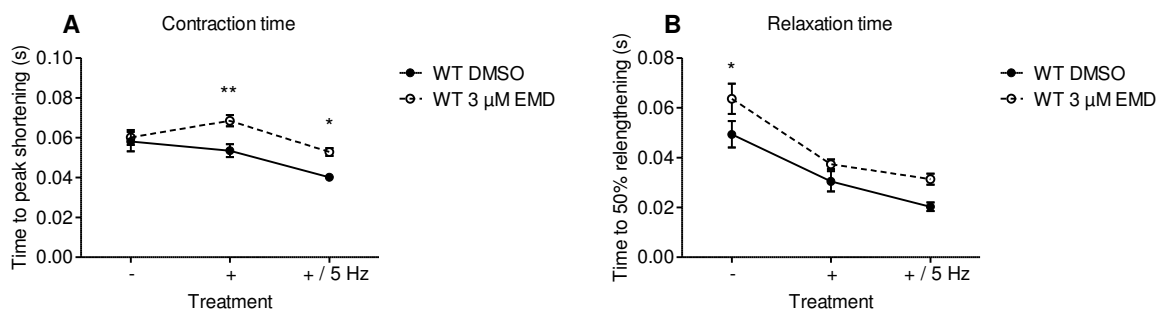
Fig. 3.9: Effect of ISO and pacing on contraction and relaxation times of EMD 57033-treated cells: A) Time from pacing signal to peak shortening of WT DMSO control cells (black, filled circles, straight lines) and WT cells treated with 3 µM EMD 57033 (black, hollow circles, dotted lines) at 1 Hz pacing (-), 1 Hz pacing and 30 nM ISO (+), 5 Hz pacing and 30 nM ISO (+ / 5 Hz). B) Time from peak shortening to 50% relaxation of the same cells; n=10-13. Two-way ANOVA with Bonferroni's post-test; *$P<0.05$ and **$P<0.01$ vs. WT DMSO value.

EMD 57033 and Fura-2 both interfered with contractile processes and showed cytotoxic effects in isolated murine cardiomyocytes at concentrations used. The

combination of both led to severe performance deficits in the increased workload protocol. To investigate if EMD 57033 had a significant effect on the intracellular Ca^{2+} transient, Fura-2-loaded cells were paced at 1 Hz and stimulated with 10 µM EMD 57033. This concentration showed a pronounced impact on contraction and relaxation in concentration-response experiments (fig. 3.7).

Ten µM EMD 57033 evoked an increase of sarcomere shortening from 2.7% to 10%, while the height of the Ca^{2+} peak, measured as change in Fura-2 340/380 nm ratio, did not change (fig. 3.10A). Furthermore, the expected shortening in dSL which followed the application of EMD 57033 was accompanied by a small, but significant increase in diastolic intracellular Ca^{2+} load (fig. 3.10B). The EMD-induced changes in contraction kinetics seen in the increased workload protocol were not accompanied by changes in Ca^{2+} transient kinetics (data not shown).
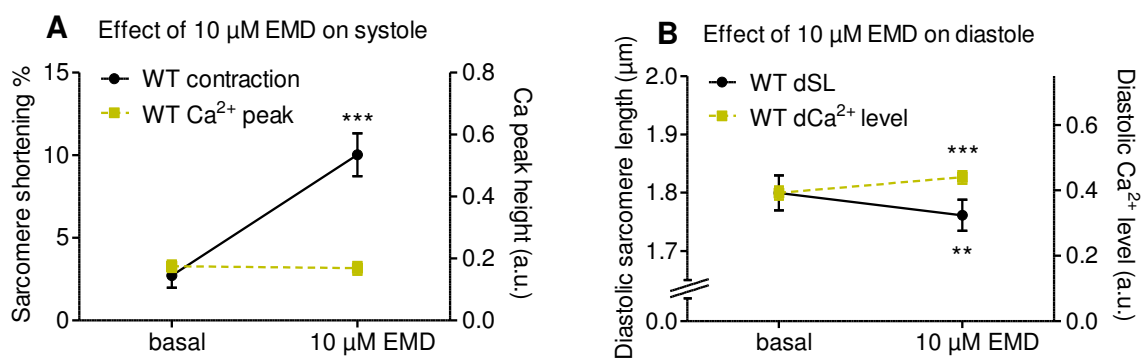
Fig. 3.10: Effect of 10 µM EMD 57033 on sarcomere shortening and diastolic sarcomere length in Fura-2 loaded WT cells paced at 1 Hz: A) Parallel recordings of sarcomere shortening (black symbol and line, left scale) and Ca^{2+} transient peak height (green symbol and dotted line, right scale) in Fura-2-loaded cells treated with 10 µM EMD 57033. B) Parallel recordings of diastolic sarcomere length and diastolic intracellular Ca^{2+} level of the same cells; n=11. Two-tailed paired t-test; **$P<0.01$ and ***$P<0.001$ vs. respective baseline value.

Overall, treatment of WT cardiomyocytes with EMD 57033 evoked a phenotype that was very similar to the one seen in KI cells concerning diastolic sarcomere length, response to ISO stimulation and contraction and relaxation behavior. Ca^{2+} transients were unaffected by the EMD 57033 concentrations used. Remarkably 10 µM EMD caused an elevated intracellular diastolic Ca^{2+} load, which had been previously seen in untreated KI cardiomyocytes.

3.2.2. Blebbistatin prevents workload-induced decrease in diastolic sarcomere length in knock-in cardiomyocytes

Before the potential of blebbistatin (BLEB) to improve KI cell performance in the increased workload protocol was tested, concentration-response curves of the drug were performed. Readout parameters were contraction values of isolated KI cardiomyocytes. Cells were under the influence of BLEB for at least 5 min before measurements to guarantee that the drug had enough time to be effective. Again, cumulative applications of BLEB did not produce reliable results, as KI cells could not withstand continuous measurements for more than 15 min. Accordingly, only one concentration of BLEB was tested per cell. BLEB produced a negative inotropic effect already at concentrations ≤ 1 µM (fig. 3.11A), with a pronounced drop of contraction amplitudes between 300 nM and 1 µM (from nearly 100% contractility after 300 nM BLEB to ~50% after 1 µM; IC_{50} = 1.3 µM). In the same concentration range, diastolic sarcomere lengths of tested cardiomyocytes started to increase (EC_{50} = 740 nM). At concentrations of ≥ 3 µM, diastolic sarcomere lengths were almost equal to those seen in untreated WT cells, but in addition, contractions were not executed anymore. For further experiments, 300 nM BLEB was used, as this concentration did not have a too profound impact on cardiomyocyte contractility.
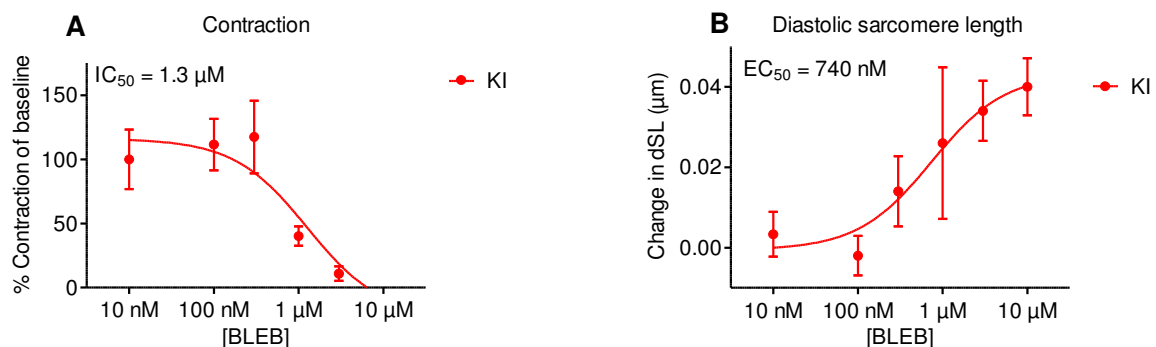
Fig. 3.11: Blebbistatin concentration-response curves on contractile parameters of KI cardiomyocytes: A) Decrease in KI cardiomyocyte sarcomere shortening upon stimulation with different concentrations of BLEB. B) Corresponding changes of diastolic sarcomere length of the same cells measured in A); n=6.

As for EMD 57033, cells were pre-incubated with BLEB 5 min prior to the increased workload protocol. The control group was pre-incubated with the solvent DMSO

(0.03%). Diastolic sarcomere length of KI cardiomyocytes treated with 300 nM BLEB did not change, but BLEB prevented shortening of dSL under the influence of ISO and at 5-Hz pacing (fig. 3.12A). Contraction amplitude was already decreased at baseline and also did not reach the same level as the control group after ISO stimulation (fig. 3.12B). However, the ISO response was still stronger than the one seen in WT cells. Contraction and relaxation times in BLEB-treated cells did not mimic the contractile behavior of WT cells (fig. 3.12 C and D). Instead, relaxation time was actually significantly longer in KI cells under the influence of BLEB before the ISO effect set in.
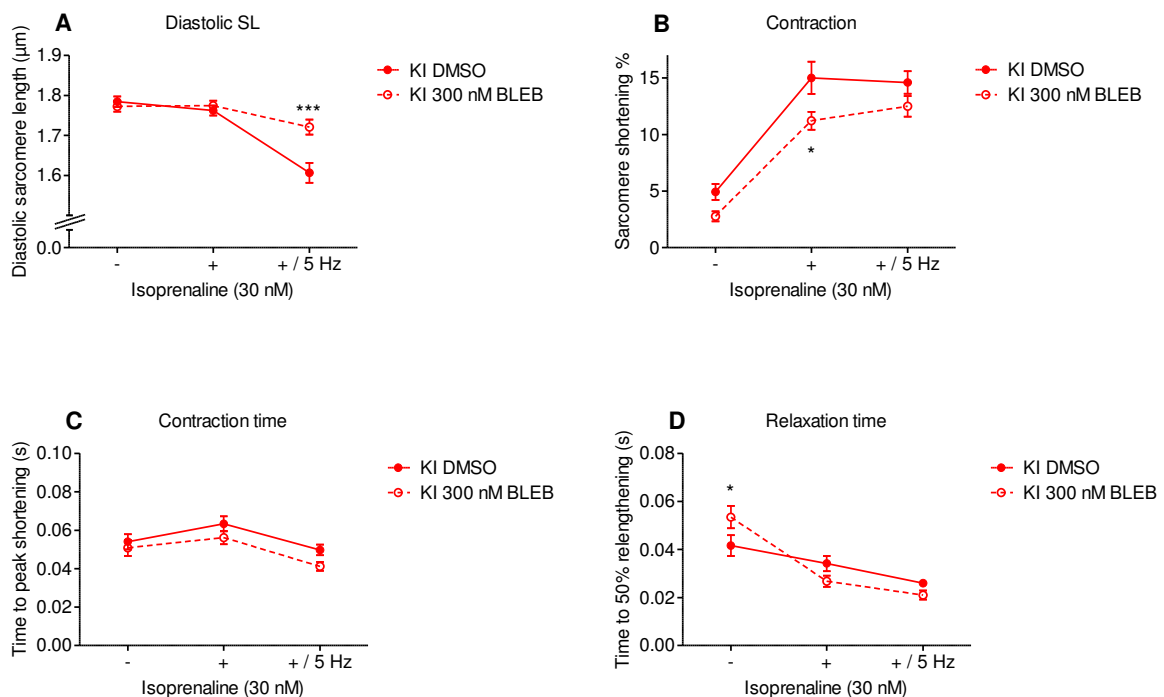
Fig. 3.12: Effect of 300 nM blebbistatin (BLEB) on contractile behavior of KI cardiomyocytes: A) Diastolic sarcomere length (SL) of DMSO control KI cells (red, filled circles, straight lines) and KI cells treated with 300 nM BLEB (red, hollow circles, dotted lines) at 1-Hz pacing (-), 1-Hz pacing and 30 nM ISO (+), 5-Hz pacing and 30 nM ISO (+ / 5 Hz). B) Contraction amplitudes of the same cells undergoing the same protocol. C) Contraction (pacing stimulus to peak) and D), Relaxation (peak to 50% relaxation) times of the same cells measured in A); n=14-15. Two-way ANOVA with Bonferroni's post-test; *P<0.05 and ***P<0.001 vs. KI DMSO value in the same condition.

Fura-2-loaded WT cells paced at 1 Hz were used to test the influence of 3 μM BLEB on the intracellular Ca^{2+} transients. This concentration showed severe effects on contractility and diastolic sarcomere length in the concentration-response experiments on KI cardiomyocytes (fig. 3.12). Parallel recordings of contractile

behavior of the cells and Ca^{2+} transients revealed that the loss of contraction amplitude was accompanied by a decrease in Ca^{2+} transient peak height (fig. 3.13A). Additionally, BLEB induced a significant increase in diastolic intracellular Ca^{2+} level (fig. 3.13B).
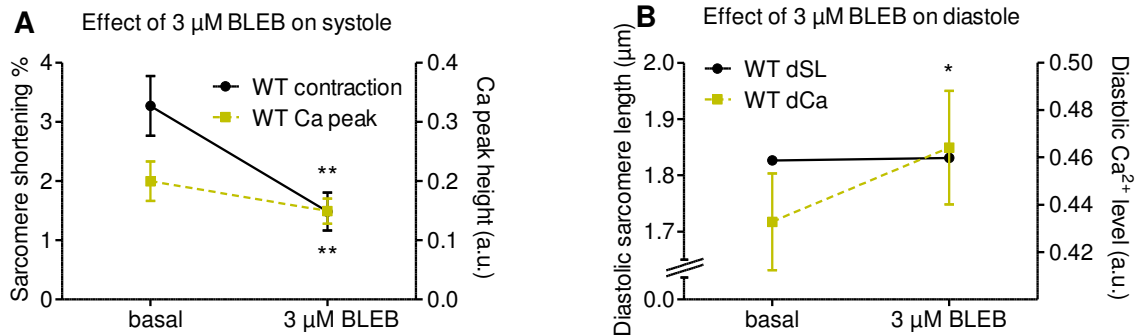
Fig. 3.13: Effect of 3 µM BLEB on sarcomere shortening, diastolic sarcomere length and intracellular Ca^{2+} levels in Fura-2-loaded wild-type cells paced at 1 Hz: A) Parallel recordings of sarcomere shortening (black symbol and line, left scale) and Ca^{2+} transient peak height (green symbol and dotted line, right scale) in Fura-2-loaded cells treated with 3 µM BLEB. B) Parallel recordings of diastolic sarcomere length and diastolic intracellular Ca^{2+} level of the same cells; n=11. Two-tailed paired t-test; *P<0.05 and **P<0.01 vs. respective baseline value.

In summary, BLEB improved the performance of isolated KI cardiomyocytes in the increased workload protocol and attenuated their hypersensitive reaction to ISO. However, diastolic sarcomere length was stabilized under full workload (30 nM ISO + 5-Hz pacing) but did not reach WT length. In addition, the response to ISO remained higher in KI than in WT cells and contraction and relaxation times did not change under the influence of BLEB. It also influenced Ca^{2+} transient peak height and diastolic Ca^{2+} level in WT cells. Taken together, BLEB showed protective effects in HCM cardiomyocytes, but was not a perfect drug to rescue the KI phenotype because it lacked the ability to fully rescue myofilament properties and seemed to have off-target effects influencing Ca^{2+} homeostasis in the concentration used in these experiments.

3.3. Acute application of EMD 57033 has different effects in wild-type and knock-in mice

As EMD 57033 showed the ability to evoke a KI-like phenotype in WT cardio-myocytes, I decided to test its efficacy in 14 to 17 week-old mice to see if phenotypic aspects of HCM, especially diastolic dysfunction, could be evoked acutely *in vivo*. At this age, mice are full-grown and those carrying the *Mybpc3* mutation at the homozygous state display diastolic and systolic dysfunction (Fraysse et al. 2012). To get a first impression about the efficacy of EMD 57033 *in vivo*, dose-response experiments were performed. Birgit Geertz, a technician from the institute, performed echocardiographic measurements, which I analyzed. Isoflurane-anaesthetized mice were injected IP with cumulating doses of EMD 57033 up to 6.4 mg/kg BW. Five min after the injection, their heart function was determined by echocardiography. EMD 57033 dose-dependently increased both heart rate (HR) and FAS, which was increased by ~90% in WT mice at highest EMD doses given (fig. 3.14B).
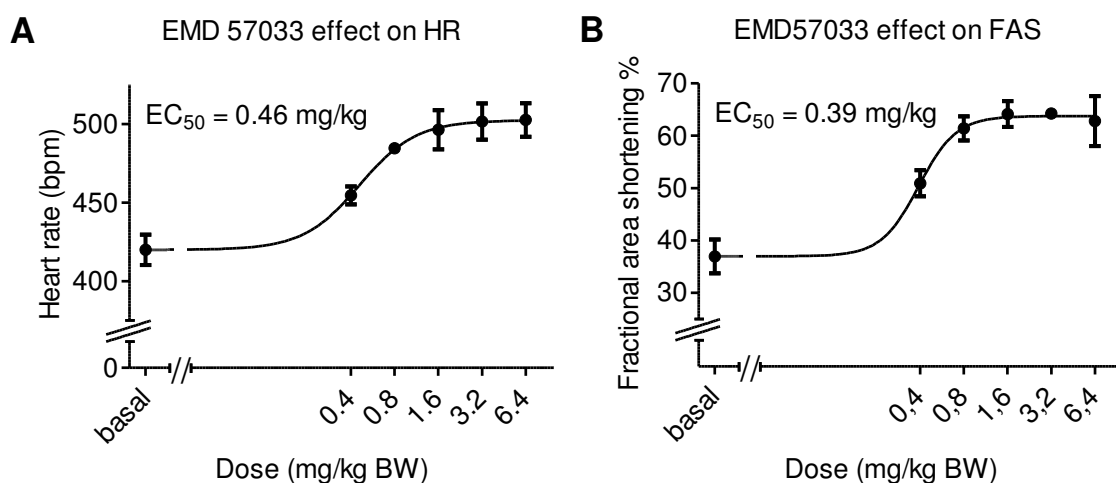
Fig. 3.14: In vivo dose-response curves of EMD 57033 on heart rate and fractional area shortening: Efficacy of EMD 57033 on heart rate (A) and fractional area shortening (B) in IP-injected WT mice. EC_{50} designates the dose of half-maximal effect; n=3.

For further experiments in WT and KI mice, an IP bolus injection of 0.6 mg/kg was used, a dose slightly above the measured EC_{50}, but without saturating effects for all parameters evaluated. Before the injection, WT and KI mice had similar HRs, while FAS was significantly lower in KI mice (fig. 3.15A and 3.15B). Additionally KI mice tended to have a lower E/A ratio, a parameter which indicates the ability of the left

ventricle to relax by relating the early, passive filling of the ventricle (E) to the late, active filling (A) (fig. 3.15C). After injection of EMD 57033, HRs accelerated in mice of both genotypes, but a higher FAS only occurred in WT mice, while the cardiac output of KI mouse hearts remained at their low level. E/A ratio was slightly decreased in KI mice, which was significantly different between WT and KI after EMD injection. Morphologic parameters like wall thicknesses and inner ventricular diameter were unaffected by EMD 57033 injection, except for those affected by the positive inotropic effect of the drug.
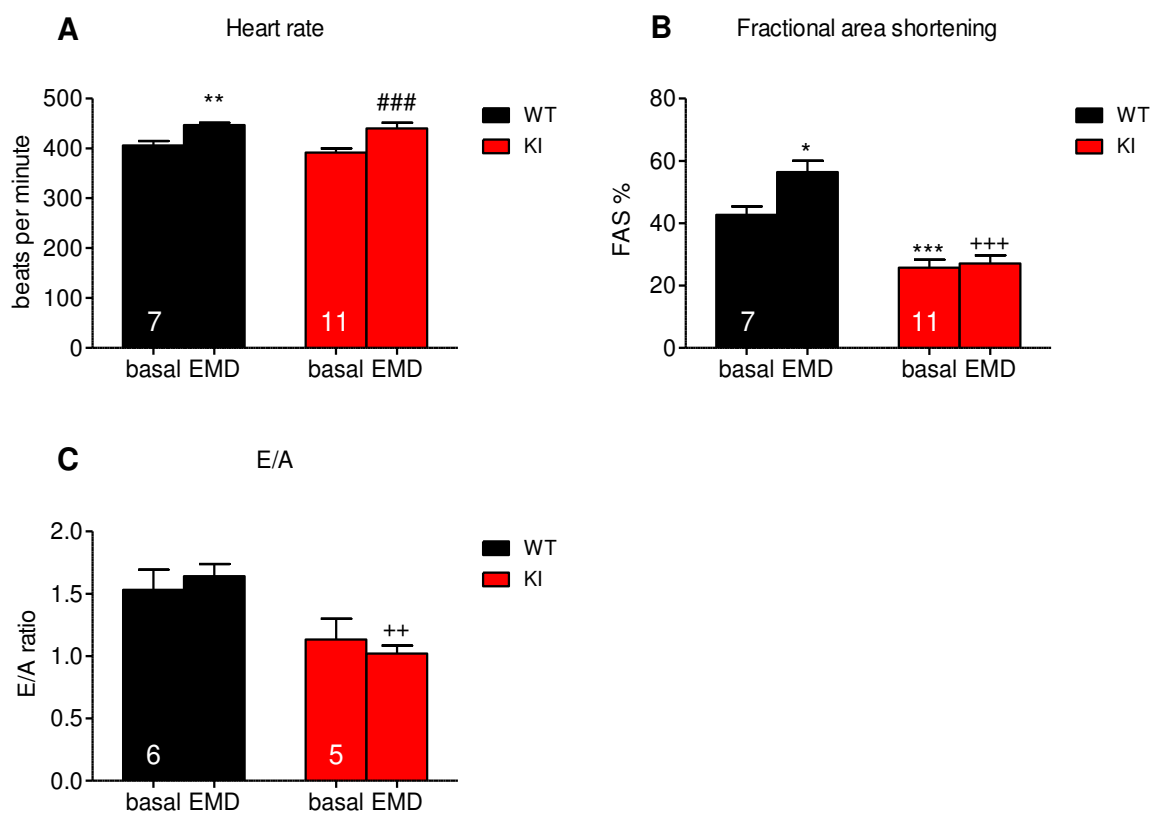
Fig. 3.15: Effect of acute IP injection of EMD 57033 on heart parameters: Effect of 0.6 mg/kg EMD 57033 on heart rate (A), fractional area shortening (B) and diastolic relaxation (E/A ratio, C) in WT (black bars) and KI (red bars) mice. Two-tailed paired t-test; *$P<0.05$, **$P<0.01$ and ***$P<0.001$ vs. WT basal; ###$P<0.005$ vs. KI basal; ++$P<0.01$, +++$P<0.005$ vs. WT EMD.

In contrast to the findings in isolated adult ventricular cardiomyocytes, acute application of EMD 57033 did not induce diastolic dysfunction *in vivo* in WT mice and only slightly decreased diastolic performance in KI animals further. Instead, it accelerated heart rates of anaesthetized animals and had positive inotropic effects in

WT animals. These effects did not occur in KI mice, which generally showed worse systolic performance than their WT counterparts.

3.4. Test of therapy approaches targeting Ca^{2+} homeostasis in isolated cardiomyocytes

Following the hypothesis that the elevated myofilament Ca^{2+} sensitivity is the major cause for the shorter dSL, the stronger response to ISO and the significant decrease of dSL under increased workload of KI cardiomyocytes seen in previous experiments, I tested the therapeutic potential of approved drugs that influence cardiomyocyte Ca^{2+} homeostasis. The increased workload protocol experiments, in which the intracellular Ca^{2+} level was increased by β-adrenergic stimulation and Ca^{2+} cycling was forced to accelerate by rapid pacing, revealed that KI cardiomyocytes struggle to stand these conditions. Concurrently, their intracellular Ca^{2+} level changes under stress conditions did not significantly differ from those of WT cells. To improve their working endurance, two therapy approaches were tested:

a) a decrease in intracellular Ca^{2+} load with the calcium channel blocker diltiazem

b) a combination of indirect decrease in ($[Ca^{2+}]_{i)}$) and myofilament Ca^{2+}
desensitization with the late sodium current blocker ranolazine.

3.4.1. Diltiazem stabilizes diastolic sarcomere length of knock-in cardiomyocytes under increased workload, but induces negative force-frequency relationship

The non-dihydropyridine Ca^{2+} channel antagonist is an antianginal and antiarrhythmic drug which is already in use in HCM therapy as an alternative to the most commonly prescribed L-type Ca^{2+} channel blocker verapamil (ESC guidelines 2014). To assess its therapeutic index in isolated cardiomyocytes, I first performed concentration-response curves looking at effects on cell contractility and Ca^{2+} transient amplitude. Again, contractile behavior and calcium homeostasis analysis were separated because of the impact of Fura-2 on contraction and only one concentration per cell was tested to avoid long measuring times which would have had undermined result

reliability. First effects of the drug were seen at concentrations ≥ 300 nM, where contraction and Ca^{2+} transient amplitudes started to decrease (fig. 3.16). At 30 µM and above, cells were almost quiescent and finally stopped to beat when treated with 1 mM diltiazem. Notably, the IC_{50} for contraction (~7.2 µM) was lower than the one for Ca^{2+} transient amplitude (~246 µM). Even at 100 µM, where cells did barely beat anymore, a Ca^{2+} transient was clearly visible (fig. 3.16B). Probably Fura-2 buffered most of the Ca^{2+} released from the SR, so myofilament contraction could not be initiated anymore.
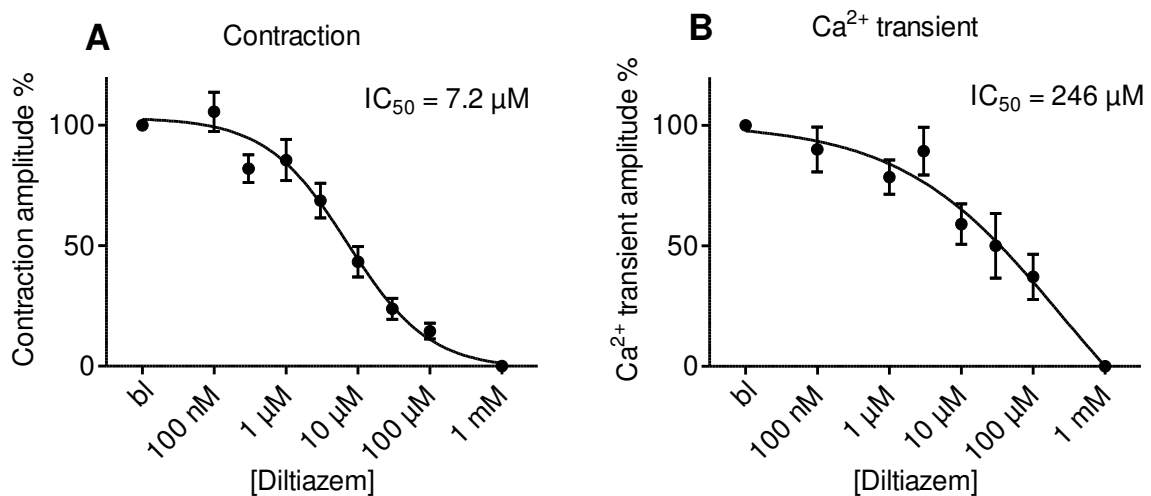
Fig. 3.16: Diltiazem concentration-response curves on contraction and Ca^{2+} transient of wild-type cardiomyocytes paced at 1 Hz: A) Percentage of decrease in WT cardiomyocyte sarcomere shortening upon exposure to different concentrations of diltiazem; n=12. B) Percentage of decrease in Ca^{2+} transient peak height measured by Fura-2 340/380 nm ratio; n=6.

Considering that mice at the age of >12 weeks, which were investigated in this part of the study, already displayed severe systolic dysfunction, I wanted to avoid lowering contractile ability of single cardiomyocytes. Hence, for further experiments 1 µM diltiazem was used to avoid excessively negative inotropic effects. The diltiazem effect could be seen in the first 2 min when applied in the concentration response experiments. To make sure diltiazem was fully active in the increased workload experiments, cells were pre-incubated for 5 min with the Ca^{2+} channel blocker.

At baseline (1-Hz pacing, no ISO stimulation), diltiazem did not influence dSL, although Ca^{2+} load in diastole was a bit smaller in KI cells treated with diltiazem (fig. 3.17A and B). KI cells treated with diltiazem did not decrease in dSL and their diastolic Ca^{2+} load was not significantly different from WT controls under increased

workload. ISO-induced increase in amplitude of both contraction and Ca^{2+} transient was attenuated in WT and in KI cardiomyocytes by diltiazem (fig. 3.17C and D).
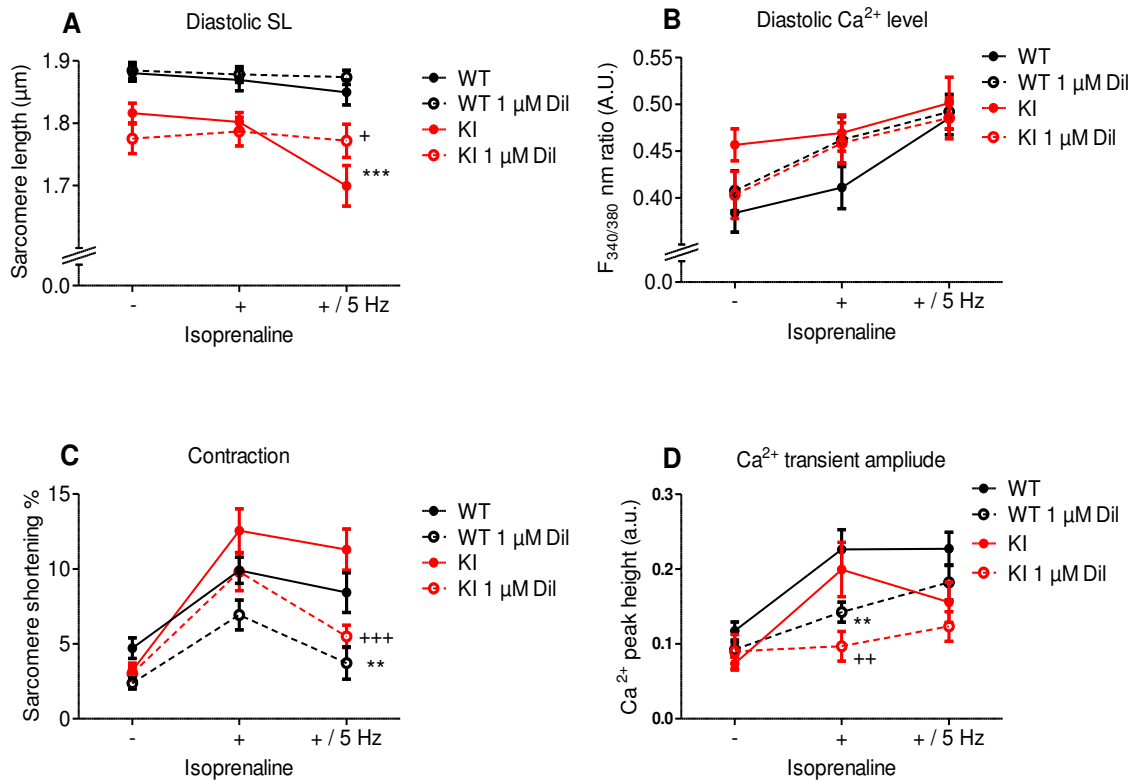
Fig. 3.17: Contraction and Ca^{2+} transient parameters of WT and KI cells in increased workload protocol and influence of 1 µM diltiazem. A) Diastolic sarcomere lengths of WT (black) and KI (red) cardiomyocytes stimulated at 1 Hz (-), 1 Hz and 30 nM ISO (+) and 5 Hz and 30 nM ISO (+ / 5 Hz). Hollow symbols and dotted lines indicate the presence of 1 µM diltiazem during the measurement: n=12. B) Diastolic Ca^{2+} level of WT and KI cells undergoing the same stimulation protocol and treatment as in A). Ca^{2+} was measured by Fura-2 340/380 nm ratio; n=6-9. C) Contraction amplitude of cells measured in A). D) Relative Ca^{2+} transient amplitude of cells measured in D). Two-way ANOVA with Bonferroni's post-test; **$P<0.01$ and ***$P<0.001$ vs. WT value in the same condition; +$P<0.05$, ++$P<0.01$, +++$P<0.001$ vs. KI value in the same condition.

When pacing was increased from 1 to 5 Hz, cells treated with 1 µM diltiazem showed a negative force-frequency relation (fig. 3.17C). This frequency-dependent effect of diltiazem also appeared in the absence of ISO stimulation (fig. 3.18).
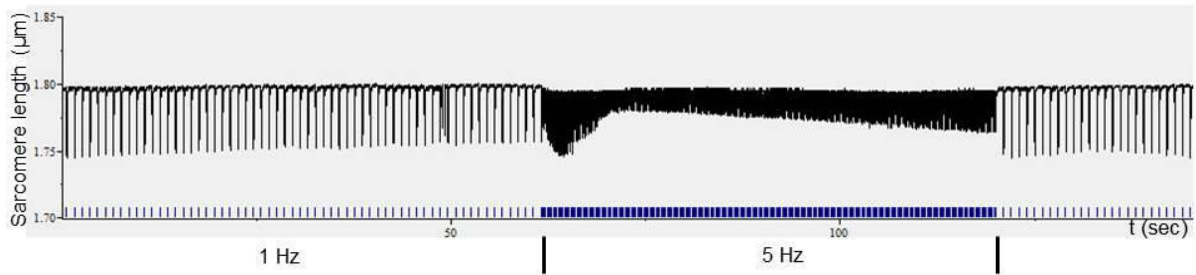
Fig. 3.18: Sarcomere shortening of a wild-type cardiomyocyte paced at 1 and 5 Hz under the influence of diltiazem: Representative sarcomere shortening trace of an electrically stimulated (blue marks) WT cardiomyocyte which was incubated with 1 µM diltiazem. Pacing frequency for the first 60 seconds is 1 Hz, followed by 60 seconds of 5 Hz and a subsequent switch back to 1 Hz.

Figure 3.19 shows representative traces of a control and a diltiazem-treated KI cell undergoing the increased workload protocol. Despite the negative force-frequency effect, Ca^{2+} transients did not decrease in diltiazem-treated cells when pacing was switched from 1 to 5 Hz (fig. 3.17D).
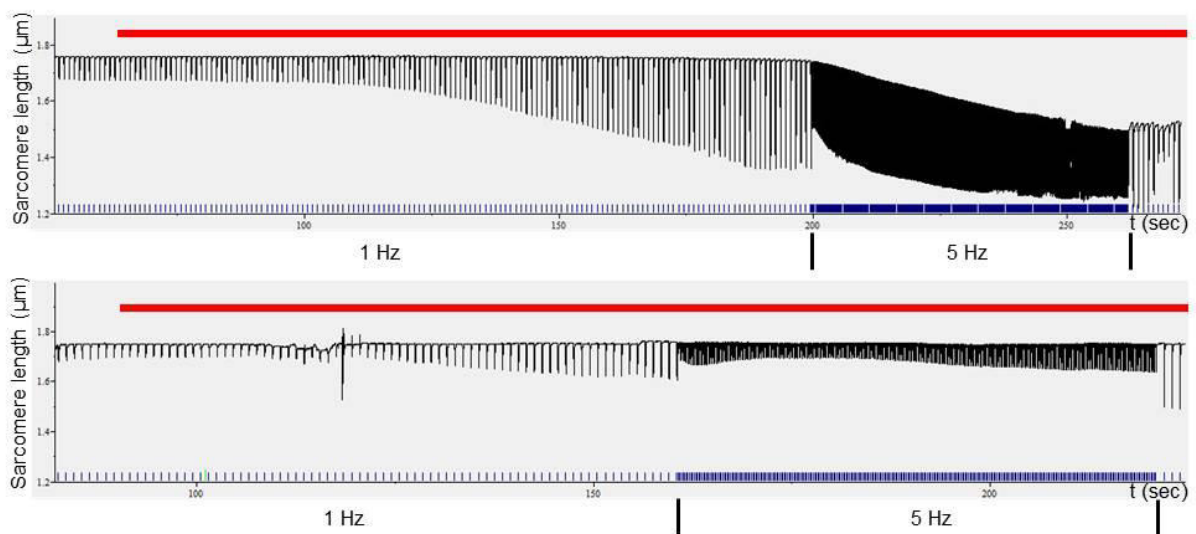
Fig. 3.19: Representative traces of an untreated (top) and a diltiazem-treated (bottom) knock-in cardiomyocyte paced at 1 and 5 Hz and stimulated with 30 nM ISO: Representative sarcomere length measurements of KI in the absence (top) or presence (bottom) of 1 µM diltiazem. The change of sarcomere length upon electrical field stimulation (blue marks) is recorded over time. The red line indicates the period of ISO stimulation.

Diltiazem also influenced contraction kinetics. ISO-induced differences in contraction and relaxation times between KI and WT cells were absent when cells were treated with diltiazem (fig. 3.20A and C), although their Ca^{2+} rise and decay times were not significantly shorter (fig. 3.20 B and D). Therefore, the shorter contraction and

relaxation times were caused by the partial blunting of the ISO effect on the Ca^{2+} transient peak amplitude.
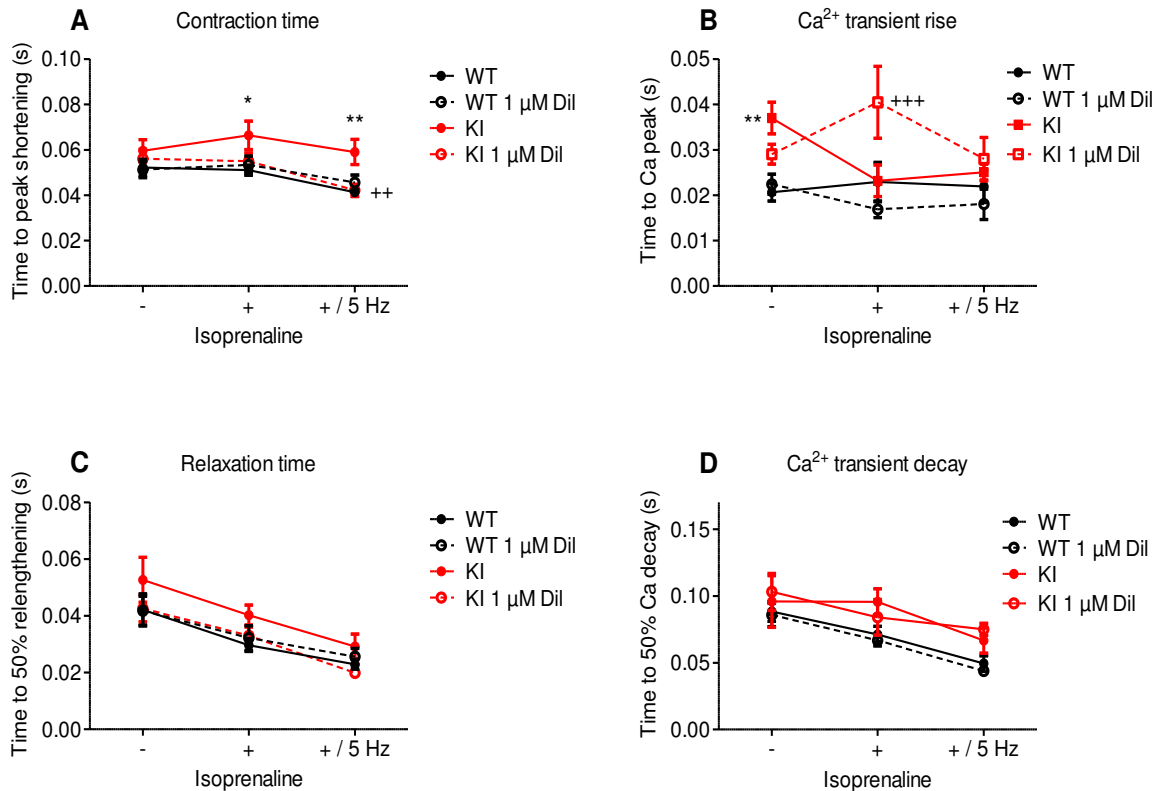
Fig. 3.20: Contraction and Ca^{2+} transient kinetics of WT and KI cells in increased workload protocol and influence of 1 µM diltiazem: A) Contraction time (from pacing signal to peak of contraction) of WT (black) and KI (red) cardiomyocytes stimulated at 1 Hz (-), 1 Hz and 30 nM ISO (+) and 5 Hz and 30 nM ISO (+ / 5 Hz). Hollow symbols and dotted lines indicate the presence of 1 µM diltiazem during the measurement; n=12. B) Ca^{2+} transient rise time of WT and KI cells undergoing the same stimulation protocol and treatment as in A). Ca^{2+} was measured by Fura-2 340/380 nm ratio; n=6-9. C) Time from peak of contraction to 50% of relengthening of cells measured in A). D) Time to 50% Ca^{2+} transient decay of cells measured in D). Two-way ANOVA with Bonferroni's post-test; *$P<0.05$ and **$P<0.01$ vs. WT value; ++$P<0.01$ and +++$P<0.001$ vs. respective KI value.

Altogether, diltiazem was protective in the increased workload protocol in KI cells, as it stabilized their diastolic sarcomere lengths under conditions of 30 nM ISO stimulation and 5-Hz pacing and prevented ISO-induced differences to WT of their contraction and relaxation times. In doing so, diltiazem partially blunted the positive inotropic effect and the elevation of maximal Ca^{2+} transient amplitude of ISO. Additionally, it led to a negative force-frequency relationship in WT and KI cardiomyocytes, an effect that should be considered in treatment.

3.4.2. Ranolazine stabilizes diastolic sarcomere length of knock-in cardiomyocytes under increased workload and blunts isoprenaline efficacy

Ranolazine is primarily known as a blocker of the late sodium current (Antzelevitch et al. 2004, Sossalla et al. 2008) and is used as an anti-anginal drug. It also has been shown to have beneficial effects in isolated cardiomyocytes of HCM patients (Barajas-Martinez et al. 2013, Coppini et al. 2013). Additionally, there is a report of myofilament Ca^{2+} desensitization through ranolazine (Lovelock et al. 2012). Therefore, it was very interesting to test ranolazine's therapeutic potential in the *Mybpc3*-KI mouse model. Its impact on contractility and Ca^{2+} transient is rather subtle, and, therefore, concentration-response curves could not be performed with the methods used for this thesis. In literature, especially in those publications dealing with ranolazine treatment of phenotypic aspects of HCM, the most commonly used ranolazine concentration was 10 µM (Sossalla et al. 2008, Lemoine et al. 2011, Parikh et al. 2012, Barajas-Martinez et al. 2013, Coppini et al. 2013). Higher concentrations had negative inotropic effects in control experiments which occurred after a few min of incubation, so cardiomyocytes were pre-incubated for 10 min with ranolazine before the increased workload protocol was applied.

Diastolic sarcomere length was not affected by ranolazine at baseline in WT and KI cells (fig. 3.21A). In WT cells, it completely blunted ISO-induced positive inotropy and partially blunted workload-induced increase in diastolic Ca^{2+} load and Ca^{2+} transient peak height (fig. 3.21B-D). Notably, there was a tendency in ranolazine-treated cells to higher Ca^{2+} transients at baseline (fig. 3.21D). In KI cells, ranolazine treatment prevented the decrease in dSL under increased workload and partially blunted ISO-induced increase in contraction amplitude as well as ISO- and pacing-induced increase in Ca^{2+} transient peak height (fig. 3.21A, C and D). The increase in diastolic Ca^{2+} load of KI cells under full workload was unaffected by ranolazine (fig. 3.21B).
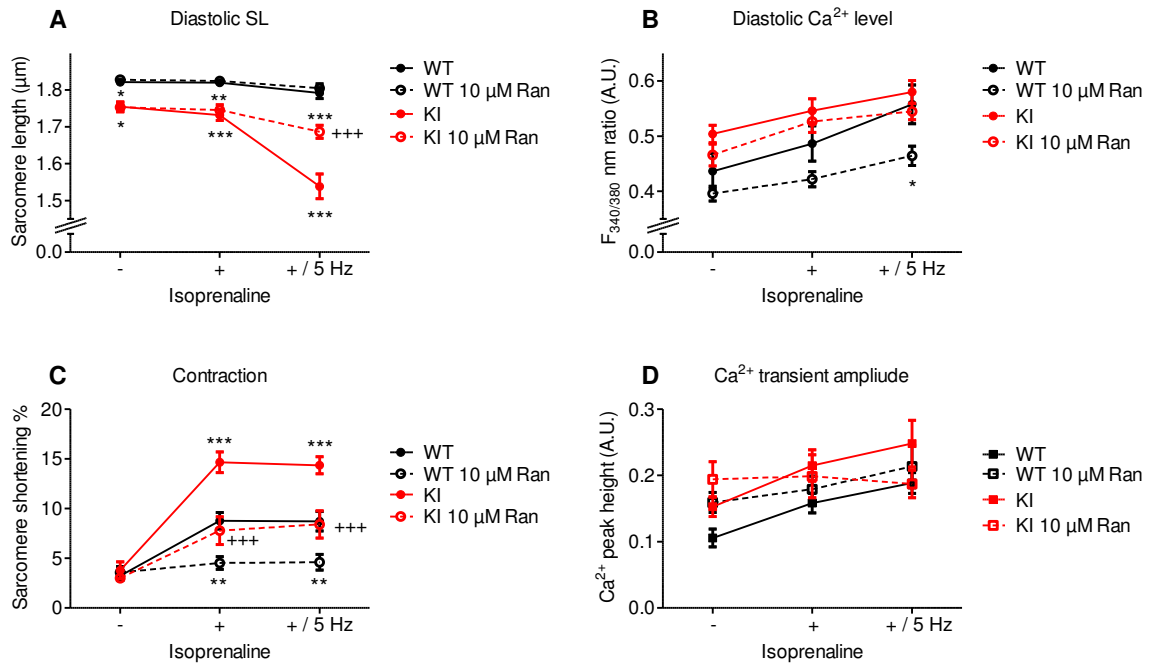
Fig. 3.21: Contraction and Ca^{2+} transient parameters of WT and KI cells in increased workload protocol and influence of 10 µM ranolazine. A) Diastolic sarcomere lengths of WT (black) and KI (red) cardiomyocytes stimulated at 1 Hz (-), 1 Hz and 30 nM ISO (+) and 5 Hz and 30 nM ISO (+ / 5 Hz). Hollow symbols and dotted lines indicate the presence of 10 µM ranolazine during the measurement, n=12-14. B) Diastolic Ca^{2+} levels of WT and KI cells undergoing the same stimulation protocol and treatment as in A). Ca^{2+} was measured by Fura-2 340/380 nm ratio; n=10-13. C) Contraction amplitude of cells measured in A). D) Relative Ca^{2+} transient amplitude of cells measured in D). Two-way ANOVA with Bonferroni's post-test; *P<0.05, **P<0.01 and ***P<0.001 vs. respective WT value; +++P<0.001 vs. respective KI value.

Effects of ranolazine on contraction and Ca^{2+} transient kinetics were somewhat opposite to those seen with diltiazem. Contraction and transient rise time was largely unaffected by ranolazine, with the exception for a slight prolongation of contraction time in KI cells under 30 nM ISO and 5 Hz (fig. 3.22A). However, relaxation times were longer in cardiomyocytes treated with ranolazine and under the influence of β-adrenergic stimulation, meaning ranolazine antagonized the positive lusitropic effect of ISO (fig. 3.22C). This was suggestively also visible in Ca^{2+} transient shapes, but ranolazine did not evoke significantly different times to 50% relaxation or decay (fig. 3.22C and D).
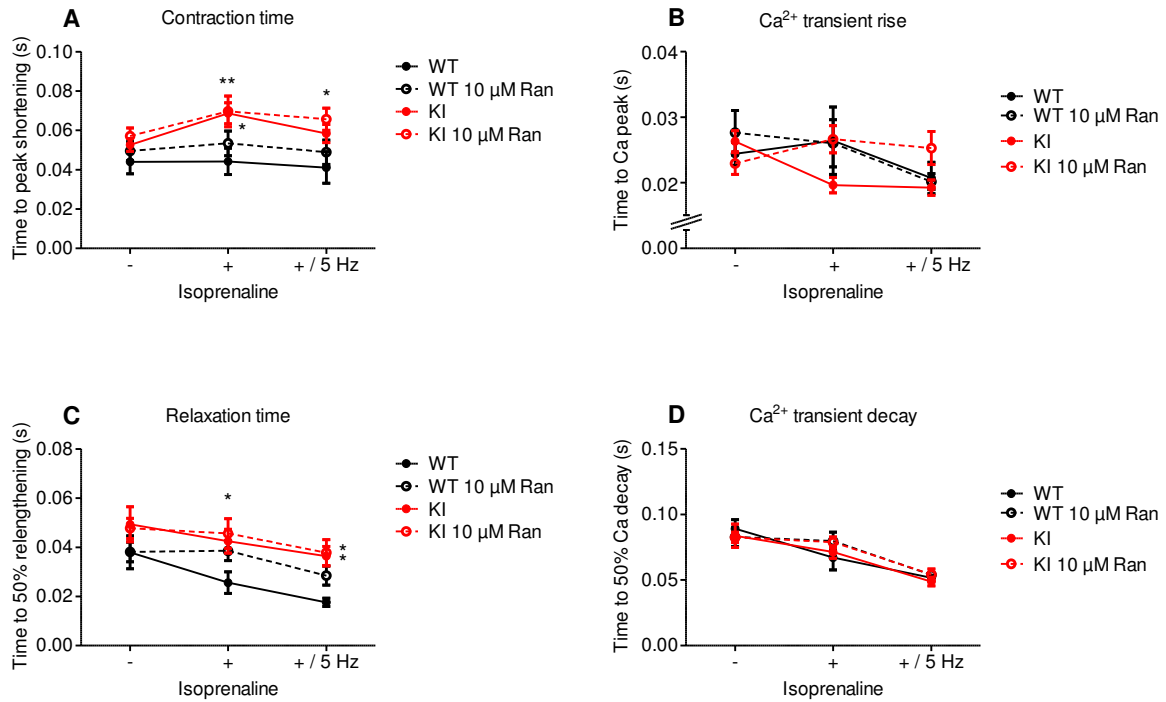
Fig. 3.22: Contraction and Ca²⁺ transient kinetics of WT and KI cells in increased workload protocol and influence of 10 µM ranolazine: A) Contraction times (from pacing signal to peak of contraction) of WT (black) and KI (red) cardiomyocytes stimulated at 1 Hz (-), 1 Hz and 30 nM ISO (+) and 5 Hz and 30 nM ISO (+ / 5 Hz). Hollow symbols and dotted lines indicate the presence of 10 µM ranolazine during the measurement; n=12-14. B) Ca²⁺ transient rise times of WT and KI cells undergoing the same stimulation protocol and treatment as in A). Ca²⁺ was measured by Fura-2 340/380 nm ratio; n=10-13. C) Time from peak of contraction to 50% of relengthening of cells measured in A).D) Time to 50% Ca²⁺ transient decay of cells measured in D). Two-way ANOVA with Bonferroni's post-test; *P<0.05 and **P<0.01 vs. respective WT value.

Ranolazine treatment of isolated KI cardiomyocytes improved their ability to endure increased workload of 30 nM ISO stimulation and 5-Hz pacing frequency. It caused stabilization of their diastolic sarcomere length and normalized KI cell response to ISO. This alleviative effect on ISO efficacy was also visible on Ca²⁺ transient amplitude and relaxation, where the positive lusitropic effect of β-adrenergic stimulation was blunted with 10 µM ranolazine. In WT myocytes, this concentration of ranolazine almost completely blunted the effect of 30 nM ISO. Therefore, I decided to evaluate the interactions of ranolazine and ISO in other experiments to get a more detailed view on its mode of action.

3.5. Ranolazine counteracts isoprenaline in isometric force measurements

Ranolazine is known to not exclusively act on the late sodium current and has already been reported in earlier studies to have β-blocker-like activity (Letienne et al. 2001, Antzelevitch et al. 2004, Zhao et al. 2011). To take a closer look on its potential to antagonize ISO stimulation, PD Dr. Torsten Christ and Klaus Soeren, a technician working in our institute, performed isometric force measurements on ventricular muscle strips isolated from WT and KI mouse hearts. ISO concentration-response curves were performed in the presence and absence of different ranolazine concentrations. Changes in contractile force of the strips were used as a read-out in the experiment.

In contrast to the findings of the experiments done with isolated cardiomyocytes, no significant differences in ISO sensitivity between WT and KI specimen occurred (ISO EC_{50} WT: 33 nM, KI: 45 nM) (fig. 3.23A). Ten µM ranolazine, the concentration used in the other experiments of this thesis and also predominantly found in literature (Lemoine et al. 2011, Barajas-Martinez et al. 2013, Coppini et al. 2013), shifted concentration-response curves of ISO to the right in both WT and KI muscle strips. The EC_{50} values for ISO were significantly higher in ranolazine-treated strips than in the respective control group when compared with extra sum-of-squares F-test (ISO EC_{50} 10 µM Ran WT: 135 nM, KI: 158 nM). Schild plot analysis, in which the dose-shift of the ISO EC_{50} was plotted against the respectively used ranolazine concentration, revealed an antagonizing effect of ranolazine on β-adrenergic stimulation – the higher the applied ranolazine concentrations were, the larger ISO EC_{50} values became. In detail, ranolazine shifted ISO concentration response curves in WT and KI muscle strips with a slope of 0.88 and an x-axis intersection of -5.7 (fig. 3.23B), indicating an antagonizing effect on β-adrenergic receptor level.
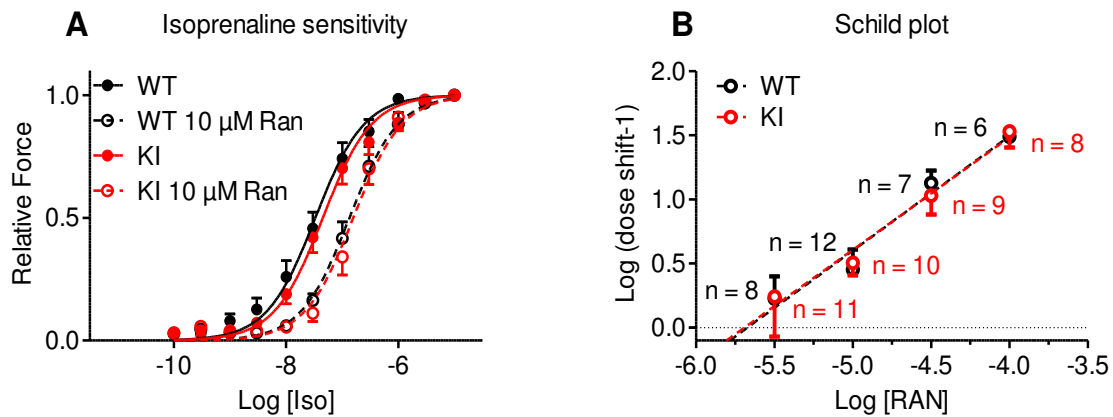
Fig. 3.23: Influence of ranolazine on ISO effect in ventricular muscle strips from wild-type and _Mybpc3_-targeted knock-in hearts: A) ISO concentration-response curves measured as relative increase in isometric force in WT (black) and KI (red) ventricular muscle strips. Hollow circles and dotted lines indicate measurements on muscles under the influence of 10 µM ranolazine. For ISO EC_{50} values, see text; n=12-19. B) Schild plot analysis of different ranolazine doses shifting the ISO EC_{50} in WT (black) and KI (red) muscle preparations.

3.6. Ranolazine blunts isoprenaline-induced protein kinase A-dependent protein phosphorylation in isolated cardiomyocytes

To assess the effect of ranolazine on β-adrenergic signaling, I investigated ISO-induced PKA-dependent protein phosphorylation in ISO-stimulated (30 nM, 30 min, room temperature) adult murine ventricular cardiomyocytes in the presence or absence of 10 µM ranolazine. The control group of cells was not stimulated at all. Subsequently, proteins were isolated and identified by Western blot with antibodies directed against the PKA-phosphorylated forms of cTnI (phosphorylation site serines 23/24) and phospholamban (phosphorylation site serine 16). The phospho-signals were normalized to total cTnI and phospholamban protein amounts, respectively. Total cTnI and phospholamban amounts tended to be lower in KI cells, but were not influenced by treatment (data not shown).

ISO stimulation induced a visible increase in protein phosphorylation in WT and KI cells. While cTnI phosphorylation at serines 23/24 was increased up to 2-fold, phospholamban phosphorylation at serine 16 was increased up to 7-fold (fig. 3.24).

Ten µM ranolazine almost completely blunted ISO-induced phosphorylation of both proteins in both genotypes.
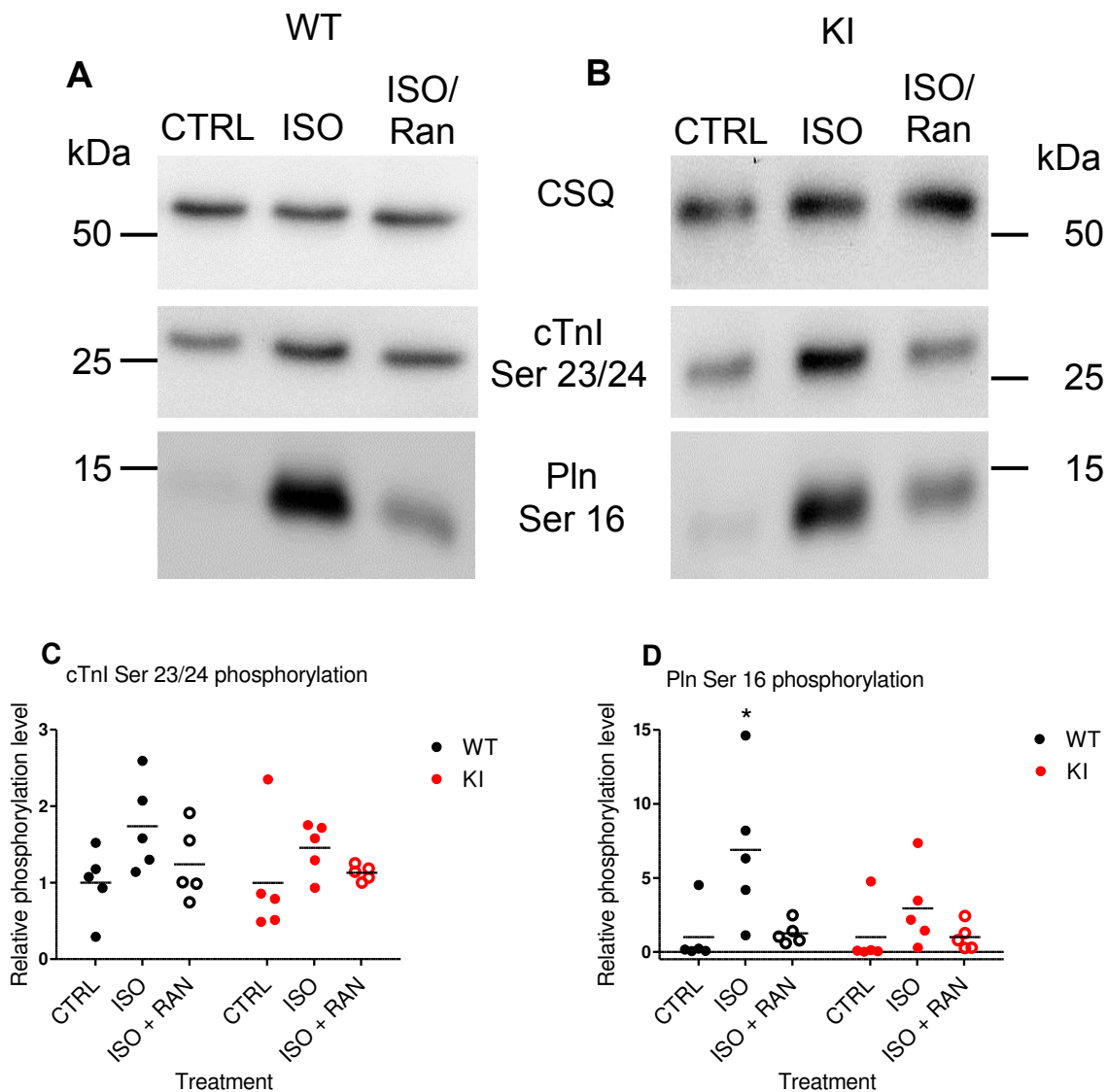
Fig. 3.24: Influence of 10 µM ranolazine on PKA-induced protein phosphorylation: A, B) Representative blots of proteins extracted from cells, which were incubated with 30 nM ISO in the absence or presence of 10 µM ranolazine. Blots were stained with antibodies directed against calsequestrin (CSQ), phospho-cardiac troponin I (cTnI) serines 23/24 (cTnI Ser 23/24) and phospho-phospholamban (Pln) serine 16 (Pln Ser 16). C, D) Quantification of cTnI Ser 23/24 and Pln Ser 16 blots; n=5. One-way ANOVA with Dunnett's post-test; *P<0.05 vs. CTRL.

In summary, ranolazine counteracted effects of ISO stimulation on various levels:
1) ISO-induced increase in contractile force of ventricular muscle strips was decreased in a concentration-dependent manner.

2) Schild plot analysis revealed an ISO EC_{50} shift typical for β-adrenoreceptor antagonists.

3) Ranolazine blunted ISO-induced PKA-dependent protein phosphorylation, as 30 nM ISO was not able to increase PKA-mediated phosphorylation when 10 µM ranolazine was present.

3.7. Long-term treatment of HCM *Mybpc3*-targeted knock-in mice

To evaluate the long-term effect of the drugs used in the single-cell experiments, food or water of groups of HCM and control WT mice were supplemented with diltiazem or ranolazine. For a comparison to classical HCM treatment with β-blockers, metoprolol-treated mice were included in the study. Basal heart function was evaluated by echocardiography before the start of treatment when mice were 6-8 weeks old. Treatment effects were assessed by additional echocardiographic measurements every 8 weeks until the end of the study after 6 months. In a subset of mice, pressure-volume loop measurements were performed at the end of the treatment period.

Ranolazine was given in combination with the cytochrome P450 inhibitor ketoconazole, which was also fed to the control groups. Therefore, the analysis of the ranolazine treatment approach was separated from the ones with diltiazem and metoprolol. However, food supply with ketoconazole did not lead to significant differences compared to non-ketoconazole control groups in any parameter examined in this study.

Mouse body weights were not significantly different between WT and KI groups at the start of the study (fig. 3.25C and D) and increased from ~20 g to up to 30 g until the end of the study. LVM, the most prominent marker of hypertrophy in HCM, was higher in all KI groups before the start of the treatment (fig. 3.25A and B). Typically, LVM in WT mice was around 65-70 mg in 6-8 week-old WT mice and 105-125 mg in age-matched KI animals. LVM values increased with time, but to a lesser degree than body weights. Therefore, LVM/BW ratios decreased over time (fig. 3.25E and F). Treatment did not lead to significant differences in BW development, but ranolazine-

fed mice showed a tendency to lower body weights (around 25 g). Age-dependent increase in LVM was not influenced by any treatment, and, accordingly, LVM/BW ratios in all treatment groups were not different from the ratios of the control groups.
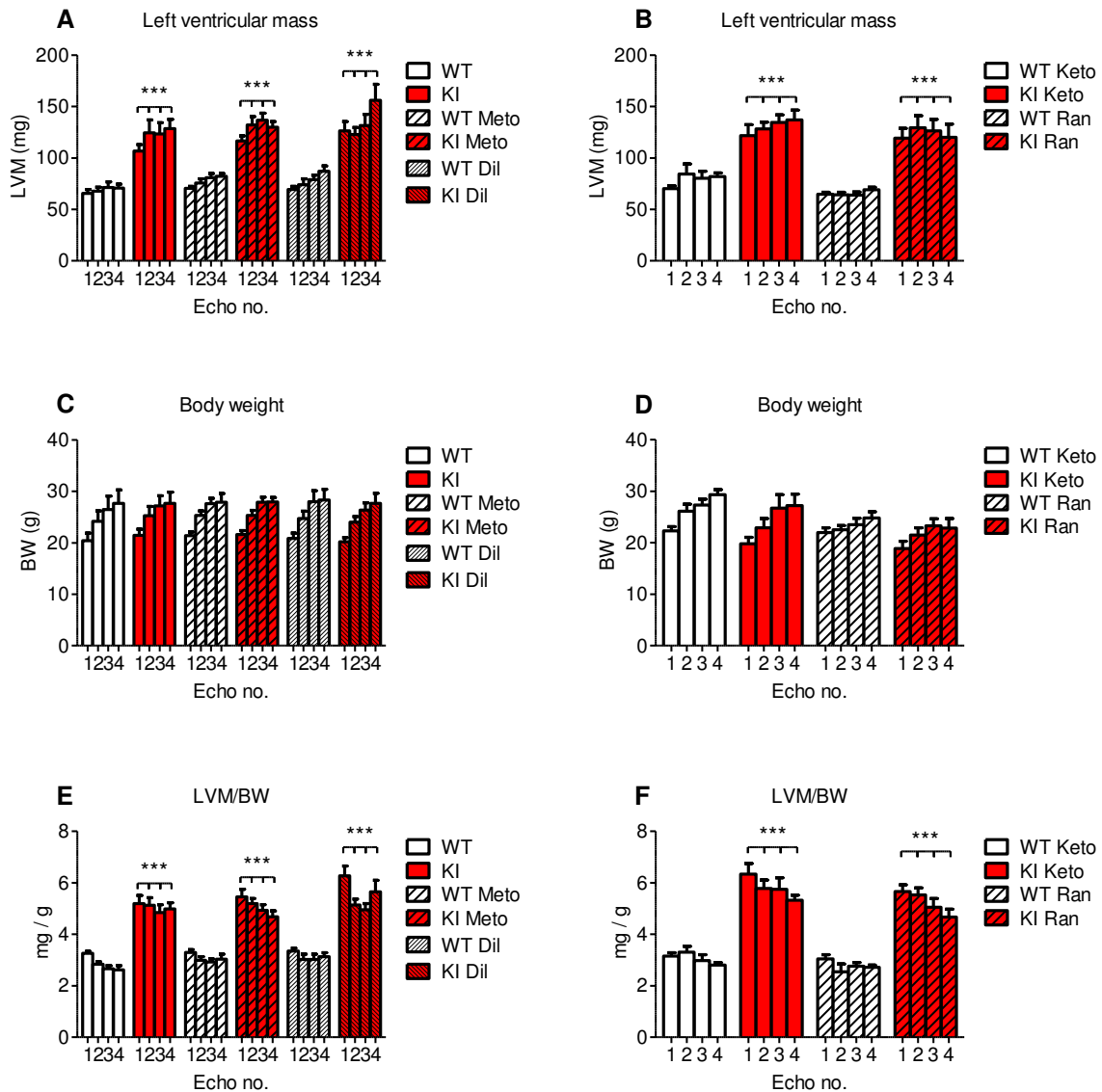
Fig. 3.25: Left ventricular masses and body weights of long-term treatment groups: A) Left ventricular mass of metoprolol (Meto), diltiazem (Dil) and B) ranolazine (Ran)-treated WT (white bars) and KI (red bars) mouse groups including the respective controls (no description and Keto). LVM was measured by echocardiography. Echo no. 1 was performed before the start of treatment, echoes 2-4 followed in intervals of 8 weeks. C, D) Body weights of the treatment groups represented in A) and B). E, F) LVM/BW ratios of the treatment groups shown in the other figures; n=7-10 Two-way ANOVA with Bonferroni's post-test; ***$P<0.001$ vs. respective WT control group with the same treatment. Abbreviations used are: BW, body weight; Dil, diltiazem; Keto, ketoconazole; KI, knock-in; LVM, left ventricular mass; Meto, metoprolol; Ran, ranolazine; WT, wild-type.

Throughout the whole study, KI mice displayed higher inner left ventricular diameters than WT mice (fig. 3.26A-D), indicating a dilated phenotype. This was true in diastole, where the inner diameter of the ventricles of WT mice normally were around 4.2 mm and the one of KI mice ~5 mm (= ~15% higher), and also in systole (WT: 3.5-3.9 mm, KI: 4.2-4.8 mm). Fractional area shortening (FAS), a parameter to evaluate systolic performance of the left ventricle, tended to be lower in KI mice than in WT mice at the beginning of the study (fig. 3.26E and F). While FAS increased in WT control mice with time, it decreased in KI controls, which produced statistically significant differences between WT and KI from the second echocardiography on. Treatments did not change the dilated phenotype of KI mice, while ranolazine-fed WT mice tended to have smaller inner left ventricular diameters than WT mice of the ketoconazole control group (fig. 3.26D). For FAS, treatments did not have influence on the increase in systolic function in WT mice or, in case of ranolazine, even enhanced this increase (fig. 3.26F). In KI, metoprolol could not prevent a decrease in FAS, while diltiazem stabilized FAS values and mice of the ranolazine-treated group displayed slight increases in this value, but overall, FAS was still significantly lower in all KI groups than in the respective WT control group (fig. 3.26E).
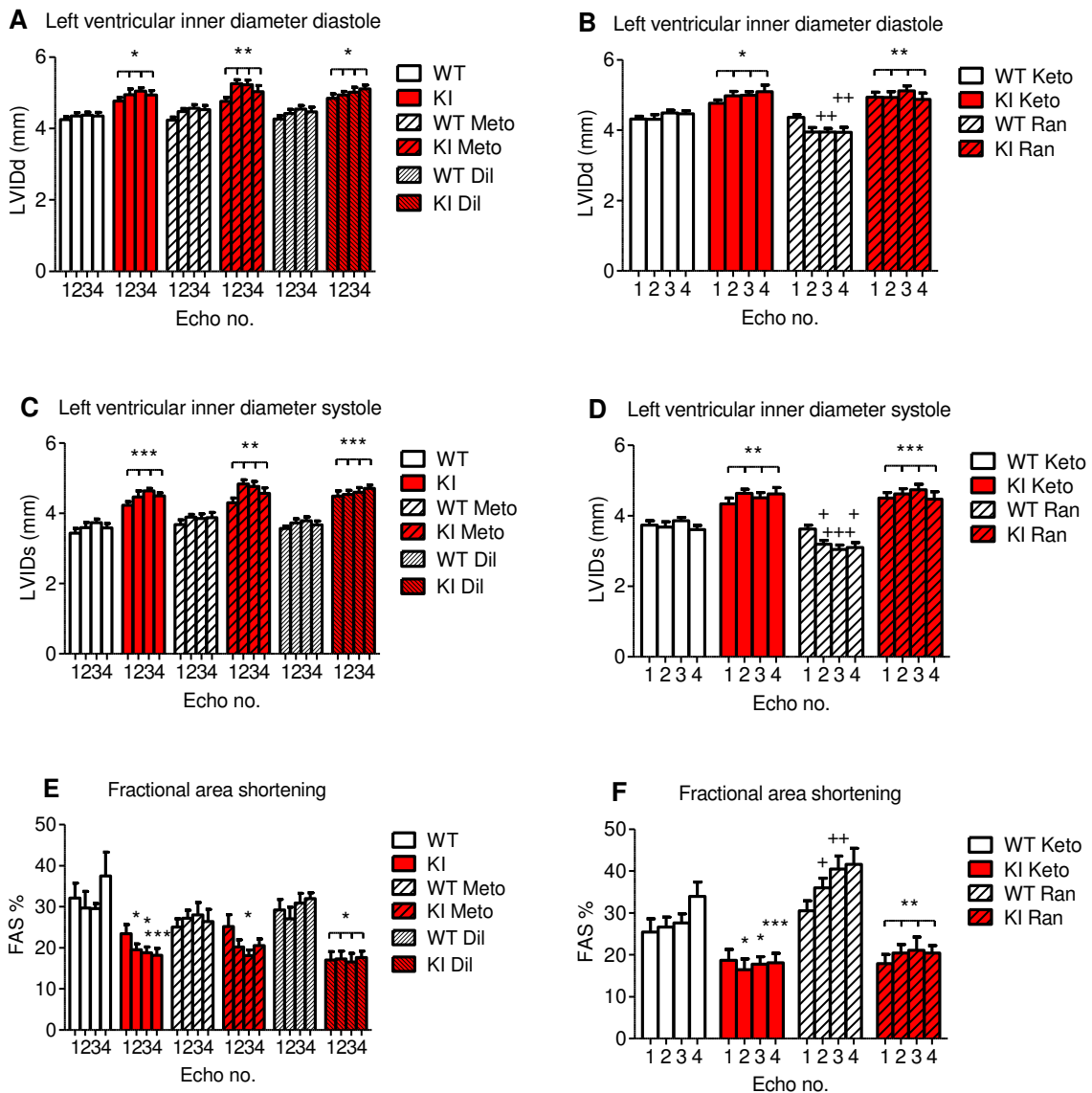
Fig. 3.26: Left ventricular inner diameters and fractional area shortening of long-term treatment groups: A. C) Left ventricular inner diameters (LVIDd and LVIDs) of metoprolol (Meto), diltiazem (Dil) and B, D) ranolazine (Ran) treated WT (white bars) and KI (red bars) mouse groups including the respective controls (no description and Keto). LVIDd and LVIDs were measured by echocardiographical B-mode recordings. Echo no. 1 was performed before the start of treatment, echoes 2-4 followed in intervals of 8 weeks. E, F) Fractional area shortening of the treatment groups shown in the other figures; n=7-10. Two-way ANOVA with Bonferroni's post-test; *P<0.05, **P<0.01 and ***P<0.001 vs. respective WT control group with the same treatment; +P<0.05, ++P<0.01 and +++P<0.001 WT Ran vs WT Keto. Abbreviations used are: d, diastole; Dil, diltiazem; FAS, fractional area shortening; Keto, ketoconazole; KI, knock-in; LVID, left ventricular inner diameter; Meto, metoprolol; Ran, ranolazine; s, systole; WT, wild-type.

For a more detailed view on systolic function, pulsed-wave Doppler images were analyzed (fig. 3.28). The times between diastolic filling phases of the left ventricle

(non-filling time, NFT) were not different between the untreated groups at the start of the study (~ 100 ms), but the period of blood ejection, measured as aortic ejection time (AET), tended to be shorter in KI than in WT mice (fig. 3.27A-D). This difference remained throughout the whole study, with AETs generally >50 ms in WT animals and only ~40 ms in KI mice. This resulted in up to 2-fold higher myocardial performance index (MPI) values, a parameter which calculates the quota of cardiac output during the non-filling time (fig. 3.27E and F). Treatments did not influence these parameters in WT mice. Metoprolol- and diltiazem-treated KI mice also showed no changes in these parameters over time, while ranolazine treatment prolonged NFT and AET in KI mice and therefore produced some slight, but non-significant improvements in their MPI (fig. 3.27).
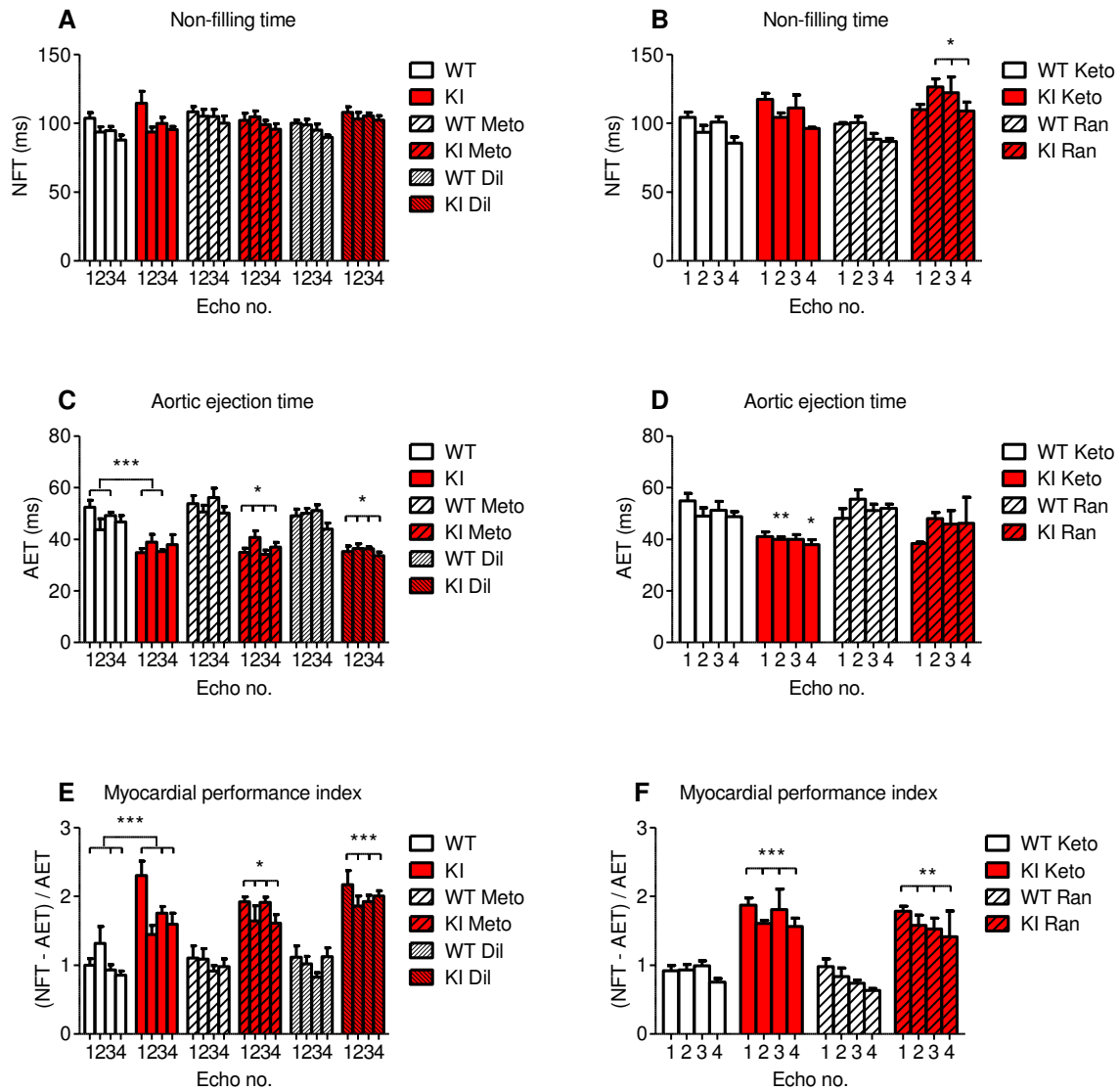
Fig. 3.27: Times of ventricular non-filling and aortic ejection, calculated myocardial performance index of long-term treatment groups: A) Left ventricular non-filling time of metoprolol (Meto), diltiazem (Dil) and B) ranolazine (Ran) treated WT (white bars) and KI (red bars) mouse groups including the respective controls (no description and Keto). Times were measured by pulsed-wave Doppler echocardiography. Echo no. 1 was performed before the start of treatment, echoes 2-4 followed in intervals of 8 weeks. C, D) Aortic ejection times of the treatment groups represented in A) and B). E, F) Myocardial performance indices calculated from values of A-D) of the treatment groups; n=4-9. Two-way ANOVA with Bonferroni's post-test; *P<0.05, **P<0.01 and ***P<0.001 vs. respective WT control group with the same treatment. Abbreviations used are: AET, aortic ejection time; Dil, diltiazem; Keto, ketoconazole; KI, knock-in; Meto, metoprolol; NFT, non-filling time; Ran, ranolazine; WT, wild-type

Diastolic function was evaluated by measuring blood flow velocities at the mitral valve in the early (MV E) and late (MV A) phases of left ventricular filling (fig. 3.27). These

measurements were difficult to execute, and especially A waves in KI mice were often not obtainable.
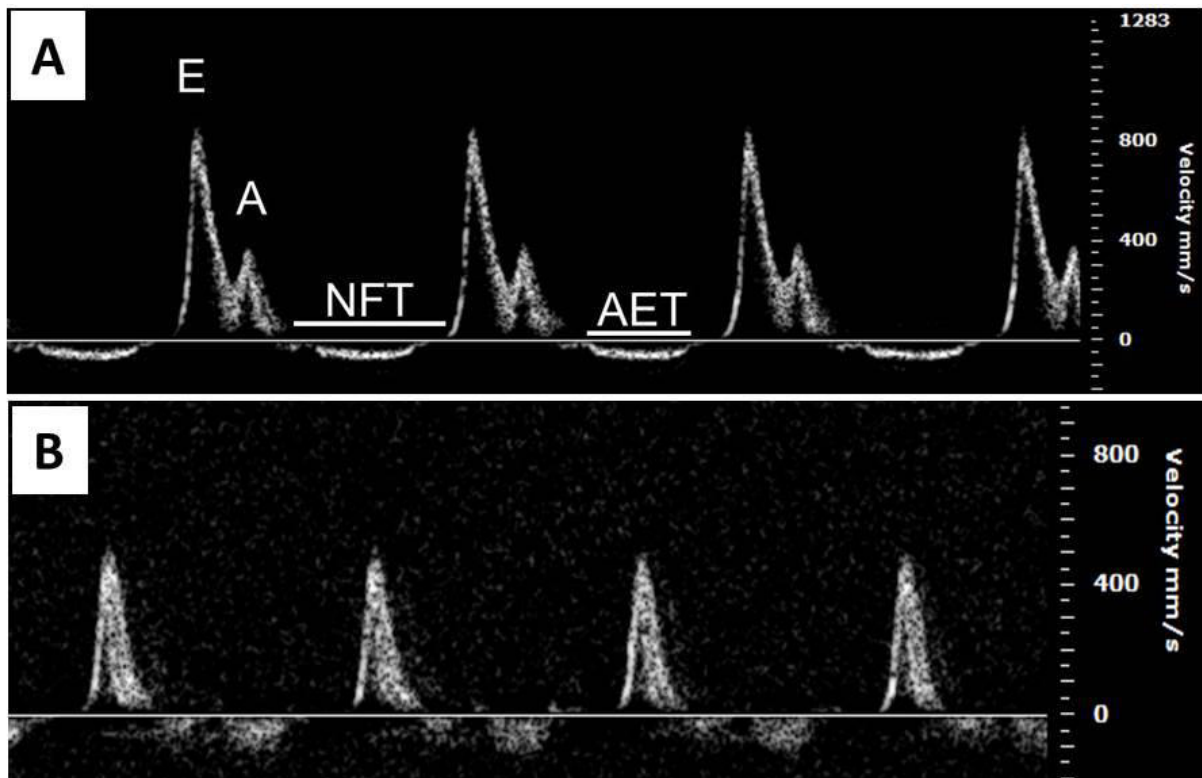
Fig. 3.28: Representative blood flow velocity measurements at the mitral walve with pulsed-wave tissue Doppler in a wild-type (A) and a knock-in (B) mouse: A) WT blood flow trace which was easy to analyze, B) KI blood flow trace in which only E waves are clearly obtainable. E = Peak velocity of early diastolic filling; A = Peak velocity of late diastolic filling; NFT = non-filling time; AET = aortic ejection time.

Nevertheless, lower E wave values were repeatedly found in KI groups (fig. 3.29A-D), showing that their maximal blood flow velocity reached only ~400 mm/s, while it was generally around 700 mm/s in WT animals. Despite the high variation caused by the small number of usable A wave measurements, values for this parameter also showed a tendency to be lower in KI mice (200-300 mm/s in KI and ≥400 mm/s in WT, fig 3.29C and D). This finding resulted in similar E/A ratios in WT and KI groups (fig. 3.29E and F). Ranolazine treatment decreased E waves in WT mice and, to a lesser extent, also in KI animals (fig. 3.29B). This decrease was already visible 8 weeks after beginning of the treatment and persisted until the end of the study. All other treatments did not induce changes in E waves in WT and KI mice (fig. 3.29A and B). A wave peaks were slightly increased in WT mice supplied with diltiazem and in KI mice treated with metoprolol, which in both cases led to small, but non-

significant reductions in E/A ratios, while all other groups did not show treatment-related changes in A waves or E/A ratios (fig. 3.29C-F).
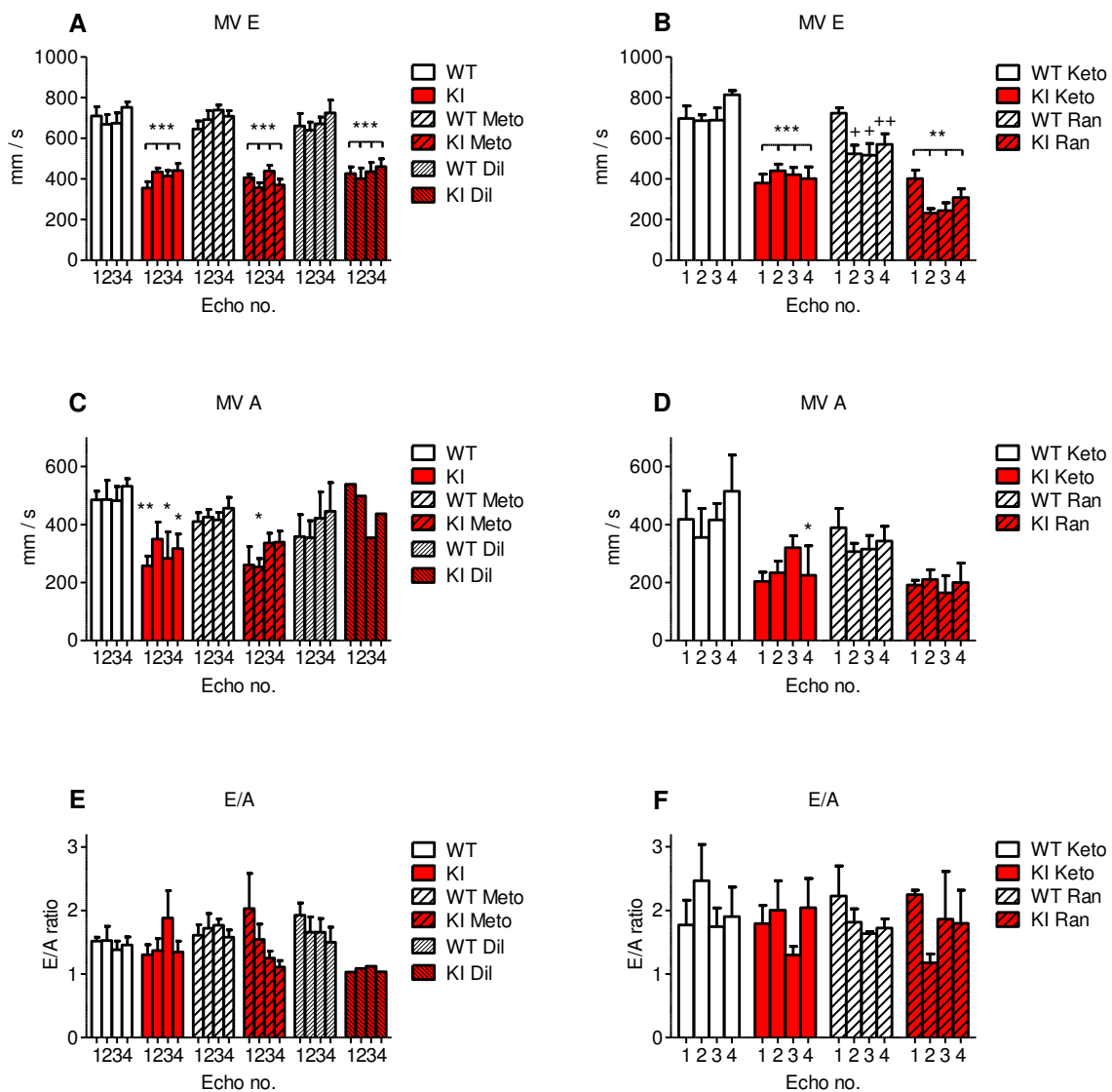
Fig. 3.29: Blood flow velocities at the mitral valve in early and late phases of left ventricular filling, ratio of those in long-term treatment groups: A) Mitral valve blood flow velocities in the early diastolic filling phase in metoprolol (Meto), diltiazem (Dil) and B) ranolazine (Ran) treated WT (white bars) and KI (red bars) mouse groups including the respective controls (no description and Keto). Velocities were measured by pulsed-wave Doppler echocardiography. Echo no. 1 was performed before the start of treatment, echoes 2-4 followed in intervals of 8 weeks. C, D) Mitral valve blood flow velocities in the late diastolic filling phase of the treatment groups represented in A) and B). E, F) Ratios of values measured for A-D); n=1-8. Two-way ANOVA with Bonferroni's post-test; *P<0.05, **P<0.01, ***P<0.001 vs respective WT control group with the same treatment; $^+$P<0.05, $^{++}$P<0.01 WT Ran vs WT Keto. Abbreviations used are: Dil, diltiazem; Keto, ketoconazole; KI, knock-in; Meto, metoprolol; MV E, Peak velocity of early diastolic filling; MV A, Peak velocity of late diastolic filling; Ran, ranolazine; WT, wild-type.

In a subgroup of animals, left ventricular hemodynamic measurements were performed by insertion of a catheter into the LV. The technique had only recently been established in the institute by Dr. Florian Weinberger and Birgit Geertz, therefore not all attempted measurements were usable. Nonetheless, PV loop data for the ranolazine treatment group, which were in focus in these measurements as ranolazine-treated mice showed slight improvements in systolic parameters (fig. 3.26F and 3.27F), could be analyzed. Because of low amount of data in these groups, data from ketoconazole and normal control groups were pooled. Heart rates were similar in all investigated animals, therefore measurements were comparable (fig. 3.30C). Maximal and minimal rates of pressure change, used as indicators of left ventricular systolic and diastolic function, were lower in the untreated KI control animals than in the WT controls (fig. 3.30A and B). The ranolazine-treated KI group showed marginally higher values for systolic and diastolic parameters than untreated KI mice.
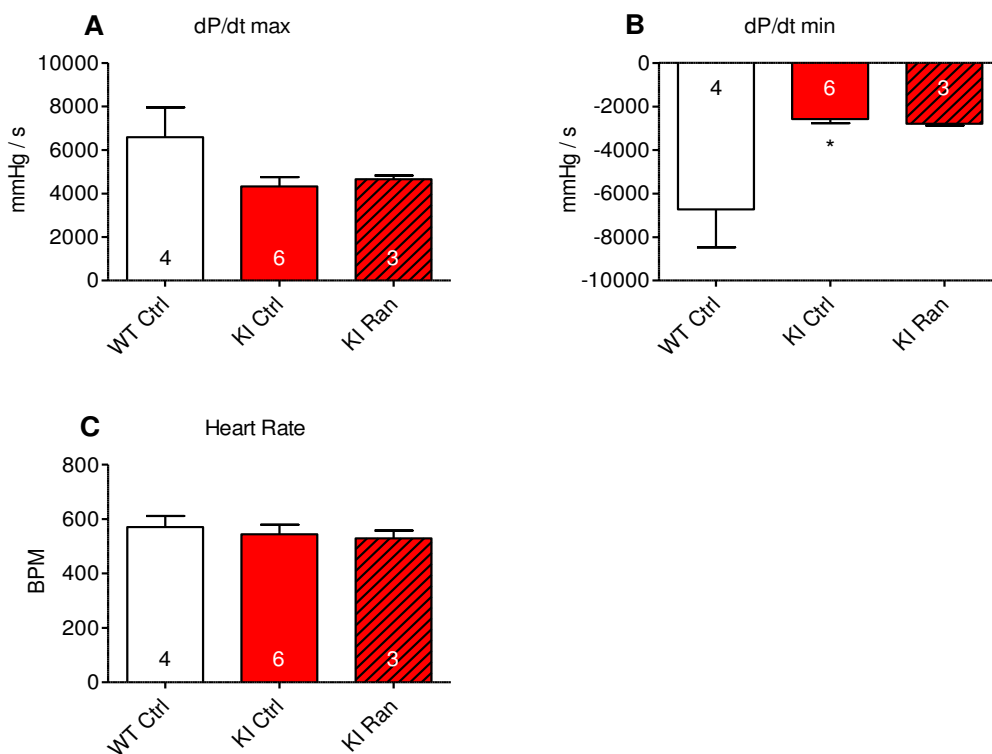
Fig. 3.30: Hemodynamic measurements of cardiac function of selected treatment groups: A) Maximal rate of pressure change (dP/dt$_{max}$) of WT (white bar) and KI (red bar) control mice and ranolazine-treated KI animals (red bar with back stripes). B) Minimal rate of pressure change (dP/dt$_{min}$) of the same animal groups. C) Heart rates of investigated mice during measurements. One-way ANOVA with Bonferroni's post-test; *$P<0.05$ vs. WT ctrl.

In summary (table 3.1), KI mice showed characteristics of LV hypertrophy combined with dilatation. These two findings were already made at the beginning of the study, when mice were only 6-8 weeks old, and persisted during the whole 6 months of investigation. Systolic as well as diastolic performance parameters obtained in echocardiography and hemodynamic measurements demonstrated functional deficits in *Mybpc3*-KI mice. This included lower fractional area shortening, shorter aortic ejection times, slower ventricular filling during the early and late phases of diastole and lower maximal and minimal rates of pressure change in the LV. Supply with metoprolol, diltiazem or ranolazine did not markedly reduce cardiac hypertrophy of KI mice, as their LVM/BW ratios were high from the beginning of the study and showed no treatment-related decrease. Ranolazine-treated mice showed a slight tendency to display improved systolic and diastolic performance with prolonged aortic ejection times and slightly higher maximal and minimal rates of pressure change than in the control group. Treatment with diltiazem or metoprolol did not have an impact on functional parameters.

Table 3.1: Summary of drug effects in isolated cardiomyocytes and on mouse heart function *in vivo.*

Drug	Effect in cardiomyocytes	Effect on heart function
EMD 57033	- induced a KI-like phenotype in WT cardiomyocytes	- acutely increased HR in WT and KI, but increased systolic function only in WT
Blebbistatin	- improved dSL in KI cardio-myocytes under increased workload	*not tested*
Diltiazem	- improved dSL in KI cardio-myocytes under increased workload, but induced negative force-frequency-relationship	- no effect on hypertrophy, systolic and diastolic function in KI mice (6 months treatment)
Ranolazine	- improved dSL in KI cardio-myocytes under increased workload, had an anti-β-adrenergic effect	- no effect on hypertrophy, marginal effects on systolic and diastolic parameters in KI mice (6 months treatment)
Metoprolol	*not tested*	- no effect on hypertrophy, systolic and diastolic function in KI mice (6 months treatment)

Abbreviations used are: dSL, diastolic sarcomere length; HR, heart rate; KI, knock-in; WT, wild-type.

4. Discussion

The first aim of this study was to characterize the contractile and Ca^{2+} homeostasis phenotype of cardiac myocytes of a HCM *Mybpc3*-KI mouse model at baseline and under physiological stress conditions. Also, the cardiac phenotype of KI mice was characterized by echocardiography and compared to WT.

The second aim was to evaluate whether the seen phenotype characteristics were based on the pathomechanism of increased myofilament Ca^{2+} sensitivity and if pharmacological agents which influence intracellular Ca^{2+} homeostasis or myofilament Ca^{2+} sensitivity woud improve the phenotype of isolated KI cardiomyocytes and heart function *in vivo*.

The main findings of this study are:

1. KI mice showed LV hypertrophy, LVID increase, impaired systolic and diastolic function already at young age (6-8 weeks). In the next 6 months, their cardiac function remained altered, but did not deteriorate further or affect overall survival or behavior of KI mice.

2. KI cardiomyocytes had shorter diastolic sarcomere lengths than WT cells, showed stronger inotropic response to ISO with prolonged contraction and relaxation times. Their diastolic Ca^{2+} load tended to be higher than in WT cells, while their Ca^{2+} transient response to β-adrenergic stimulation was similar to the one of WT cells. In response to increased workload with ISO stimulation and high pacing frequency, KI myocytes developed drastic shortening of diastolic sarcomere length, but still showed normal Ca^{2+} transient response.

3. The Ca^{2+} sensitizer EMD 57033 evoked a KI-like phenotype in WT cardiomyocytes undergoing a high workload protocol of ISO stimulation and high pacing frequencies, whereas the Ca^{2+} desensitizer BLEB partially rescued the phenotype of KI cardiomyocytes during this protocol.

4. The LTCC antagonist diltiazem and the late sodium current inhibitor ranolazine both improved KI cardiomyocyte performance in the increased workload protocol.

However, diltiazem induced a negative force-frequency relationship, while ranolazine antagonized β-adrenergic stimulation.

5. Long-term application of diltiazem, ranolazine or the β-blocker metoprolol could not reverse hypertrophy and had only minor positive effects on systolic and diastolic function.

Therefore, the results of this study support the hypothesis that the elevated myofilament Ca^{2+} sensitivity is a major elicitor of phenotypic HCM aspects. Modulation of this and decrease in intracellular Ca^{2+} load could improve the phenotype of isolated cardiomyocytes acutely, but failed to substantially improve established HCM *in vivo*. Furthermore, this study demonstrates that ranolazine has therapeutic potential in HCM, but is also a potent β-adrenergic antagonist at so-called therapeutic concentrations in mice, which should be considered for application in patients.

4.1. *Mypbc3*-targeted knock-in phenotype

HCM is characterized by morphological and functional abnormalities on organ, tissue and single cell level. Some of these aspects have already been studied in the *Mybpc3*-KI mouse model (Vignier et al. 2009, Fraysse et al. 2012) and typical features of HCM such as cardiac hypertrophy with increased LV wall thickness, fibrosis, abnormal sarcomere structure and impaired diastolic and systolic function have been observed.

This study underlined these findings, as echocardiographic measurements of heart morphology and function showed higher LVM/BW ratios and impaired systolic and diastolic function, represented by lower FAS and lower AET, respectively in KI mice than in WT mice. These phenotypic aspects were visible already at young age (6-8 weeks), which is in line with a recent report about development of hypertrophy and heart function deficits in homozygous KI mice very early after birth (Gedicke-Hornung et al. 2013). Noteworthy, assessment of diastolic function via echocardiography was

very difficult and the E/A ratios which could be determined were higher than the ones reported by Fraysse et al. 2012. This was caused by very low E values (a correlate for early, passive ventricular filling) in KI mice examined in the present study, which indicates that disturbance of cardiac compliance in these mice occurred already at very young age. In addition, results of this study revealed increased LVID, a sign of a dilated ventricular phenotype, which also occurred in juvenile mice. Throughout the whole study, all these parameters remained different in comparison to the WT group, but did not deteriorate further.

Isolated ventricular muscle strips of KI mouse hearts developed similar forces like WT muscle strips and reacted similarly to 2-Hz pacing. On single cell level, KI cardiomyocytes paced at 1 Hz (and also at rest) showed shorter diastolic sarcomere lengths than WT cells. This has already been reported before for this mouse model (Fraysse et al. 2012) and the *Mybpc3*-KO mouse (Pohlmann et al. 2007). Considering the low cMyBP-C amount present in the mouse model used in this study (Vignier et al. 2009, Fraysse et al. 2012), which also had been observed in engineered heart tissue (EHT) of neonatal *Mybpc3*-KI cardiac myocytes (Stohr et al. 2013), protein insufficiency seems to be an important trigger for this phenotypic aspect.

Ca^{2+} transients were not different in height or shape in KI cardiomyocytes at baseline compared to WT cells. This is in contrast to Fraysse et al. 2012, who reported faster Ca^{2+} transient kinetics in KI cells. This finding was surprising in the first place since at the same time both NCX mRNA and protein levels were lower in KI cells than in the WT control. It was supposed that the remaining NCX molecules compensate this phenomenon with higher activity. In that study, cells were kept at room temperature, while in the present study, measurements were performed at 37 °C. Apparently, at this temperature the lower NCX protein amount does not have such high impact anymore. This illustrates the low percentage of Ca^{2+} cycling at the sarcolemma in rodents, in which 90-95% of the myofilament-activating Ca^{2+} is cycled through the SR (Bers 2008). Nevertheless, alterations in Ca^{2+} handling pose an important feature of the HCM phenotype, since a reproducible difference in diastolic Ca^{2+} levels between both genotypes at baseline could be observed in the experiments of this study. This finding has already been reported in HCM patient sample cells (Coppini et al. 2013), therefore it seems to be a general consequence of HCM, which, in combination with increased myofilament Ca^{2+} sensitivity, surely has dangerous potential concerning

arrhythmia development. Besides the problem of altered Ca^{2+} handling itself, the increased Ca^{2+} sensitivity might cause a prolonged phase of myosin-actin interaction, which in this study was visible in increased contraction and relaxation times in ISO-stimulated KI cardiac myocytes. This contributes to an oftentimes seen increase in ATP consumption in HCM (Sweeney et al. 1998, Crilley et al. 2003), which can also be acutely arrhythmogenic (Huke et al. 2013).

Ventricular muscle strips of KI mice did not show higher sensitivity to ISO than WT muscles, but in isolated KI cardiomyocytes, 30 nM ISO lead to a higher positive inotropic response than in WT cells. This inconsistency could be explained in two opposing ways: i) the hypercontractile reaction to ISO in isolated cells reflects a compensatory mechanism of single cells to work against the rigidity of the fibrotic ventricular tissue or ii) the hypercontractile behavior is an innate property of the cells, which does not have an impact on overall cardiac function because of the fibrotic and stiff LV morphology. The latter one seems more likely as neonatal KI myocytes embedded in an EHT display a hypercontractile phenotype when they have matured and start to beat (Stohr et al. 2013). Interestingly, a higher density of β-adrenergic receptors was reported in the *Mybpc3*-KO mouse model (Pohlmann 2008). The density of β-adrenergic receptors could be tested for the KI model as well. Additionally, KI cell contraction and relaxation kinetics were slower than in WT cells under ISO stimulation. These findings are new and contribute to the characterization of the KI phenotype, but could have been anticipated because of the findings by Fraysse et al. 2012, in which a tendency to longer relaxation times in KI paced at 2 Hz was already visible. Interestingly, EHTs of neonatal *Mybpc3*-KI cardiac myocytes also displayed contractile abnormalities, but showed a tendency towards shorter contraction and relaxation times (Stohr et al. 2013). These differences in ISO efficacy in ventricular muscle strips, isolated cardiomyocytes and EHTs show the importance of cell and tissue organization for contractile properties, as e.g. measured isolated cardiomyocytes were unloaded. When they are organized in a united cell structure like the myocardium, their sarcomere lengths and contractile behavior are influenced by the condition of the whole tissue. However, the findings of this study again emphasize that cMyBP-C is necessary for proper mechanical action of the contractile apparatus. The higher inotropic ISO response in KI cells while displaying an ISO-

induced increase in the Ca^{2+} transient amplitude similar to WT cells underlines the Ca^{2+} hypersensitivity of the KI myofilaments.

KI cells were unable to keep a stable dSL under increased workload conditions (30 nM ISO + 5-Hz pacing), while their Ca^{2+} transient response to these conditions was similar to WT cells. This decrease in dSL could reflect the functional contraction deficits seen in HCM mouse models and patients, as HCM symptoms often surface when patients are exercising (Maron et al. 2006) and are attributed to diastolic dysfunction.

In general, the tested conditions revealed more and more phenotypic aspects of KI cardiomyocytes by a stepwise increase in workload:

1) lower dSL and higher diastolic Ca^{2+} levels at baseline

2) higher inotropic response to ISO with slower contraction and relaxation kinetics

3) drastic decrease in dSL under ISO and 5-Hz pacing.

Maybe this connects to the fact that HCM is considered one of the main causes of SCD in young athletes, with SCD often occurring during or just after exercise (Maron et al. 2009). Interestingly, detailed analysis of the isometric force measurements on ventricular muscle strips revealed a ~3-fold higher incidence of arrhythmic events in KI muscles than in WT muscles under ISO stimulation, which will be analyzed further in a subsequent study.

4.2. Increased myofilament Ca^{2+} sensitivity as a cause for hypertrophic cardiomyopathy

Myofilament Ca^{2+} sensitivity in skinned cardiac muscle fibers of *Mybpc3*-KI mice (Fraysse et al. 2012), skinned cardiomyocytes of *Mybpc3*-KO mice (Cazorla et al. 2006) and different HCM patient cell samples (van Dijk et al. 2009, van Dijk et al. 2012, Sequeira et al. 2013) has been reported to be higher than in controls. In this study I tried to evaluate if this high myofilament Ca^{2+} sensitivity is responsible for phenotypic aspects of intact cardiomyocytes and if Ca^{2+} desensitization can improve their condition. Pharmacological Ca^{2+} sensitizers and desensitizers have been used in proof-of-principle studies before, and they have been able to mimic or rescue

phenotypic aspects related to HCM (Sirenko et al. 2006, Baudenbacher et al. 2008, Huke et al. 2013).

WT cardiomyocytes under the influence of the calcium sensitizer EMD 57033 (3 µM) had a diastolic sarcomere length as low as KI cardiomyocytes and behaved very similar to KI cells in the increased workload protocol, where they had trouble to tolerate the entire recording protocol. These findings support the thesis that increased myofilament Ca^{2+} sensitivity, a common finding in HCM (Michele et al. 1999, van Dijk et al. 2009, van Dijk et al. 2012, Sequeira et al. 2013), is a functional deficit that is causal for at least some phenotypic aspects of HCM, especially those concerning contractile properties.

Furthermore, it is highly interesting in this context that EMD 57033 treatment of WT cardiomyocytes led to an almost immediate elevation in diastolic Ca^{2+} load similar to the high diastolic Ca^{2+} levels seen in KI cells and in HCM patient samples (Coppini et al. 2013). The finding of this study points to an influence of increased myofilament Ca^{2+} sensitivity on intracellular Ca^{2+} concentration which leads to changes in cytosolic Ca^{2+} levels within minutes and is not based on remodeling processes. A possible explanation is that sensitized myofilaments buffer Ca^{2+} until a late phase of diastole, when cytosolic Ca^{2+} export processes are already declining. If myofilaments release their bound Ca^{2+} not till then, it might contribute to an elevation of the cytosolic Ca^{2+} level. This, in turn, has been speculated to be a starting point for hypertrophic signaling pathways (for review, see Wilkins et al. 2004, Kreusser et al. 2014). In short, elevated cytosolic Ca^{2+} can lead to hyperactivation of the Ca^{2+}-binding messenger protein calmodulin. This in turn leads to an increased activation of the serine/threonine phosphatase calcineurin, either indirectly via calmodulin-mediated increase in activation of CaMKII or directly by calmodulin itself. Calcineurin regulates transcriptional effectors like nuclear factor of activated T cells (NFAT) and myocyte enhancer factor 2 (MEF2), and increased activity of NFAT and MEF2 can lead to an activation of transcription of hypertrophic response genes (fig. 4.1).
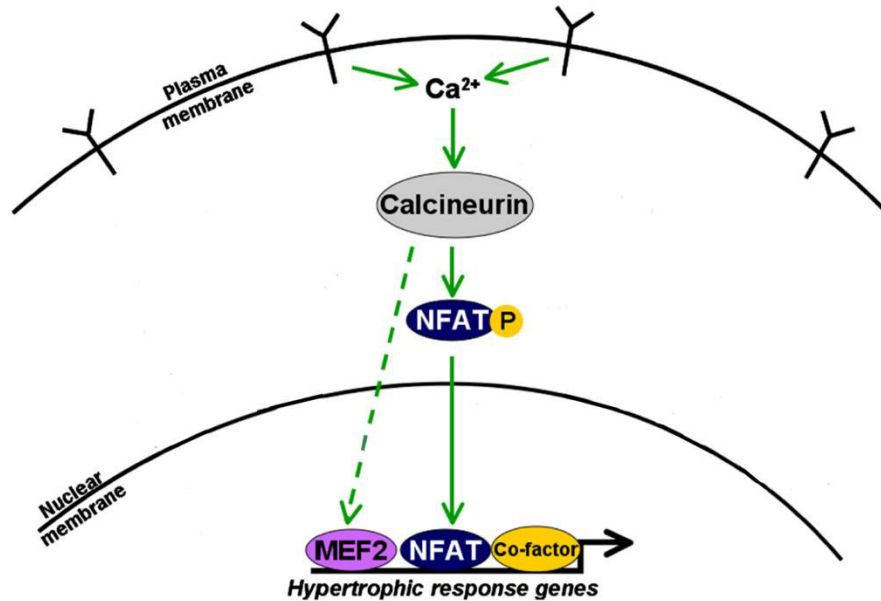
Fig. 4.1: Activation of hypertrophic response genes through calcineurin activation (adapted from Wilkins et al. 2004): Elevated $[Ca^{2+}]_i$ leads to higher calmodulin and CaMKII activation (not shown), which in turn increase calcineurin activation. This leads to increased activity of transcriptional effectors nuclear factor of activated T cells (NFAT) and myocyte enhancer factor 2 (MEF2), which induce a hypertrophic gene response.

Admittedly, EMD 57033 does not exclusively act on the myofilament and might elevate intracellular Ca^{2+} by an off-target mechanism like PDE III inhibition (White et al. 1993).

Somewhat puzzling is the lack of EMD 57033 efficacy on contraction seen *in vivo* after IP injection in *Mybpc3*-KI mice. Isolated KI adult cardiac myocytes responded to EMD 57033 in similar order like WT cells (fig. 3.7). When organized in an EHT format, KI response to EMD 57033 was blunted, but still visible (Stohr et al. 2013). Therefore, similar to the observations made with ISO stimulation discussed above, organization format of the cells seems to play a role in this context. Ventricular tissue of adult homozygous *Mybpc3*-KI (and -KO) mice is already remodeled and probably highly fibrotic, and systolic function is impaired (Vignier et al. 2009, Fraysse et al. 2012). Nevertheless, contractile reserve is still existent in these mice, as their muscles still reacted to β-adrenergic stimulation in the organ bath experiments. Additionally, the increase in heart rate after IP injection of EMD 57033 argues for a PDE III-inhibiting effect at the used dose (0.6 mg/kg). This leads to an increased activation of pacemaking HCN channels in the sino-atrial node, and also has

additional inotropic effects in the ventricle. Still, the positive inotropic effects of EMD 57033 were apparently too weak to overcome the contractile deficits of the KI ventricle.

BLEB, which desensitizes the myofilament towards Ca^{2+}, prevented decrease in dSL length in KI cells in the increased workload protocol, but at the applied concentration of 300 nM, it failed to increase basal diastolic sarcomere length or improve contractile kinetics. Higher concentrations induced an increase in dSL, but this was also visible in WT cells to a similar extent and additionally impaired contractility profoundly. In contrast to EMD 57033, which directly acts on Ca^{2+} sensing elements of the sarcomere (for review, see Endoh 2008), BLEB inhibits myosin ATPase function (Kovacs et al. 2004, Dou et al. 2007, Farman et al. 2008) and is therefore not an optimal therapeutic approach considering the systolic deficits in KI mice *in vivo*. This is underlined by the finding that 3 µM BLEB reduced Ca^{2+} transient peaks, but elevated diastolic Ca^{2+} load. Given the fact that diastolic Ca^{2+} is elevated in KI cardiomyocytes at baseline, an additional increase in $[Ca^{2+}]_i$ has detrimental potential. Ca^{2+} levels and transients should be measured in BLEB-treated cells undergoing the increased workload protocol.

4.3. Evaluation of drug therapies with diltiazem, ranolazine and metoprolol

Pharmacological therapy according to guidelines (Maron et al. 2003, Gersh et al. 2011, ESC guidelines 2014) is based on β-adrenoceptor and Ca^{2+} channel blockers. The β-blockers and the most frequently used Ca^{2+} antagonist verapamil relieve patients from symptoms, but fail to stop or even reverse disease progression. Despite the incomplete penetrance of HCM-associated mutations and the broad phenotypic variability of symptoms, there is evidence that in those who suffer from severe HCM, disease progression to heart failure is the probable course of the disease (Hamada 1993). Therefore, to antagonize this progress is of course one of the major tasks of HCM therapy.

4.3.1. Diltiazem improved the phenotype of isolated knock-in cardiomyocytes, but not the *in vivo* phenotype

Diltiazem, like verapamil a Ca^{2+} channel blocker of the non-dihydropyridine class which is already used in HCM treatment (ESC guidelines 2014), displayed the potential to prevent full development of HCM in mouse models (Semsarian et al. 2002, Westermann et al. 2006) and was therefore an interesting substance to test in the *Mybpc3*-targeted KI mouse model.

In acute application on single KI cardiac myocytes, diltiazem improved their diastolic function in the increased workload protocol. Diastolic Ca^{2+} in KI cells was lower in baseline condition with diltiazem, and the ISO- and pacing-induced increase in Ca^{2+} transient peak heights was attenuated, which had a protective effect in KI cells. This finding can be explained by diltiazem limiting the ISO-induced increase of LTCC channel opening, which has two consequences: First, less Ca^{2+} is available to be pumped into the SR than normally after ISO stimulation, and the Ca^{2+} balancing mechanisms will lead to lower SR loading (Eisner et al. 2013). Second, less RyRs will be activated and less Ca^{2+} will be released from the SR upon stimulation compared to a situation in which LTCCs are fully activated by ISO-induced phosphorylation.

The inhibition of LTCCs by diltiazem also led to a negative force-frequency relationship in isolated WT and KI cells. Force-frequency relationships are distinct in different species and not necessarily positive. In fact, there are usually two phases, of which the first one describes a positive relationship in lower frequency ranges. Above a species-specific threshold frequency, force is declining again due to complex mechanisms including oxygen limitation (for review, see Endoh 2004). However, untreated murine cardiac myocytes measured in this study showed stable contraction amplitudes at 1 and 5 Hz, so the effect of diltiazem must be considered detrimental. A closer look to a contraction trace of a control experiment without ISO stimulation shows that immediately after switching to 5-Hz pacing, contraction amplitude increased slightly, then rapidly declined and subsequently recovered slowly and not to full extent (fig. 3.18). It seems that diltiazem shifted Ca^{2+} flux balance towards export of Ca^{2+} to the extracellular space temporarily: In the early phase, 5-Hz pacing led to an increased activation of RyRs and therefore higher Ca^{2+} release from the SR (Endoh 2004). This then increased NCX-driven export of Ca^{2+} from the cytosol, which

is normally balanced by increased Ca^{2+} influx through LTCCs, which were here blocked by diltiazem. Oftentimes, cells slowly recovered and showed a steady increase in contraction during the fast pacing phase. This might have been mediated by the activation of CaMKII in the early phase of high Ca^{2+} release from the SR. CaMKII then phosphorylated SERCA and RyRs and subsequently, the SR Ca^{2+} content and its total Ca^{2+} release per beat increased to a certain extent (Huke et al. 2007).

In homozygous *Mybpc3*-KI mice treated with diltiazem for 6 months, the LTCC antagonist failed to improve their phenotype on morphological and functional level. Cardiac hypertrophy as well as systolic and diastolic function of diltiazem-treated mice were not significantly different from those of untreated KI mice. In previous studies (Semsarian et al. 2002, Westermann et al. 2006), early start of diltiazem treatment could prevent full HCM development. As described above, although 6-8 week old KI mice were not fully grown at the beginning of the treatment, they already displayed high LVM which did not increase much during the study. Accordingly, their LV hypertrophy was almost fully developed at this young age and could not be reversed by diltiazem treatment. The same was true for LV dilation, which occurred already at the beginning of the study and did not improve with diltiazem treatment, and for systolic and diastolic function, which were worse than in WT mice from the beginning on and remained low throughout the whole treatment period. Therefore, it could be speculated that diltiazem treatment started too late in this study and was therefore not able to produce a phenotypic rescue of established HCM.

4.3.2. Ranolazine improved the phenotype of knock-in cardiomyocytes, but only marginally improved cardiac function of knock-in mice

The second tested drug, the late sodium current blocker ranolazine, possesses anti-anginal and anti-arrhythmic efficacies (Verrier et al. 2013, Banon et al. 2014). Recently, studies reported high late sodium currents in HCM patient cardiac cells which could be lowered by ranolazine (Barajas-Martinez et al. 2013, Coppini et al. 2013). Additionally, ranolazine improved diastolic dysfunction in rodent models (Lovelock et al. 2012, Williams et al. 2014), which was connected to myofilament

Ca^{2+} desensitization (Lovelock et al. 2012). These findings made it an attractive substance to test in the therapy concept of this study.

Ranolazine blunted ISO efficacy in isolated cells and ventricular muscle strips significantly. Furthermore, ranolazine improved KI cardiomyocyte performance in the increased workload protocol and also reduced the occurrence of arrhythmic events, which were not quantified in this study. Schild plot analysis of concentration-response curves on ventricular muscle strips in the presence of different ranolazine concentrations revealed a pattern typical for direct receptor antagonism. The phosphorylation analysis of PKA targets, in which ranolazine significantly blunted ISO-induced PKA phosphorylation, underlined the finding that ranolazine interferes with β-adrenergic signaling. This finding has been reported before (Letienne et al. 2001, Zhao et al. 2011), but is usually not considered in therapeutical concepts. Additionally, the impact on β-adrenergic receptors found in this work is much higher than the one reported in earlier studies, which were done in rats and dogs. This species-dependent difference might be very important, as the sensitivity of human β-adrenoceptors to ranolazine is not known. Also, in many studies in which ranolazine is tested *ex vivo* or *in vitro*, 10 μM is the used concentration, which shifted the ISO sensitivity of LV muscle strips in this study half a log unit to the right. In patients, plasma concentrations of 2-6 μM are considered as therapeutic (Chaitman et al. 2004, Chaitman et al. 2004); at least in mice, these plasma concentrations would already lead to a significant influence on β-adrenergic signaling. Considering the broad range of targets of ranolazine (Antzelevitch et al. 2004), findings of this study make it even harder to evaluate which mode of action of ranolazine finally led to the effect in the respective studies, as β-adrenergic signaling in the end affects many targets involved in excitation-contraction coupling. This should be considered when applying ranolazine in HCM patients.

In mice, ranolazine treatment did not improve LV hypertrophy or dilation when applied for 6 months in KI mice starting at the age of 6-8 weeks. However, in contrast to KI controls, systolic parameters measured by echocardiography (FAS and MPI) showed a slight tendency to improve in ranolazine-treated KI mice, and in haemodynamic measurements, diastolic performance of the LV was marginally better in treated than in untreated KI mice. If these faint improvements seen in these

parameters translate into better function or, transferred to patients, in improvement of symptoms, is unsure, but the tendency of this study is in line with what has been reported for ranolazine used in a canine model of heart failure, though treatment impact was more pronounced in these studies (Chandler et al. 2002, Sabbah et al. 2002).

4.3.3. Metoprolol did not improve phenotype of knock-in mice

The most classical and prevalent class of therapeutic agents in HCM are β-blockers (ACCF/AHA guidelines 2011, ESC guidelines 2014). To compare the effect of a β-blocker therapy with the ones of diltiazem and ranolazine, a metoprolol-treated group was included in the long-term treatment approach.

In general, metoprolol failed to significantly improve LV hypertrophy, dilation and cardiac function in KI mice. An improvement of ventricular relaxation, which is sometimes attributed to β-blocker therapy (for review, see Spirito et al. 1997, Marian 2009) was not visible and also, systolic function was unaltered in metoprolol-treated KI mice. This might be a hint at the fact that although ranolazine showed β-blocker properties in several experiments, it has additional effects which could be beneficial in HCM treatment. To further compare the efficacies of metoprolol and ranolazine, metoprolol will be tested in the increased workload protocol with isolated WT and KI cardiomyocytes. The overall results of the metoprolol-treated group underline that this classical HCM treatment is only relieving patients from symptoms partially and cannot reverse established HCM.

4.3.4. Limitations of long-term treatment in *Mybpc3*-targeted knock-in mice

In general, the evaluation of the long-term treatment results was complicated because of special properties of the *Mybpc3*-KI model, which also make it difficult to find a proper design for studies which aim at counteracting disease progression. In the homozygous state, KI mice develop cardiac dysfunction and pronounced hypertrophy already a few days after birth (Gedicke-Hornung et al. 2013), but

pharmacological therapy in pups is difficult to establish. Direct application of drugs is hardly possible and supplementation via the mother is at least difficult to dose, and in cases of full metabolism of the drug, simply impossible. Furthermore, this study now shows that at juvenile age of 6-8 weeks, phenotypic HCM aspects are fully present and cannot be reversed by the pharmacological therapies tested. Then again, the HCM-associated cardiac dysfunctions do not progress further and do not seem to significantly trouble the mice in any way. Regardless of all measured impairments of cardiac function in KI mice, they did not display any apparent differences in overall development, behavior, food consumption or longevity; during the study, 3 of 100 mice died randomly, two of those were ranolazine-treated KI males and one was a WT male in the water-supplied control group. Also, our mouse facility never reported any complications in KI mice breeding, and KI mice do not show higher mortality than WT animals of the same genetic background. Therefore, studies with homozygous KI mice will require establishment of a second readout of therapy, like exercise performance and its change upon treatment.

Interestingly, heterozygous *Mybpc3*-KI mice display increased myofilament Ca^{2+} sensitivity, but generally have a rather mild phenotype and do not develop hypertrophy (Vignier et al. 2009, Fraysse et al. 2012). However, HCM-like hypertrophy can be evoked by one week of ISO stimulation (Schlossarek et al. 2012). Closer investigation how fast this process happens and subsequent development of study designs intervening at early HCM stages can be an option to test therapeutic success concerning disease development. The approach to intervene with HCM development at early stages is currently also tested in humans by application of diltiazem in pre-hypertrophic patients (NCT00319982). Ranolazine is also a subject of a clinical study, but it is applied in HCM patients already suffering from chest pain or dyspnea despite treatment with standard medical therapy (NCT01721967).

Additionally, it might be worthwhile to use mice with another genetic background, as the outbred black swiss mice used in this study seem to be resistant to heart failure related death even at the homozygous *Mybpc3*-KI or -KO state. The *Mybpc3*-KO model has been established in our laboratory on the congenic C57BL/6j background, and at least in the homozygous state, mice displayed a more severe phenotype and died earlier than black swiss KO animals (FW Friedrich, data not shown). Hence, it is

not unlikely that the heterozygous *Mybpc3*-KI genotype could evoke a more pronounced disease pattern in C57BL/6j mice.

4.4. Outlook

The findings of this study support the hypothesis that increased myofilament Ca^{2+} sensitivity is an important underlying mechanism of HCM. Pharmacological intervention on the level of intracellular Ca^{2+} levels with the LTCC blocker diltiazem and the late sodium current blocker ranolazine improved HCM-associated phenotypic aspects of isolated HCM cardiomyocytes acutely. This could indicate usefulness of these drugs in preventive treatment of HCM mutation carriers at risk for sudden cardiac death, and for amelioration of symptoms under physical stress, although the induction of negative force-frequency relationship by diltiazem in murine cardiac myocytes also urges to be cautious in treatment of e.g. athletes. A first approach to test the efficacy of diltiazem and ranolazine in this context should be to test their anti-arrhythmic potential in electrophysiological measurements on cardiac tissue and isolated myocytes.

In addition, it would be important to know if the faint improvements seen in long-term treatment of KI mice with ranolazine is accompanied by a reduction of genetic hypertrophic markers like natriuretic peptides, β-myosin heavy chain or α-skeletal actin (Swynghedauw 1999) or the amount of cardiac fibrosis in cardiac tissue. Maybe also the treatments with metoprolol and diltiazem were able to induce some changes on these parameters of HCM. Therefore, analysis of the impact of treatments on mRNA and protein markers as well as assessment of heart morphologies on histological level in treated and untreated mouse groups will help to evaluate treatment impact in more detail.

Furthermore, it would be very interesting to reveal the mode of action causing the ranolazine-related effects. This study provides evidence of ranolazine blocking β-adrenergic stimulation, but an equivalent dose of metoprolol did not improve of cardiac function in the long-term study. Long-term metoprolol usage has been reported to increase β-adrenoceptor density in heart failure (Gilbert et al. 1996); a

comparative analysis of this parameter between tissue samples of metoprolol- and ranolazine-treated mice will reveal if this therapeutic aspect is also happening in ranolazine-treated mice. Electrophysiological analysis of the effects of ranolazine will provide more information, and the possible Ca^{2+}-desensitizing effect of ranolazine should be tested acutely in skinned ventricular muscle preparations to evaluate if this pathway also plays a role.

In general, the therapeutical approach to desensitize myofilaments to Ca^{2+} is tempting, as it could be applied in most HCM cases regardless of the underlying mutations and might be a very central mechanism for many HCM phenotype aspects (fig. 4.2).
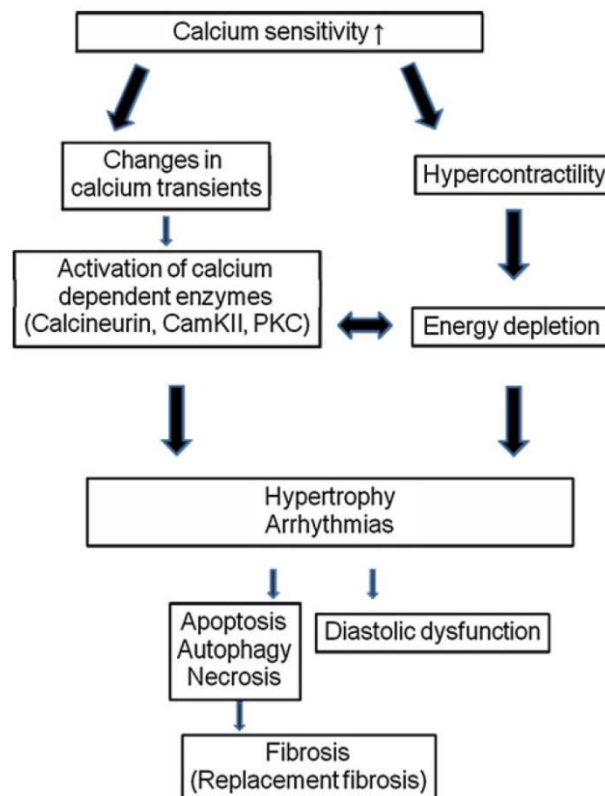
Fig. 4.2: Involvement of increased myofilament Ca²⁺ sensitivity in HCM (Knoll 2012).

A pharmacological solution for this aim is difficult though, as selective agents are lacking. The green tea component EGCg is a promising substance, but has also been reported to have multiple adverse off-target effects (Tadano et al. 2010, Feng et al. 2012) which can lead to a detrimental increase in intracellular Ca^{2+}. Recently, myofilament Ca^{2+} desensitization by gene therapy was successful: Expression of a

pseudophosphorylated cTnI was able to prevent HCM development in a α-tropomyosin HCM mouse model (Alves et al. 2014). Gene therapies might in general provide a more promising approach to HCM therapy, especially as *MYBPC3* mutations cause haploinsufficiency (Marston et al. 2009, van Dijk et al. 2009). Elevation of mRNA and protein levels, either by repair of mutated RNA (reviewed by Behrens-Gawlik et al. 2014) or by introduction of the correct full-length gene (Mearini et al. 2014) have led to substantial and, in the latter case, long-lasting prevention of HCM in mouse models. Finally, the establishment of larger animal models (cat and pig), which is currently pursued by our institute, will help to answer if therapy achievements in mice are translatable to cardiac models which are closer to the human situation.

5. Summary

Cardiovascular diseases are the number one cause of death worldwide. A part of these diseases is caused by genetic defects, and the most common genetic cardiovascular disorder is hypertrophic cardiomyopathy (HCM). The vast majority of the mutations underlying HCM are in genes encoding for sarcomeric proteins, and one of the two most frequently affected genes is *MYBPC3*, which encodes cardiac myosin binding protein C (cMyBP-C). This protein is associated to the thick filament and interacts with myosin and titin, but also with the thin filament protein actin. Thereby, it regulates myosin-actin interaction and, consequently, contraction. Mutations in *MYBPC3* and other myofilament-associated genes oftentimes lead to protein insufficiencies and are commonly accompanied by a sensitization of the myofilament to Ca^{2+}, which is considered one of the underlying defects of HCM and, therefore, a possible target for HCM therapy.

In this study, the used murine *Mybpc3*-targeted knock-in (KI) mouse model recapitulates these phenotypic aspects of HCM. The aim of this work was to evaluate if increased myofilament Ca^{2+} sensitivity is the underlying cause of the contractile and Ca^{2+} transient phenotype of cardiac myocytes isolated from *Mybpc3*-KI mice and to test pharmacological therapy approaches intervening at the level of Ca^{2+} homeostasis and myofilament Ca^{2+} sensitivity.

Isolated cardiac myocytes of *Mybpc3*-KI mice displayed shorter diastolic sarcomere lengths than wild-type cells, showed a higher inotropic response to β-adrenergic stimulation with increased contraction and relaxation times, and suffered from a drastic reduction of diastolic sarcomere length when challenged with high workload of β-adrenergic stimulation and high pacing frequency. A similar phenotype could be elicited in WT cardiac myocytes with the Ca^{2+} sensitizer EMD 57033, and the Ca^{2+}-desensitizing myosin ATPase inhibitor blebbistatin could partially improve the KI phenotype. This supports the theory of myofilament Ca^{2+} hypersensitivity being an underlying problem in HCM.

The Ca^{2+} channel blocker diltiazem and the late sodium current inhibitor ranolazine, which has also been reported to have Ca^{2+} desensitizing properties, were both able

to improve diastolic sarcomere length of *Mybpc3*-KI cells challenged with high workload. Diltiazem also induced the adverse side effect of a negative force-frequency relationship, while concentration-response experiments with isoprenaline and protein phosphorylation analysis revealed β-adrenergic antagonism of ranolazine at concentrations which are considered to be its therapeutic range of action. This should be considered in pharmacological therapy of HCM patients.

Six month treatment of hypertrophic *Mybpc3*-KI mice with diltiazem or the β-blocker metoprolol failed to significantly improve cardiac function or hypertrophy. Ranolazine induced slight tendencies to improved systolic and diastolic function parameters, indicating its possible usefulness in HCM therapy. Its effects should be further evaluated by measurement of mRNA and protein hypertrophy markers, and subsequently, ranolazine can be tested in a larger animal model.

5.1.   Zusammenfassung

Kardiovaskuläre Erkrankungen sind weltweit die häufigste Todesursache. Viele dieser Erkrankungen haben einen genetischen Hintergrund, und die häufigste durch Mutationen verursachte Herzerkrankung ist die hypertrophe Kardiomyopathie (HCM). Fast alle mit der HCM assoziierten Mutationen treten in Genen auf, die für Proteine des Sarkomers kodieren. Eins von den zwei am häufigsten betroffenen Genen ist dabei *MYBPC3*, welches für das Sarkomerprotein cMyBP-C kodiert. Dieses Protein interagiert sowohl mit Komponenten des dicken Filaments (Myosin und Titin) als auch mit Aktin, dem Hauptbestandteil des dünnen Filaments. Hierdurch nimmt cMyBP-C eine regulierende Funktion bezüglich der Interaktion von Myosin und Aktin, und damit im Endeffekt der Kontraktion, ein. Mutationen in *MYBPC3* sowie anderen HCM-assoziierten Genen führen häufig zu einer Haploinsuffizienz und verursachen oft eine Sensitisierung des Myofilaments gegenüber Ca^{2+}. Diese wird als mögliche Ursache der HCM angesehen und ist deshalb potentieller Ansatzpunkt für die Therapie der Krankheit.

In dieser Arbeit wurde ein knock-in (KI) Mausmodell untersucht, welches eine Mutation im *Mybpc3* Gen trägt und die angesprochenen phänotypischen Aspekte der HCM aufweist. Erstes Ziel der Arbeit war zu evaluieren, ob die hohe Ca^{2+}-Sensitivität der Myofilamente Ursache für phänotypische Aspekte bezüglich der kontraktilen Eigenschaften und des intrazellulären Ca^{2+} Transienten in isolierten *Mybpc3*-KI Herzmuskelzellen ist. Im zweiten Teil der Arbeit wurde getestet, wie sich pharmakologische Therapien auswirken, die den intrazellulären Ca^{2+}-Haushalt und die Ca^{2+}-Sensitivität der Myofilamente verändern.

Isolierte Herzmuskelzellen von *Mybpc3*-KI Mäusen zeigten eine kürzere diastolische Sarkomerlänge als Zellen von Wildtyp-Mäusen (WT). Beta-adrenerge Stimulation rief in ihnen einen stärkeren Anstieg der kontraktilen Verkürzung mit verlängerten Kontraktions- und Relaxationszeiten hervor. Eine erhöhte Arbeitslast durch β-adrenerge Stimulation in Kombination mit hoher Stimulationsfrequenz führte zu einer drastischen Verkürzung der diastolischen Sarkomerlänge. Ein ähnlicher Phänotyp konnte in WT-Herzmuskelzellen durch die Anwendung des Ca^{2+}-Sensitisierers EMD 57033 hervorgerufen werden, und der Ca^{2+}-desensitisierende Myosin-ATPase-

Inhibitor Blebbistatin konnte den Phänotyp von KI-Zellen partiell verbessern. Dies spricht dafür, dass die erhöhte Ca^{2+}-Sensitivität der Myofilamente in der Tat ein grundlegendes Problem der HCM ist.

Sowohl der Ca^{2+}-Kanalblocker Diltiazem als auch Ranolazin, ein Blocker des späten Natriumstroms, der auch Ca^{2+}-desensitierende Eigenschaften besitzen soll, konnten die diastolische Funktion von *Mybpc3*-KI Herzmuskelzellen unter erhöhter Arbeitslast verbessern. Dabei verursachte Diltiazem als Nebenwirkung eine negative Kraft-Frequenz-Beziehung. Konzentrations-Wirkungs-Experimente mit Isoprenalin und die Messung von Phosporylierungszuständen kardialer Proteine zeigten, dass Ranolazin in den eingesetzten Konzentrationen einen β-adrenergen Antagonismus ausübt. Da dies Konzentrationen sind, die als therapeutisch angesehen werden, sollte dies bei der pharmakologischen Therapie der HCM berücksichtigt werden.

Die sechsmonatige Behandlung von hypertrophen *Mybpc3*-KI Mäusen mit Diltiazem oder dem β-Blocker Metoprolol konnte weder die Herzfunktion verbessern noch die Hypertrophie verringern. Der Einsatz von Ranolazin führte tendenziell zu leichten Verbesserungen in Parametern der systolischen und diastolischen Herzfunktion, was einen möglichen Nutzen von Ranolazin in der HCM-Therapie unterstreicht. Zur weiteren Charakterisierung der Wirkung von Ranolazin sollten Hypertrophiemarker auf mRNA- und Protein-Ebene gemessen werden. Im nächsten Schritt kann Ranolazin dann im Großtiermodell getestet werden.

6. Appendix

6.1. Literature

Abozguia, K., P. Elliott, W. McKenna, T. T. Phan, G. Nallur-Shivu, I. Ahmed, A. R. Maher, K. Kaur, J. Taylor, A. Henning, H. Ashrafian, H. Watkins and M. Frenneaux (2010). "Metabolic modulator perhexiline corrects energy deficiency and improves exercise capacity in symptomatic hypertrophic cardiomyopathy." Circulation **122**(16): 1562-1569.

Alcalai, R., J. G. Seidman and C. E. Seidman (2008). "Genetic basis of hypertrophic cardiomyopathy: from bench to the clinics." J Cardiovasc Electrophysiol **19**(1): 104-110.

Alves, M. L., F. A. Dias, R. D. Gaffin, J. N. Simon, E. M. Montminy, B. J. Biesiadecki, A. C. Hinken, C. M. Warren, M. S. Utter, R. T. Davis, 3rd, S. Sadayappan, J. Robbins, D. F. Wieczorek, R. J. Solaro and B. M. Wolska (2014). "Desensitization of myofilaments to Ca2+ as a therapeutic target for hypertrophic cardiomyopathy with mutations in thin filament proteins." Circ Cardiovasc Genet **7**(2): 132-143.

American College of Cardiology Foundation/American Heart Association Task Force on, P., S. American Association for Thoracic, E. American Society of, C. American Society of Nuclear, A. Heart Failure Society of, S. Heart Rhythm, A. Society for Cardiovascular, Interventions, S. Society of Thoracic, B. J. Gersh, B. J. Maron, R. O. Bonow, J. A. Dearani, M. A. Fifer, M. S. Link, S. S. Naidu, R. A. Nishimura, S. R. Ommen, H. Rakowski, C. E. Seidman, J. A. Towbin, J. E. Udelson and C. W. Yancy (2011). "2011 ACCF/AHA guideline for the diagnosis and treatment of hypertrophic cardiomyopathy: a report of the American College of Cardiology Foundation/American Heart Association Task Force on Practice Guidelines." J Thorac Cardiovasc Surg **142**(6): e153-203.

Antzelevitch, C., L. Belardinelli, L. Wu, H. Fraser, A. C. Zygmunt, A. Burashnikov, J. M. Di Diego, J. M. Fish, J. M. Cordeiro, R. J. Goodrow, Jr., F. Scornik and G. Perez (2004). "Electrophysiologic properties and antiarrhythmic actions of a novel antianginal agent." J Cardiovasc Pharmacol Ther **9 Suppl 1**: S65-83.

Antzelevitch, C., L. Belardinelli, A. C. Zygmunt, A. Burashnikov, J. M. Di Diego, J. M. Fish, J. M. Cordeiro and G. Thomas (2004). "Electrophysiological effects of ranolazine, a novel antianginal agent with antiarrhythmic properties." Circulation **110**(8): 904-910.

Arad, M., J. G. Seidman and C. E. Seidman (2002). "Phenotypic diversity in hypertrophic cardiomyopathy." Hum Mol Genet **11**(20): 2499-2506.

Ashrafian, H. and H. Watkins (2007). "Reviews of translational medicine and genomics in cardiovascular disease: new disease taxonomy and therapeutic implications cardiomyopathies: therapeutics based on molecular phenotype." J Am Coll Cardiol **49**(12): 1251-1264.

Authors/Task Force, m., P. M. Elliott, A. Anastasakis, M. A. Borger, M. Borggrefe, F. Cecchi, P. Charron, A. A. Hagege, A. Lafont, G. Limongelli, H. Mahrholdt, W. J. McKenna, J. Mogensen, P. Nihoyannopoulos, S. Nistri, P. G. Pieper, B. Pieske, C. Rapezzi, F. H. Rutten, C. Tillmanns, H. Watkins and m. Authors/Task Force (2014). "2014 ESC Guidelines on diagnosis and management of hypertrophic cardiomyopathy: The Task Force for the Diagnosis and Management of Hypertrophic Cardiomyopathy of the European Society of Cardiology (ESC)." Eur Heart J **35**(39): 2733-2779.

Ball, W., J. Ivanov, H. Rakowski, E. D. Wigle, M. Linghorne, A. Ralph-Edwards, W. G. Williams, L. Schwartz, A. Guttman and A. Woo (2011). "Long-term survival in patients with resting obstructive hypertrophic cardiomyopathy comparison of conservative versus invasive treatment." J Am Coll Cardiol **58**(22): 2313-2321.

Banon, D., K. B. Filion, T. Budlovsky, C. Franck and M. J. Eisenberg (2014). "The usefulness of ranolazine for the treatment of refractory chronic stable angina pectoris as determined from a systematic review of randomized controlled trials." Am J Cardiol **113**(6): 1075-1082.

Barajas-Martinez, H., D. Hu, R. J. Goodrow, Jr., F. Joyce and C. Antzelevitch (2013). "Electrophysiologic characteristics and pharmacologic response of human cardiomyocytes isolated from a patient with hypertrophic cardiomyopathy." Pacing Clin Electrophysiol **36**(12): 1512-1515.

Bardswell, S. C., F. Cuello, J. C. Kentish and M. Avkiran (2012). "cMyBP-C as a promiscuous substrate: phosphorylation by non-PKA kinases and its potential significance." J Muscle Res Cell Motil **33**(1): 53-60.

Barefield, D. and S. Sadayappan (2010). "Phosphorylation and function of cardiac myosin binding protein-C in health and disease." J Mol Cell Cardiol **48**(5): 866-875.

Baudenbacher, F., T. Schober, J. R. Pinto, V. Y. Sidorov, F. Hilliard, R. J. Solaro, J. D. Potter and B. C. Knollmann (2008). "Myofilament Ca2+ sensitization causes susceptibility to cardiac arrhythmia in mice." J Clin Invest **118**(12): 3893-3903.

Behrens-Gawlik, V., G. Mearini, C. Gedicke-Hornung, P. Richard and L. Carrier (2014). "MYBPC3 in hypertrophic cardiomyopathy: from mutation identification to RNA-based correction." Pflugers Arch **466**(2): 215-223.

Bers, D. M. (2002). "Cardiac excitation-contraction coupling." Nature **415**(6868): 198-205.

Bers, D. M. (2008). "Calcium cycling and signaling in cardiac myocytes." Annu Rev Physiol **70**: 23-49.

Bos, J. M., J. A. Towbin and M. J. Ackerman (2009). "Diagnostic, prognostic, and therapeutic implications of genetic testing for hypertrophic cardiomyopathy." J Am Coll Cardiol **54**(3): 201-211.

Carrier, L., R. Knoell, N. Vignier, D. I. Keller, P. Bausero, B. Prudhon, R. Isnard, M. L. Ambroisine, M. Fiszman, J. Ross, Jr., K. Schwartz and K. R. Chien (2004).

"Asymmetric septal hypertrophy in heterozygous cMyBP-C null mice." <u>Cardiovasc Res</u> **63**(2): 293-304.

Carrier, L., S. Schlossarek, M. S. Willis and T. Eschenhagen (2010). "The ubiquitin-proteasome system and nonsense-mediated mRNA decay in hypertrophic cardiomyopathy." <u>Cardiovascular Research</u> **85**(2): 330-338.

Cazorla, O., S. Szilagyi, N. Vignier, G. Salazar, E. Kramer, G. Vassort, L. Carrier and A. Lacampagne (2006). "Length and protein kinase A modulations of myocytes in cardiac myosin binding protein C-deficient mice." <u>Cardiovasc Res</u> **69**(2): 370-380.

Chaitman, B. R., C. J. Pepine, J. O. Parker, J. Skopal, G. Chumakova, J. Kuch, W. Wang, S. L. Skettino, A. A. Wolff and I. Combination Assessment of Ranolazine In Stable Angina (2004). "Effects of ranolazine with atenolol, amlodipine, or diltiazem on exercise tolerance and angina frequency in patients with severe chronic angina: a randomized controlled trial." <u>JAMA</u> **291**(3): 309-316.

Chaitman, B. R., S. L. Skettino, J. O. Parker, P. Hanley, J. Meluzin, J. Kuch, C. J. Pepine, W. Wang, J. J. Nelson, D. A. Hebert, A. A. Wolff and M. Investigators (2004). "Anti-ischemic effects and long-term survival during ranolazine monotherapy in patients with chronic severe angina." <u>J Am Coll Cardiol</u> **43**(8): 1375-1382.

Chandler, M. P., W. C. Stanley, H. Morita, G. Suzuki, B. A. Roth, B. Blackburn, A. Wolff and H. N. Sabbah (2002). "Short-term treatment with ranolazine improves mechanical efficiency in dogs with chronic heart failure." <u>Circ Res</u> **91**(4): 278-280.

Choudhury, L., P. Elliott, O. Rimoldi, M. Ryan, A. A. Lammertsma, H. Boyd, W. J. McKenna and P. G. Camici (1999). "Transmural myocardial blood flow distribution in hypertrophic cardiomyopathy and effect of treatment." <u>Basic Res Cardiol</u> **94**(1): 49-59.

Colson, B. A., T. Bekyarova, M. R. Locher, D. P. Fitzsimons, T. C. Irving and R. L. Moss (2008). "Protein kinase A-mediated phosphorylation of cMyBP-C increases proximity of myosin heads to actin in resting myocardium." <u>Circ Res</u> **103**(3): 244-251.

Coppini, R., C. Ferrantini, L. Yao, P. Fan, M. Del Lungo, F. Stillitano, L. Sartiani, B. Tosi, S. Suffredini, C. Tesi, M. Yacoub, I. Olivotto, L. Belardinelli, C. Poggesi, E. Cerbai and A. Mugelli (2013). "Late sodium current inhibition reverses electromechanical dysfunction in human hypertrophic cardiomyopathy." <u>Circulation</u> **127**(5): 575-584.

Crilley, J. G., E. A. Boehm, E. Blair, B. Rajagopalan, A. M. Blamire, P. Styles, W. J. McKenna, I. Ostman-Smith, K. Clarke and H. Watkins (2003). "Hypertrophic cardiomyopathy due to sarcomeric gene mutations is characterized by impaired energy metabolism irrespective of the degree of hypertrophy." <u>J Am Coll Cardiol</u> **41**(10): 1776-1782.

Decker, J. A., J. W. Rossano, E. O. Smith, B. Cannon, S. K. Clunie, C. Gates, J. L. Jefferies, J. J. Kim, J. F. Price, W. J. Dreyer, J. A. Towbin and S. W. Denfield (2009). "Risk factors and mode of death in isolated hypertrophic cardiomyopathy in children." <u>J Am Coll Cardiol</u> **54**(3): 250-254.

Detweiler, D. K. and H. H. Erickson (2004). Regulation of the Heart. Dukes' Physiology of Domestic Animals. R. W.O., Cornell University. **12th ed.**

Dou, Y., P. Arlock and A. Arner (2007). "Blebbistatin specifically inhibits actin-myosin interaction in mouse cardiac muscle." Am J Physiol Cell Physiol **293**(3): C1148-1153.

Eisner, D., E. Bode, L. Venetucci and A. Trafford (2013). "Calcium flux balance in the heart." J Mol Cell Cardiol **58**: 110-117.

El-Armouche, A., L. Pohlmann, S. Schlossarek, J. Starbatty, Y. H. Yeh, S. Nattel, D. Dobrev, T. Eschenhagen and L. Carrier (2007). "Decreased phosphorylation levels of cardiac myosin-binding protein-C in human and experimental heart failure." J Mol Cell Cardiol **43**(2): 223-229.

Elliott, P. M., J. Poloniecki, S. Dickie, S. Sharma, L. Monserrat, A. Varnava, N. G. Mahon and W. J. McKenna (2000). "Sudden death in hypertrophic cardiomyopathy: identification of high risk patients." J Am Coll Cardiol **36**(7): 2212-2218.

Endoh, M. (2004). "Force-frequency relationship in intact mammalian ventricular myocardium: physiological and pathophysiological relevance." Eur J Pharmacol **500**(1-3): 73-86.

Endoh, M. (2008). "Cardiac Ca2+ signaling and Ca2+ sensitizers." Circ J **72**(12): 1915-1925.

Eschenhagen, T. (2010). "Is ryanodine receptor phosphorylation key to the fight or flight response and heart failure?" J Clin Invest **120**(12): 4197-4203.

Farman, G. P., K. Tachampa, R. Mateja, O. Cazorla, A. Lacampagne and P. P. de Tombe (2008). "Blebbistatin: use as inhibitor of muscle contraction." Pflugers Arch **455**(6): 995-1005.

Feng, W., H. S. Hwang, D. O. Kryshtal, T. Yang, I. T. Padilla, A. K. Tiwary, B. Puschner, I. N. Pessah and B. C. Knollmann (2012). "Coordinated regulation of murine cardiomyocyte contractility by nanomolar (-)-epigallocatechin-3-gallate, the major green tea catechin." Mol Pharmacol **82**(5): 993-1000.

Flashman, E., C. Redwood, J. Moolman-Smook and H. Watkins (2004). "Cardiac myosin binding protein C: its role in physiology and disease." Circ Res **94**(10): 1279-1289.

Flavigny, J., M. Souchet, P. Sebillon, I. Berrebi-Bertrand, B. Hainque, A. Mallet, A. Bril, K. Schwartz and L. Carrier (1999). "COOH-terminal truncated cardiac myosin-binding protein C mutants resulting from familial hypertrophic cardiomyopathy mutations exhibit altered expression and/or incorporation in fetal rat cardiomyocytes." J Mol Biol **294**(2): 443-456.

Force, T., R. O. Bonow, S. R. Houser, R. J. Solaro, R. E. Hershberger, B. Adhikari, M. E. Anderson, R. Boineau, B. J. Byrne, T. P. Cappola, R. Kalluri, M. M. LeWinter, M. S. Maron, J. D. Molkentin, S. R. Ommen, M. Regnier, W. H. Tang, R. Tian, M. A.

Konstam, B. J. Maron and C. E. Seidman (2010). "Research priorities in hypertrophic cardiomyopathy: report of a Working Group of the National Heart, Lung, and Blood Institute." Circulation **122**(11): 1130-1133.

Fraysse, B., F. Weinberger, S. C. Bardswell, F. Cuello, N. Vignier, B. Geertz, J. Starbatty, E. Kramer, C. Coirault, T. Eschenhagen, J. C. Kentish, M. Avkiran and L. Carrier (2012). "Increased myofilament Ca2+ sensitivity and diastolic dysfunction as early consequences of Mybpc3 mutation in heterozygous knock-in mice." J Mol Cell Cardiol **52**(6): 1299-1307.

Frey, N., M. Luedde and H. A. Katus (2012). "Mechanisms of disease: hypertrophic cardiomyopathy." Nat Rev Cardiol **9**(2): 91-100.

Friedrich, F. W. and L. Carrier (2012). "Genetics of hypertrophic and dilated cardiomyopathy." Curr Pharm Biotechnol.

Gautel, M., O. Zuffardi, A. Freiburg and S. Labeit (1995). "Phosphorylation switches specific for the cardiac isoform of myosin binding protein-C: a modulator of cardiac contraction?" Embo J **14**(9): 1952-1960.

Gedicke-Hornung, C., V. Behrens-Gawlik, S. Reischmann, B. Geertz, D. Stimpel, F. Weinberger, S. Schlossarek, G. Precigout, I. Braren, T. Eschenhagen, G. Mearini, S. Lorain, T. Voit, P. A. Dreyfus, L. Garcia and L. Carrier (2013). "Rescue of cardiomyopathy through U7snRNA-mediated exon skipping in Mybpc3-targeted knock-in mice." EMBO Mol Med **5**(7): 1060-1077.

Gersh, B. J., B. J. Maron, R. O. Bonow, J. A. Dearani, M. A. Fifer, M. S. Link, S. S. Naidu, R. A. Nishimura, S. R. Ommen, H. Rakowski, C. E. Seidman, J. A. Towbin, J. E. Udelson and C. W. Yancy (2011). "2011 ACCF/AHA guideline for the diagnosis and treatment of hypertrophic cardiomyopathy: a report of the American College of Cardiology Foundation/American Heart Association Task Force on Practice Guidelines." J Thorac Cardiovasc Surg **142**(6): e153-203.

Gilbert, E. M., W. T. Abraham, S. Olsen, B. Hattler, M. White, P. Mealy, P. Larrabee and M. R. Bristow (1996). "Comparative hemodynamic, left ventricular functional, and antiadrenergic effects of chronic treatment with metoprolol versus carvedilol in the failing heart." Circulation **94**(11): 2817-2825.

Gilbert, R., J. A. Cohen, S. Pardo, A. Basu and D. A. Fishman (1999). "Identification of the A-band localization domain of myosin binding proteins C and H (MyBP-C, MyBP-H) in skeletal muscle." J. Cell Science **112**: 69-79.

Girolami, F., C. Y. Ho, C. Semsarian, M. Baldi, M. L. Will, K. Baldini, F. Torricelli, L. Yeates, F. Cecchi, M. J. Ackerman and I. Olivotto (2010). "Clinical features and outcome of hypertrophic cardiomyopathy associated with triple sarcomere protein gene mutations." J Am Coll Cardiol **55**(14): 1444-1453.

Gruen, M. and M. Gautel (1999). "Mutations in beta-myosin S2 that cause familial hypertrophic cardiomyopathy (FHC) abolish the interaction with the regulatory domain of myosin binding protein-C." J Mol Biol **286**: 933-949.

Hamada, M. (1993). "[Progression of hypertrophic cardiomyopathy to dilated cardiomyopathy]." Nihon Naika Gakkai Zasshi **82**(2): 188-193.

Hamada, M., S. Ikeda and Y. Shigematsu (2014). "Advances in medical treatment of hypertrophic cardiomyopathy." J Cardiol.

Hanrath, P., D. G. Mathey, P. Kremer, F. Sonntag and W. Bleifeld (1980). "Effect of verapamil on left ventricular isovolumic relaxation time and regional left ventricular filling in hypertrophic cardiomyopathy." Am J Cardiol **45**(6): 1258-1264.

Harris, S. P., C. R. Bartley, T. A. Hacker, K. S. McDonald, P. S. Douglas, M. L. Greaser, P. A. Powers and R. L. Moss (2002). "Hypertrophic cardiomyopathy in cardiac myosin binding protein-C knockout mice." Circ Res **90**(5): 594-601.

Herron, T. J., E. Rostkova, G. Kunst, R. Chaturvedi, M. Gautel and J. C. Kentish (2006). "Activation of myocardial contraction by the N-terminal domains of myosin binding protein-C." Circ Res **98**(10): 1290-1298.

Ho, C. Y., H. M. Lever, R. DeSanctis, C. F. Farver, J. G. Seidman and C. E. Seidman (2000). "Homozygous mutation in cardiac troponin T. Implications for hypertrophic cardiomyopathy." Circulation **102**: 1950-1955.

Howarth, J. W., S. Ramisetti, K. Nolan, S. Sadayappan and P. R. Rosevear (2012). "Structural insight into unique cardiac myosin-binding protein-C motif: a partially folded domain." J Biol Chem **287**(11): 8254-8262.

Huke, S. and D. M. Bers (2007). "Temporal dissociation of frequency-dependent acceleration of relaxation and protein phosphorylation by CaMKII." J Mol Cell Cardiol **42**(3): 590-599.

Huke, S. and B. C. Knollmann (2010). "Increased myofilament Ca2+-sensitivity and arrhythmia susceptibility." J Mol Cell Cardiol **48**(5): 824-833.

Huke, S., R. Venkataraman, M. Faggioni, S. Bennuri, H. S. Hwang, F. Baudenbacher and B. C. Knollmann (2013). "Focal energy deprivation underlies arrhythmia susceptibility in mice with calcium-sensitized myofilaments." Circ Res **112**(10): 1334-1344.

Ingles, J., A. Doolan, C. Chiu, J. Seidman, C. Seidman and C. Semsarian (2005). "Compound and double mutations in patients with hypertrophic cardiomyopathy: implications for genetic testing and counselling." J Med Genet **42**(10): e59.

Iorga, B., N. Blaudeck, J. Solzin, A. Neulen, I. Stehle, A. J. Lopez Davila, G. Pfitzer and R. Stehle (2008). "Lys184 deletion in troponin I impairs relaxation kinetics and induces hypercontractility in murine cardiac myofibrils." Cardiovasc Res **77**(4): 676-686.

Jacques, A. M., O. Copeland, A. E. Messer, C. E. Gallon, K. King, W. J. McKenna, V. T. Tsang and S. B. Marston (2008). "Myosin binding protein C phosphorylation in normal, hypertrophic and failing human heart muscle." J Mol Cell Cardiol **45**(2): 209-216.

Kawai, M., J. A. Lee and C. H. Orchard (2000). "Effects of the Ca2+ sensitizer EMD 57033 on intracellular Ca2+ in rat ventricular myocytes: relevance to arrhythmogenesis during positive inotropy." Clin Sci (Lond) **99**(6): 547-554.

Klues, H. G., A. Schiffers and B. J. Maron (1995). "Phenotypic spectrum and patterns of left ventricular hypertrophy in hypertrophic cardiomyopathy: morphologic observations and significance as assessed by two-dimensional echocardiography in 600 patients." J. Am. Coll. Cardiol. **26**(7): 1699-1708.

Knoll, R. (2012). "Myosin binding protein C: implications for signal-transduction." J Muscle Res Cell Motil **33**(1): 31-42.

Kooij, V., R. J. Holewinski, A. M. Murphy and J. E. Van Eyk (2013). "Characterization of the cardiac myosin binding protein-C phosphoproteome in healthy and failing human hearts." J Mol Cell Cardiol **60**: 116-120.

Kovacs, M., J. Toth, C. Hetenyi, A. Malnasi-Csizmadia and J. R. Sellers (2004). "Mechanism of blebbistatin inhibition of myosin II." J Biol Chem **279**(34): 35557-35563.

Kreusser, M. M. and J. Backs (2014). "Integrated mechanisms of CaMKII-dependent ventricular remodeling." Front Pharmacol **5**: 36.

Kulikovskaya, I., G. McClellan, J. Flavigny, L. Carrier and S. Winegrad (2003). "Effect of MyBP-C binding to actin on contractility in heart muscle." J Gen Physiol **122**: 1-15.

Kunst, G., K. R. Kress, M. Gruen, D. Uttenweiler, M. Gautel and R. H. Fink (2000). "Myosin binding protein C, a phosphorylation-dependent force regulator in muscle that controls the attachment of myosin heads by its interaction with myosin S2." Circ Res **86**(1): 51-58.

Kuster, D. W., A. C. Bawazeer, R. Zaremba, M. Goebel, N. M. Boontje and J. van der Velden (2012). "Cardiac myosin binding protein C phosphorylation in cardiac disease." J Muscle Res Cell Motil **33**(1): 43-52.

Landstrom, A. P. and M. J. Ackerman (2010). "Mutation type is not clinically useful in predicting prognosis in hypertrophic cardiomyopathy." Circulation **122**(23): 2441-2449; discussion 2450.

Lemoine, M. D., J. E. Duverger, P. Naud, D. Chartier, X. Y. Qi, P. Comtois, L. Fabritz, P. Kirchhof and S. Nattel (2011). "Arrhythmogenic left atrial cellular electrophysiology in a murine genetic long QT syndrome model." Cardiovasc Res **92**(1): 67-74.

Letienne, R., B. Vie, A. Puech, S. Vieu, B. Le Grand and G. W. John (2001). "Evidence that ranolazine behaves as a weak beta1- and beta2-adrenoceptor antagonist in the rat [correction of cat] cardiovascular system." Naunyn Schmiedebergs Arch Pharmacol **363**(4): 464-471.

Lovelock, J. D., M. M. Monasky, E. M. Jeong, H. A. Lardin, H. Liu, B. G. Patel, D. M. Taglieri, L. Gu, P. Kumar, N. Pokhrel, D. Zeng, L. Belardinelli, D. Sorescu, R. J.

Solaro and S. C. Dudley, Jr. (2012). "Ranolazine improves cardiac diastolic dysfunction through modulation of myofilament calcium sensitivity." Circ Res **110**(6): 841-850.

Luther, P. K., P. M. Bennett, C. Knupp, R. Craig, R. Padron, S. P. Harris, J. Patel and R. L. Moss (2008). "Understanding the organisation and role of myosin binding protein C in normal striated muscle by comparison with MyBP-C knockout cardiac muscle." J Mol Biol **384**(1): 60-72.

Marian, A. J. (2009). "Contemporary treatment of hypertrophic cardiomyopathy." Tex Heart Inst J **36**(3): 194-204.

Marian, A. J. and R. Roberts (2001). "The molecular genetic basis for hypertrophic cardiomyopathy." J Mol Cell Cardiol **33**: 655-670.

Maron, B., J. Shirani, L. Poliac, R. Mthenge, W. Roberts and F. Mueller (1996). "Sudden death in young competitive athletes. Clinical, demographic, and pathological profiles." JAMA **276**: 199-204.

Maron, B. J. (2002). "Hypertrophic cardiomyopathy: a systematic review." Jama **287**(10): 1308-1320.

Maron, B. J. (2010). "Contemporary insights and strategies for risk stratification and prevention of sudden death in hypertrophic cardiomyopathy." Circulation **121**(3): 445-456.

Maron, B. J. and E. Braunwald (2012). "Evolution of hypertrophic cardiomyopathy to a contemporary treatable disease." Circulation **126**(13): 1640-1644.

Maron, B. J., S. A. Casey, T. S. Haas, C. L. Kitner, R. F. Garberich and J. R. Lesser (2012). "Hypertrophic cardiomyopathy with longevity to 90 years or older." Am J Cardiol **109**(9): 1341-1347.

Maron, B. J., S. A. Casey, R. G. Hauser and D. M. Aeppli (2003). "Clinical course of hypertrophic cardiomyopathy with survival to advanced age." J Am Coll Cardiol **42**(5): 882-888.

Maron, B. J., J. J. Doerer, T. S. Haas, D. M. Tierney and F. O. Mueller (2009). "Sudden deaths in young competitive athletes: analysis of 1866 deaths in the United States, 1980-2006." Circulation **119**(8): 1085-1092.

Maron, B. J., J. M. Gardin, J. M. Flack, S. S. Gidding, T. T. Kurosaki and D. E. Bild (1995). "Prevalence of hypertrophic cardiomyopathy in a general population of young adults: echocardiographic analysis of 4111 subjects in the CARDIA study." Circulation **92**: 785-789.

Maron, B. J. and M. S. Maron (2013). "Hypertrophic cardiomyopathy." Lancet **381**(9862): 242-255.

Maron, B. J., M. S. Maron and C. Semsarian (2012). "Double or compound sarcomere mutations in hypertrophic cardiomyopathy: a potential link to sudden death in the absence of conventional risk factors." Heart Rhythm **9**(1): 57-63.

Maron, B. J., M. S. Maron and C. Semsarian (2012). "Genetics of hypertrophic cardiomyopathy after 20 years: clinical perspectives." J Am Coll Cardiol **60**(8): 705-715.

Maron, B. J., W. J. McKenna, G. K. Danielson, L. J. Kappenberger, H. J. Kuhn, C. E. Seidman, P. M. Shah, W. H. Spencer, 3rd, P. Spirito, F. J. Ten Cate, E. D. Wigle, D. American College of Cardiology Foundation Task Force on Clinical Expert Consensus and G. European Society of Cardiology Committee for Practice (2003). "American College of Cardiology/European Society of Cardiology Clinical Expert Consensus Document on Hypertrophic Cardiomyopathy. A report of the American College of Cardiology Foundation Task Force on Clinical Expert Consensus Documents and the European Society of Cardiology Committee for Practice Guidelines." Eur Heart J **24**(21): 1965-1991.

Maron, B. J., W. J. McKenna, G. K. Danielson, L. J. Kappenberger, H. J. Kuhn, C. E. Seidman, P. M. Shah, W. H. Spencer, 3rd, P. Spirito, F. J. Ten Cate, E. D. Wigle, C. Task Force on Clinical Expert Consensus Documents. American College of and C. Committee for Practice Guidelines. European Society of (2003). "American College of Cardiology/European Society of Cardiology clinical expert consensus document on hypertrophic cardiomyopathy. A report of the American College of Cardiology Foundation Task Force on Clinical Expert Consensus Documents and the European Society of Cardiology Committee for Practice Guidelines." J Am Coll Cardiol **42**(9): 1687-1713.

Maron, B. J., W. J. McKenna, G. K. Danielson, L. J. Kappenberger, H. J. Kuhn, C. E. Seidman, P. M. Shah, W. H. Spencer, P. Spirito, F. J. Ten Cate and E. D. Wigle (2003). "American College of Cardiology/European Society of Cardiology Clinical Expert Consensus Document on Hypertrophic Cardiomyopathy: A report of the American College of Cardiology Foundation Task Force on Clinical Expert Consensus Documents and the European Society of Cardiology Committee for Practice Guidelines." Eur Heart J. **in press**.

Maron, M. S., B. J. Maron, C. Harrigan, J. Buros, C. M. Gibson, I. Olivotto, L. Biller, J. R. Lesser, J. E. Udelson, W. J. Manning and E. Appelbaum (2009). "Hypertrophic cardiomyopathy phenotype revisited after 50 years with cardiovascular magnetic resonance." J Am Coll Cardiol **54**(3): 220-228.

Maron, M. S., I. Olivotto, A. G. Zenovich, M. S. Link, N. G. Pandian, J. T. Kuvin, S. Nistri, F. Cecchi, J. E. Udelson and B. J. Maron (2006). "Hypertrophic cardiomyopathy is predominantly a disease of left ventricular outflow tract obstruction." Circulation **114**(21): 2232-2239.

Marston, S., O. Copeland, K. Gehmlich, S. Schlossarek and L. Carrier (2012). "How do MYBPC3 mutations cause hypertrophic cardiomyopathy?" J Muscle Res Cell Motil **33**(1): 75-80.

Marston, S., O. N. Copeland, A. Jacques, K. Livesey, V. Tsang, W. J. McKenna, S. Jalilzadeh, S. Carballo, C. Redwood and H. Watkins (2009). "Evidence From Human Myectomy Samples That MYBPC3 Mutations Cause Hypertrophic Cardiomyopathy Through Haploinsufficiency." Circulation Research **105**(3): 219-222.

McLeod, C. J., M. J. Ackerman, R. A. Nishimura, A. J. Tajik, B. J. Gersh and S. R. Ommen (2009). "Outcome of patients with hypertrophic cardiomyopathy and a normal electrocardiogram." J Am Coll Cardiol **54**(3): 229-233.

McLeod, C. J., J. M. Bos, J. L. Theis, W. D. Edwards, B. J. Gersh, S. R. Ommen and M. J. Ackerman (2009). "Histologic characterization of hypertrophic cardiomyopathy with and without myofilament mutations." Am Heart J **158**(5): 799-805.

Mearini, G., D. Stimpel, B. Geertz, F. Weinberger, E. Krämer, S. Schlossarek, J. Mourot-Filiatre, A. Stoehr, A. Dutsch, P. J. Wijnker, I. Braren, H. A. Katus, O. J. Müller, T. Voit, T. Eschenhagen and L. Carrier (2014). "Mybpc3 gene therapy for neonatal cardiomyopathy enables long-term disease prevention in mice." Ncomms **in press**.

Meurs, K. M., X. Sanchez, R. M. David, N. E. Bowles, J. A. Towbin, P. J. Reiser, J. A. Kittleson, M. J. Munro, K. Dryburgh, K. A. Macdonald and M. D. Kittleson (2005). "A cardiac myosin binding protein C mutation in the Maine Coon cat with familial hypertrophic cardiomyopathy." Hum Mol Genet **14**(23): 3587-3593.

Michele, D. E., F. P. Albayya and J. M. Metzger (1999). "Direct, convergent hypersensitivity of calcium-activated force generation produced by hypertrophic cardiomyopathy mutant alpha-tropomyosins in adult cardiac myocytes." Nat Med **5**(12): 1413-1417.

Miller, T., D. Szczesna, P. R. Housman, J. Zhao, F. de Freitas, A. V. Gomes, L. Culbreath, J. McCue, Y. Wang, Y. Xu, W. G. L. Kerrick and J. D. Potter (2001). "Abnormal contractile function in transgenic mice expressing familial hypertrophic cardiomyopathy-linked troponin T (I79N) mutation." J. Biol. Chem. **276**: 3743-3755.

Mohamed, A. S., J. D. Dignam and K. K. Schlender (1998). "Cardiac myosin-binding protein C (MyBP-C): Identification of protein kinase A and protein kinase C phosphorylation sites." Arch. Biochem. Biophys. **358**: 313-319.

Moolman-Smook, J., E. Flashman, W. de Lange, Z. Li, V. Corfield, C. Redwood and H. Watkins (2002). "Identification of novel interactions between domains of Myosin binding protein-C that are modulated by hypertrophic cardiomyopathy missense mutations." Circ Res **91**(8): 704-711.

Nanni, L., M. Pieroni, C. Chimenti, B. Simionati, R. Zimbello, A. Maseri, A. Frustaci and G. Lanfranchi (2003). "Hypertrophic cardiomyopathy: two homozygous cases with "typical" hypertrophic cardiomyopathy and three new mutations in cases with progression to dilated cardiomyopathy." Biochem Biophys Res Commun **309**(2): 391-398.

Neulen, A., R. Stehle and G. Pfitzer (2009). "The cardiac troponin C mutation Leu29Gln found in a patient with hypertrophic cardiomyopathy does not alter

contractile parameters in skinned murine myocardium." Basic Res Cardiol **104**(6): 751-760.

Niimura, H., L. L. Bachinski, S. Sangwatanaroj, H. Watkins, A. E. Chudley, W. McKenna, A. Kristinsson, R. Roberts, M. Sole, B. J. Maron, J. G. Seidman and C. E. Seidman (1998). "Mutations in the gene for cardiac myosin-binding protein C and late-onset familial hypertrophic cardiomyopathy." N. Engl. J. Med. **338**: 1248-1257.

O'Connell, T. D., M. C. Rodrigo and P. C. Simpson (2007). "Isolation and culture of adult mouse cardiac myocytes." Methods Mol Biol **357**: 271-296.

Olivotto, I., F. Cecchi, S. A. Casey, A. Dolara, J. H. Traverse and B. J. Maron (2001). "Impact of atrial fibrillation on the clinical course of hypertrophic cardiomyopathy." Circulation **104**(21): 2517-2524.

Ommen, S. R., B. J. Maron, I. Olivotto, M. S. Maron, F. Cecchi, S. Betocchi, B. J. Gersh, M. J. Ackerman, R. B. McCully, J. A. Dearani, H. V. Schaff, G. K. Danielson, A. J. Tajik and R. A. Nishimura (2005). "Long-term effects of surgical septal myectomy on survival in patients with obstructive hypertrophic cardiomyopathy." J Am Coll Cardiol **46**(3): 470-476.

Pacher, P., T. Nagayama, P. Mukhopadhyay, S. Batkai and D. A. Kass (2008). "Measurement of cardiac function using pressure-volume conductance catheter technique in mice and rats." Nat Protoc **3**(9): 1422-1434.

Parikh, A., R. Mantravadi, D. Kozhevnikov, M. A. Roche, Y. Ye, L. J. Owen, J. L. Puglisi, J. J. Abramson and G. Salama (2012). "Ranolazine stabilizes cardiac ryanodine receptors: a novel mechanism for the suppression of early afterdepolarization and torsades de pointes in long QT type 2." Heart Rhythm **9**(6): 953-960.

Pohlmann, L. (2008). "The role of cardiac myosin binding protein C and its phosphorylation in the regulation of cardiac contraction " Dissertation, University of Hamburg.

Pohlmann, L., I. Kroger, N. Vignier, S. Schlossarek, E. Kramer, C. Coirault, K. R. Sultan, A. El-Armouche, S. Winegrad, T. Eschenhagen and L. Carrier (2007). "Cardiac myosin-binding protein C is required for complete relaxation in intact myocytes." Circ Res **101**(9): 928-938.

Razumova, M. V., J. F. Shaffer, A. Y. Tu, G. V. Flint, M. Regnier and S. P. Harris (2006). "Effects of the N-terminal domains of myosin binding protein-C in an in vitro motility assay: Evidence for long-lived cross-bridges." J Biol Chem **281**(47): 35846-35854.

Richard, P., P. Charron, L. Carrier, C. Ledeuil, T. Cheav, C. Pichereau, A. Benaiche, R. Isnard, O. Dubourg, M. Burban, J. P. Gueffet, A. Millaire, M. Desnos, K. Schwartz, B. Hainque and M. Komajda (2003). "Hypertrophic Cardiomyopathy: Distribution of disease genes, spectrum of mutations and implications for molecular diagnosis strategy." Circulation **107**: 2227-2232.

Richard, P., E. Villard, P. Charron and R. Isnard (2006). "The genetic bases of cardiomyopathies." J Am Coll Cardiol **48**(9 Suppl): A79-89.

Sabbah, H. N., M. P. Chandler, T. Mishima, G. Suzuki, P. Chaudhry, O. Nass, B. J. Biesiadecki, B. Blackburn, A. Wolff and W. C. Stanley (2002). "Ranolazine, a partial fatty acid oxidation (pFOX) inhibitor, improves left ventricular function in dogs with chronic heart failure." J Card Fail **8**(6): 416-422.

Sadayappan, S. and P. P. de Tombe (2014). "Cardiac myosin binding protein-C as a central target of cardiac sarcomere signaling: a special mini review series." Pflugers Arch **466**(2): 195-200.

Sadayappan, S., J. Gulick, H. Osinska, L. A. Martin, H. S. Hahn, G. W. Dorn, 2nd, R. Klevitsky, C. E. Seidman, J. G. Seidman and J. Robbins (2005). "Cardiac myosin-binding protein-C phosphorylation and cardiac function." Circ Res **97**(11): 1156-1163.

Sanders, G. D., M. A. Hlatky and D. K. Owens (2005). "Cost-effectiveness of implantable cardioverter-defibrillators." N Engl J Med **353**(14): 1471-1480.

Sarikas, A., L. Carrier, C. Schenke, D. Doll, J. Flavigny, K. S. Lindenberg, T. Eschenhagen and O. Zolk (2005). "Impairment of the ubiquitin-proteasome system by truncated cardiac myosin binding protein C mutants." Cardiovasc Res **66**(1): 33-44.

Schlossarek, S., G. Mearini and L. Carrier (2011). "Cardiac myosin-binding protein C in hypertrophic cardiomyopathy: mechanisms and therapeutic opportunities." J Mol Cell Cardiol **50**(4): 613-620.

Schlossarek, S., F. Schuermann, B. Geertz, G. Mearini, T. Eschenhagen and L. Carrier (2012). "Adrenergic stress reveals septal hypertrophy and proteasome impairment in heterozygous Mybpc3-targeted knock-in mice." J Muscle Res Cell Motil **33**(1): 5-15.

Semsarian, C., I. Ahmad, M. Giewat, D. Georgakopoulos, J. P. Schmitt, B. K. McConnell, S. Reiken, U. Mende, A. R. Marks, D. A. Kass, C. E. Seidman and J. G. Seidman (2002). "The L-type calcium channel inhibitor diltiazem prevents cardiomyopathy in a mouse model." J Clin Invest **109**(8): 1013-1020.

Sequeira, V., P. J. Wijnker, L. L. Nijenkamp, D. W. Kuster, A. Najafi, E. R. Witjas-Paalberends, J. A. Regan, N. Boontje, F. J. Ten Cate, T. Germans, L. Carrier, S. Sadayappan, M. A. van Slegtenhorst, R. Zaremba, D. B. Foster, A. M. Murphy, C. Poggesi, C. Dos Remedios, G. J. Stienen, C. Y. Ho, M. Michels and J. van der Velden (2013). "Perturbed length-dependent activation in human hypertrophic cardiomyopathy with missense sarcomeric gene mutations." Circ Res **112**(11): 1491-1505.

Sequeira, V., E. R. Witjas-Paalberends, D. W. Kuster and J. van der Velden (2014). "Cardiac myosin-binding protein C: hypertrophic cardiomyopathy mutations and structure-function relationships." Pflugers Arch **466**(2): 201-206.

Shaffer, J. F. and S. P. Harris (2009). "Species-specific differences in the Pro-Ala rich region of cardiac myosin binding protein-C." J Muscle Res Cell Motil **30**(7-8): 303-306.

Shaffer, J. F., R. W. Kensler and S. P. Harris (2009). "The myosin-binding protein C motif binds to F-actin in a phosphorylation-sensitive manner." J Biol Chem **284**(18): 12318-12327.

Shannon, T. R., K. S. Ginsburg and D. M. Bers (2000). "Reverse mode of the sarcoplasmic reticulum calcium pump and load-dependent cytosolic calcium decline in voltage-clamped cardiac ventricular myocytes." Biophys J **78**(1): 322-333.

Sigwart, U. (1995). "Non-surgical myocardial reduction for hypertrophic obstructive cardiomyopathy." Lancet **346**(8969): 211-214.

Sirenko, S. G., J. D. Potter and B. C. Knollmann (2006). "Differential effect of troponin T mutations on the inotropic responsiveness of mouse hearts--role of myofilament Ca2+ sensitivity increase." J Physiol **575**(Pt 1): 201-213.

Soergel, D. G., D. Georgakopoulos, L. B. Stull, D. A. Kass and A. M. Murphy (2004). "Augmented systolic response to the calcium sensitizer EMD-57033 in a transgenic model with troponin I truncation." Am J Physiol Heart Circ Physiol **286**(5): H1785-1792.

Sossalla, S., S. Wagner, E. C. Rasenack, H. Ruff, S. L. Weber, F. A. Schondube, T. Tirilomis, G. Tenderich, G. Hasenfuss, L. Belardinelli and L. S. Maier (2008). "Ranolazine improves diastolic dysfunction in isolated myocardium from failing human hearts--role of late sodium current and intracellular ion accumulation." J Mol Cell Cardiol **45**(1): 32-43.

Spirito, P., C. E. Seidman, W. J. Mckenna and B. J. Maron (1997). "The management of hypertrophic cardiomyopathy." New Engl. J. Med. **336**: 775-785.

Spoladore, R., M. S. Maron, R. D'Amato, P. G. Camici and I. Olivotto (2012). "Pharmacological treatment options for hypertrophic cardiomyopathy: high time for evidence." Eur Heart J **33**(14): 1724-1733.

Squire, J. M., P. K. Luther and C. Knupp (2003). "Structural evidence for the interaction of C-protein (MyBP-C) with actin and sequence identification of a possible actin-binding domain." J Mol Biol **331**(3): 713-724.

Stohr, A., F. W. Friedrich, F. Flenner, B. Geertz, A. Eder, S. Schaaf, M. N. Hirt, J. Uebeler, S. Schlossarek, L. Carrier, A. Hansen and T. Eschenhagen (2013). "Contractile abnormalities and altered drug response in engineered heart tissue from Mybpc3-targeted knock-in mice." J Mol Cell Cardiol **63**: 189-198.

Sweeney, H. L., H. S. Feng, Z. Yang and H. Watkins (1998). "Functional analyses of troponin T mutations that cause hypertrophic cardiomyopathy: insights into disease pathogenesis and troponin function." Proc. Natl. Acad. Sci. USA **95**: 14406-14410.

Swynghedauw, B. (1999). "Molecular mechanisms of myocardial remodeling." Physiol Rev **79**(1): 215-262.

Tadano, N., C. K. Du, F. Yumoto, S. Morimoto, M. Ohta, M. F. Xie, K. Nagata, D. Y. Zhan, Q. W. Lu, Y. Miwa, F. Takahashi-Yanaga, M. Tanokura, I. Ohtsuki and T. Sasaguri (2010). "Biological actions of green tea catechins on cardiac troponin C." Br J Pharmacol **161**(5): 1034-1043.

Tong, C. W., J. E. Stelzer, M. L. Greaser, P. A. Powers and R. L. Moss (2008). "Acceleration of crossbridge kinetics by protein kinase A phosphorylation of cardiac myosin binding protein C modulates cardiac function." Circ Res **103**(9): 974-982.

van Dijk, S. J., D. Dooijes, C. Dos Remedios, M. Michels, J. M. Lamers, S. Winegrad, S. Schlossarek, L. Carrier, F. J. Ten Cate, G. J. Stienen and J. van der Velden (2009). "Cardiac Myosin-Binding Protein C Mutations and Hypertrophic Cardiomyopathy. Haploinsufficiency, Deranged Phosphorylation, and Cardiomyocyte Dysfunction." Circulation **119**: 1473-1483.

van Dijk, S. J., E. R. Paalberends, A. Najafi, M. Michels, S. Sadayappan, L. Carrier, N. M. Boontje, D. W. Kuster, M. van Slegtenhorst, D. Dooijes, C. dos Remedios, F. J. ten Cate, G. J. Stienen and J. van der Velden (2012). "Contractile dysfunction irrespective of the mutant protein in human hypertrophic cardiomyopathy with normal systolic function." Circ Heart Fail **5**(1): 36-46.

Verrier, R. L., K. Kumar, T. Nieminen and L. Belardinelli (2013). "Mechanisms of ranolazine's dual protection against atrial and ventricular fibrillation." Europace **15**(3): 317-324.

Vignier, N., S. Schlossarek, B. Fraysse, G. Mearini, E. Kramer, H. Pointu, N. Mougenot, J. Guiard, R. Reimer, H. Hohenberg, K. Schwartz, M. Vernet, T. Eschenhagen and L. Carrier (2009). "Nonsense-mediated mRNA decay and ubiquitin-proteasome system regulate cardiac myosin-binding protein C mutant levels in cardiomyopathic mice." Circ Res **105**(3): 239-248.

Watkins, H., W. J. McKenna, L. Thierfelder, P. Spirito, A. Matsumori, C. S. Moravec, J. G. Seidman and C. E. Seidman (1995). "Mutations in the genes for cardiac troponin T and α-tropomyosin in hypertrophic cardiomyopathy." N. Engl. J. Med. **332**: 1058-1064.

Watkins, H., C. E. Seidman, J. G. Seidman, H. S. Feng and H. L. Sweeney (1996). "Expression and functional assessment of a truncated cardiac troponin T that causes hypertrophic cardiomyopathy." J. Clin. Invest. **98**: 2456-2461.

Wessels, M. W., J. C. Herkert, I. M. Frohn-Mulder, M. Dalinghaus, A. van den Wijngaard, R. R. de Krijger, M. Michels, I. F. de Coo, Y. M. Hoedemaekers and D. Dooijes (2014). "Compound heterozygous or homozygous truncating MYBPC3 mutations cause lethal cardiomyopathy with features of noncompaction and septal defects." Eur J Hum Genet.

Westermann, D., B. C. Knollmann, P. Steendijk, S. Rutschow, A. Riad, M. Pauschinger, J. D. Potter, H. P. Schultheiss and C. Tschope (2006). "Diltiazem

treatment prevents diastolic heart failure in mice with familial hypertrophic cardiomyopathy." Eur J Heart Fail **8**(2): 115-121.

White, J., J. A. Lee, N. Shah and C. H. Orchard (1993). "Differential effects of the optical isomers of EMD 53998 on contraction and cytoplasmic Ca2+ in isolated ferret cardiac muscle." Circ Res **73**(1): 61-70.

WHO (2012). "The top 10 causes of death."

Wigle, A. D., H. Rakowski, B. P. Kimball and W. G. Williams (1995). "Hypertrophic cardiomyopathy: clinical spectrum and treatment." Circulation **92**: 1680-1692.

Wilkins, B. J. and J. D. Molkentin (2004). "Calcium-calcineurin signaling in the regulation of cardiac hypertrophy." Biochem Biophys Res Commun **322**(4): 1178-1191.

Williams, S., M. Pourrier, D. McAfee, S. Lin and D. Fedida (2014). "Ranolazine improves diastolic function in spontaneously hypertensive rats." Am J Physiol Heart Circ Physiol **306**(6): H867-881.

Winegrad, S. (1999). "Cardiac myosin binding protein C." Circ Res **84**: 1117-1126.

Zhao, G., E. Walsh, J. C. Shryock, E. Messina, Y. Wu, D. Zeng, X. Xu, M. Ochoa, S. P. Baker, T. H. Hintze and L. Belardinelli (2011). "Antiadrenergic and hemodynamic effects of ranolazine in conscious dogs." J Cardiovasc Pharmacol **57**(6): 639-647.

6.2. Abbreviations

α-TM	α-tropomyosin
β-AR	β-adrenoreceptor
μ	micro
ADP	adenosine diphosphate
AET	aortic ejection time
AM	acetoxymethyl ester
AMP	adenosine monophosphate
ANOVA	analysis of variance
APS	ammonium persulfate
ATP	adenosine triphosphate
BDM	2,3-butanedione monoxime
BLEB	blebbistatin
BW	body weight
CaMKII	Ca^{2+}/calmodulin-dependent protein kinase II
cMyBP-C	cardiac myosin binding protein C
cTn	cardiac troponin
CICR	Ca^{2+}-induced Ca^{2+} release
DCM	dilated cardiomyopathy
Dil	diltiazem
dP	delta of pressure
DMSO	dimethyl sulfoxide
dt	delta of time
DTT	dithiothreitol
EC_{50}	half maximal effective concentration
ECG	electrocardiogram
EDTA	ethylenediaminetetraacetic acid
EF	ejection fraction
EGCG	epigallocatechin gallate
EMD	Ernst Merck Darmstadt
FAS	fractional area shortening
HCM	hypertrophic cardiomyopathy
HCN	hyperpolarization-activated cyclic nucleotide-gated

HEPES	4-(2-hydroxyethyl)-1-piperazineethanesulfonic acid
HOCM	obstructive hypertrophic cardiomyopathy
Hz	hertz
IC_{50}	half maximal inhibitory concentration
I_{Na}	sodium current
IP	Intraperitoneal
IU	injection unit
ISO	isoprenaline
KI	knock-in
KO	knock-out
LTCC	L-type calcium channel
LV	left ventricle
LVM	left ventricular mass
m	milli or meter
M	molar
MEF2	myocyte enhancer factor 2
Meto	metoprolol
MPI	myocardial performance index
mRNA	messenger RNA
MV	mitral valve
MYH7	myosin heavy chain, gene
MYBPC3	cardiac myosin binding protein C, gene
n	nano
NCX	sodium-calcium exchanger
NFAT	nuclear factor of activated T cells
NFT	non-filling time
Pln	phospholamban
PMT	photomultiplier
PKA	protein kinase A
PKC	protein kinase C
PKD	protein kinase D
PVDF	polyvinylidene difluoride
Ran	ranolazine
RV	right ventricle

RyR	ryanodine receptor
SCD	sudden cardiac death
SDS	sodium dodecyl sulfate
SEM	standard error of the mean
Ser	serine
SERCA	sarcoplasmic/endoplasmic reticulum calcium ATPase
SL	sarcomere length
SR	sarcoplasmic reticulum
TBS-T	tris-buffered saline and Tween 20
TEMED	tetramethylethylenediamine
TTP	time to peak
W	watt
WT	wild type

6.3. Antibodies

Target protein	Host species	Dilution	Company and product
Calsequestrin	Rabbit	1:2500	Dianova ABR-01164
Troponin I	Rabbit	1:1000	Cell signaling #4002
Phospho-troponin I serine 23/24 ()	Rabbit	1:1000	Cell signaling #4004
Phospholamban	Mouse	1:2000	Badrilla A10-14
Phospho-phospholamban serine 16	Rabbit	1:5000	Badrilla A10-12
Rabbit IgG horseradish peroxidase-conjugated	Goat	1:5000	Sigma-Aldrich A0545
Rabbit IgG horseradish peroxidase-conjugated	Goat	1:5000	Dianova 111-035-045
Mouse IgG horseradish peroxidase-conjugated	Sheep	1:5000	Dianova 515-035-003

Protein marker:

Precision Plus Protein^{Tm} Marker			Bio-Rad #161-0373

6.4. Chemicals

Chemical product	Company
Acrylamid/bis solution (29:1)	Bio-Rad
Ammonium persulfate (APS)	Bio-Rad
Blebbistatin	Sigma-Aldrich
Bovine serum albumin	Sigma-Aldrich
Buprenorphine	Sigma-Aldrich
Calcium chloride ($CaCl_2$)	Merck
Dimethyl sulfoxide (DMSO)	Sigma-Aldrich
Diltiazem	Sigma-Adrich
Disodium hydrogen phosphate (Na_2HPO_4)	Merck
Dithiothreitol (DTT)	Sigma-Aldrich
ECL plus Western Blotting detection system	Amersham Biosciences
Ethylenediaminetetraacetic acid (EDTA)	Sigma-Aldrich
EMD 57033	Merck
Fura-2 AM	Life technologies
Heparin	Rotexmedica
Hydrochloric acid (HCl)	Merck
Isoprenaline	Sigma-Aldrich
Isoflurane	Abbot
Ketoconazole chow	Altromin
Metoprolol	Sigma-Aldrich
Milk powder	Roth
Magnesium sulfate ($MgSO_4$)	Merck
Magnesium chloride ($MgCl_2$)	Fluka
Penicillin-streptomycin	Gibco
Potassium chloride (KCl)	Merck
Potassium hydrogen carbonate ($KHCO_3$)	Merck
Potassium dihydrogen phosphate (KH_2PO_4)	Merck
Ranolazine	Sigma-Aldrich
Ranolazine/Ketoconazole chow	Altromin
Sodium chloride (NaCl)	J.T. Baker
Sodium chloride 0.9%	B | Braun

Sodium dodecyl sulfate (SDS)	Roth
Sodium hydrogen carbonate ($NaHCO_3$)	Merck
Sodium dihydrogen phosphate(NaH_2PO_4)	Merck
Sodium hydroxide (NaOH)	Merck
Super Signal West Dura extended duration substrate	Pierce
Tetramethylethylenediamine (TEMED)	Bio-Rad
Tris-buffered saline (TBS)	Sigma-Aldrich
Tween-20	Sigma-Aldrich

6.5. Consumable material

Product	Company
Blotting paper (Whatman 3 mm)	Schleicher & Schuell
Cotton buds	Beese
Cuvette 1 ml	Sarstedt
Falcon tubes (15 and 50 ml)	Greiner bio-one
Glassware	Schott Duran
Latex gloves	Aurelia
Micro tubes (1.5 and 2 ml)	Sarstedt
Nitrile gloves	Ansell
Parafilm	Bemis
Pipette tips	Sarstedt
PVDF membrane	GE Healthcare
Serological pipettes (5, 10 and 25 ml)	Sarstedt
Serological pipettes (wide tip, 10 ml)	Sarstedt
Stirring rod 120 mm	Sarstedt
Syringes (1 ml / 50 ml)	BD Medical / B	Braun
Tissue culture dish (60 x 15 mm)	Sarstedt
Transfer pipette 3.5 ml	Sarstedt
Vacuum filtering flasks (250 and 500 ml)	Sarstedt
Weighing paper 90 x 115 mm	Macherey-Nagel

6.6. Laboratory equipment

Equipment	Company
Accu-jet pipetting aid	Brand
Blotting system	Bio-Rad
Centrifuge 5415 R	Eppendorf
Chemie Genius^2 Bio imaging system	Syngene
Electrophoresis system	Bio-Rad
Glass equipment of Langendorff perfusion system	W. Hassa Laborbedarf
Ice machine	Scotsman
Inverted microscope Eclipse TS 100	Nikon
Light source KL 1500 compact	Schott
Magnetic stirrer (IKAMAG$^®$ RCT)	Janke & Kunkel
Minipuls pump	Gibson
Myocyte contraction recording and Ca^{2+} imaging system	IonOptix
Consumables, perfusion and temperature control system	Cell MicroControls
Myocyte counting chamber (Fuchs-Rosenthal)	Assistent
Peristaltic pump P1	Pharmacia fine chemicals
pH meter	Knick
Pipettes (10, 100, 200, 1000 ml)	Eppendorf
Small rodent echocardiography system Vevo$^®$ 2100	Visual Sonics
Spectrophotometer (Smart Spec^{Tm} 3000)	Bio-Rad
Surgical instruments	Fine Science Tools / Hammacher
Ultra-pure water system Milli-Q	Millipore
Water bath Thermostat 2761	Eppendorf

7. Acknowledgements

First of all I would like to thank Prof. Dr. Lucie Carrier for giving me the opportunity to work on this project and for her critical, respectful and kind supervision and guidance. I also would like to thank Dr. Felix Friedrich for his great supervision and support and Prof. Dr. Thomas Eschenhagen for his helpful feedback on my work.

Furthermore, I would like to thank PD Dr. Hartwig Lüthen for his review of this thesis and Dr. Kent Duncan for verification of the English language I used.

I also would like to thank everyone who helped me with my work on the project, especially Lisa Krämer for teaching me how to isolate AMCMs, Birgit Geertz and Dr. Florian Weinberger for perfoming echocardiography and haemodynamic measurements, Silke Reischmann for helping me with Western Blots and PD Dr. Torsten Christ and Klaus Soeren for performing organ bath measurements.

Many thanks to the whole Institute of Pharmacology and especially the members of the AG Carrier for providing a great working atmosphere and always being helpful and supportive.

Last but not least, I would like to thank my parents, my sister, my friends and especially Kati for being the supportive, caring and wonderful people they are.